DOE/NASA/0075-82/1
NASA CR-167985

Advanced Axial Field D.C. Motor Development for Electric Passenger Vehicle

William J. Jones
Westinghouse Research Laboratories
Westinghouse Electric Corporation

December, 1982

Prepared for
NATIONAL AERONAUTICS AND SPACE ADMINISTRATION
Lewis Research Center
Cleveland, OH 44135
Under Contract DEN 3-75

for
U.S. DEPARTMENT OF ENERGY
Conservation and Renewable Energy
Office of Vehicle and Engine R&D

NOTICE

D95-23

DOE/NASA/0075-82/1
NASA CR-167985

ADVANCED AXIAL FIELD D.C. MOTOR DEVELOPMENT FOR ELECTRIC PASSENGER VEHICLE

William J. Jones
Westinghouse Research Laboratories
Westinghouse Electric Corporation

December 1982

Prepared for
National Aeronautics and Space Administration
Lewis Research Centerr
Cleveland, Ohio 44135
Under Contract DEN 3-75

for
U.S. DEPARTMENT OF ENERGY
Conservation and Renewable Energy
Office of Vehicle and Engine R&D
Washington, D.C. 20585
Under Interagency Agreement DE-AI01-77-CS51044

FOREWORD

The author would like to acknowledge the dedication and hard work of a number of persons who contributed significantly to this project. Principally among them are:

Dave Triezenberg and Henry Haller, who made major contributions to developing the electromagnetic theory and design rationale necessary to quantification of the motor performance.

Phil Ulerich, who contributed to the electromagnetic design and compiled the motor performance and vehicle simulation computer programs.

Ray Hastings, who applied his manufacturing engineering knowledge to the design of the various model motors to maximize manufacturability.

A number of DC motor design engineers in the various Westinghouse manufacturing divisions who consulted with the author at various times on specific problems, including Joe Moxie and Vern Vranna of the Large Motor Division, Jim Needles of the Transportation Division, and Harry Meyers, consultant to the Corporation.

Bob Hatvani, who while functioning as Project Manager for NASA, also contributed his knowledge, enthusiasm, and determination to the successful completion of this effort.

William J. Jones
Principle Investigator

TABLE OF CONTENTS

TABLE OF CONTENTS (cont.)

LIST OF FIGURES

LIST OF FIGURES (cont.)

LIST OF TABLES

1. SUMMARY

As part of a coordinated program to develop advanced propulsion system components for electric and hybrid vehicles, Westinghouse Electric Corporation conducted a two-phase development program of an advanced axial field D.C. motor under contract DEN 3-75 for the NASA Lewis Research Center. The work scope of this development effort was to design, fabricate and test a series of models of the proposed motor concept, leading to a demonstration of technology readiness. Selection of a wound field D.C. motor for electric vehicle propulsion was based upon its favorable impact upon the cost and reliability of the total vehicle propulsion system. The axial field geometry permits the use of higher peripheral speeds than the conventional drum armature machine because its inactive periphery can be effectively banded; this advantage should lead to higher power density and greater efficiency, and ultimately to both lower weight and cost.

The Westinghouse advanced D.C. motor is essentially an axial field version of the classical Gramme ring winding motor, but the active conductors are recessed into slots cut on the two opposite faces of the laminated, tape-wound core ring. The armature is flanked on each side with a pair of wound field pole assemblies; in later models commutating poles were added to one side. The development program was carried out in two phases. In Phase I a proof-of-principle model was built and tested, a functional model was designed, built, and tested, and the preliminary design of an engineering model was completed. In Phase II the engineering model, incorporating a number of design improvements and considerably reduced weight, was designed, built, and tested.

To guide us in the optimization of the motor design for electric vehicle propulsion, a computer simulation program was developed which predicts the performance of the motor under any specified operating condition. By exercising the motor over a sequence of quasi-steady state operating points simulating the desired vehicle operating profile, an integrated cycle efficiency and energy consumption can be calculated.

By considering the battery weight penalty associated with motor inefficiency, the concept of an "adjusted" weight was developed which allowed optimization of the motor design using a single weighted attribute. In this optimization the motor weight is penalized 12 pounds for each 1% of energy inefficiency when operating the vehicle over the SAE J227a D-cycle. This adjusted weight guideline was utilized in the design of both the functional and engineering models.

The functional model was a six pole machine which weighed 88.5 kg (195 lbs.). It developed 16.5 kw (22.0 H.P.) continuous at a base speed of 2400 rpm with an efficiency of 92%. Maximum rated speed was 4800 rpm. Its size, weight and efficiency are comparable to the best state-of-the-art D.C. motors available. Morevoer, its performance agreed quite well with that predicted by our computer model, enhancing significantly our confidence in this model. The only performance problem encountered with the functional model was that commutation was considered marginal under overload conditions, leading to commutator overheating.

It was decided that to justify additional development effort the engineering model must show the potential for a significant reduction in weight over that of the functional model, and that such a weight reduction could only be achieved by increasing motor base speed and increasing the ratio of electrical to magnetic loading. Both of these changes, however, necessitated the addition of interpoles to the engineering model to assist commutation.

The engineering model is a four-pole machine with four interpoles. Its design continuous power rating is 13.5 kw (18.0 H.P.) at a base speed of 3000 rpm, with a 2:1 overload capability. Maximum speed was 7200 rpm. The engineering model weighs 47 kg (104 lbs.), and was constructed in a standard 250 frame size. The initial performance of the model was unsatisfactory; commutation was poor, and efficiency was approximately 10% lower than expected. A brief theoretical review of the motor design fundamentals was conducted by a consultant, but no design weaknesses were uncovered. Although the difficulties experienced with the engineering model appear

soluable, additional effort was judged to be inappropriate when the projected results were compared with other advanced electric motor alternatives; therefore, work on the engineering model was discontinued.

The major uncertainties concerning the ultimate utility of this new motor technology are related to its manufacturability, and its compatibility with an optimal vehicle propulsion system.

Manufacturability problems include the development of an inexpensive method for volume production of slotted cores, and automated winding techniques and equipment for armature winding. Apparently feasible solutions to both of these problems have been conceptualized, but the development of the manufacturing technology and equipment was clearly beyond the scope of this effort.

Propulsion system compatibility problems are centered around the very high rotational kinetic energy of the engineering model, and the problems this may pose when mating the motor to a shifting transmission.

2. INTRODUCTION

2.1 Background

The Electric and Hybrid Vehicle (EHV) Program is sponsored by the U.S. Department of Energy (DOE). The overall objective of the EHV research and development activity is to increase the national petroleum savings potential of electric and hybrid vehicles by providing advanced technologies having attributes necessary to ensure their widespread use. The NASA Lewis Research Center (LRC) was given the authority by DOE to administer contracts for Research and Development of Advanced Propulsion Systems and Components. The development effort described in this report is one element of that program to develop and demonstrate advanced propulsion system components employing new technology.

Electric motors available at present to the electric vehicle industry may, in general, be characterized as heavy, expensive, and inefficient when operated over a wide range of speed and load. The objective of the work performed under the Advanced Electric Vehicle Motor Development Program was to overcome these limitations by developing advanced electric propulsion motors optimized to meet the specific requirements and constraints of electric vehicle service, using technology that can be incorporated into volume production at reasonable cost in the mid-1980's.

Based upon extensive development and evaluation of electric vehicle technologies during the previous decade, Westinghouse concluded that only a D.C. motor linked to a multi-speed transmission and using field modulation as the primary control mode could possibly be cost effective for volume production in the mid-1980's.

2.2 Program Scope

The development was carried out in two phases. The objective of Phase I, a demonstration of feasibility, via design, fabrication and testing of a functional model, and preliminary design and performance

prediction of an engineering model motor. The objective of the optional Phase II was to demonstrate technology readiness, via design, fabrication and testing of an engineering model, and preliminary design and performance prediction of a production model motor.

3. MOTOR CONCEPT

3.1 Background

The Westinghouse Axial Field D.C. Motor was conceived as an outgrowth of an extensive in-house electric vehicle hardware development program at the Corporate Research and Development Center during the 1970's. The design objective was to develop an inexpensive wound field D.C. machine that was both lightweight and efficient. A wound field D.C. motor was chosen as the preferred motor design concept because of its favorable impact on the cost and reliability of the total vehicle propulsion system. By operating it in conjunction with a suitable transmission and low-power field controller, the noisy, expensive, and unreliable SCR armature chopper can be eliminated. Although a permanent magnet field offers both cost and weight advantages to the motor, the use of a wound field machine was dictated by overall propulsion system considerations which simplified the transmission and vehicle control system.

Our interest in the axial field D.C. machine was caused by its apparent suitability for high speed operation. In high volume production, the price of a motor is material-cost-intensive; thus a low-cost motor must be a lightweight motor. Because the periphery of the axial field machine is not active material (but end turns), it can be effectively banded and should, therefore, be capable of higher peripheral speeds than the conventional drum armature machine. Furthermore, by placing the active materials at a greater working radius, there were theoretical reasons to believe that higher efficiencies and power densities were simultaneously available in a given frame size.

3.2 Concept Description

One of the initial construction concepts proposed for the axial field machine is illustrated in Figure 1. A slotted tape-wound core ring is wound toroidally with a continuous conductor which is tapped periodically for commutator connections. This is simply a two-sided

axial field version of the classical Gramme-ring winding. But whereas the classical ring winding had only one active element per turn (the peripheral coil element) and therefore had relatively long end turns, the proposed winding with two active coil sides overcomes this limitation. Because the field flux enters the opposed faces of the armature and travels circumferentially in the core ring, the core must be laminated circumferentially; thus a continuous steel strip tape-wound into a ring is utilized for the armature core.

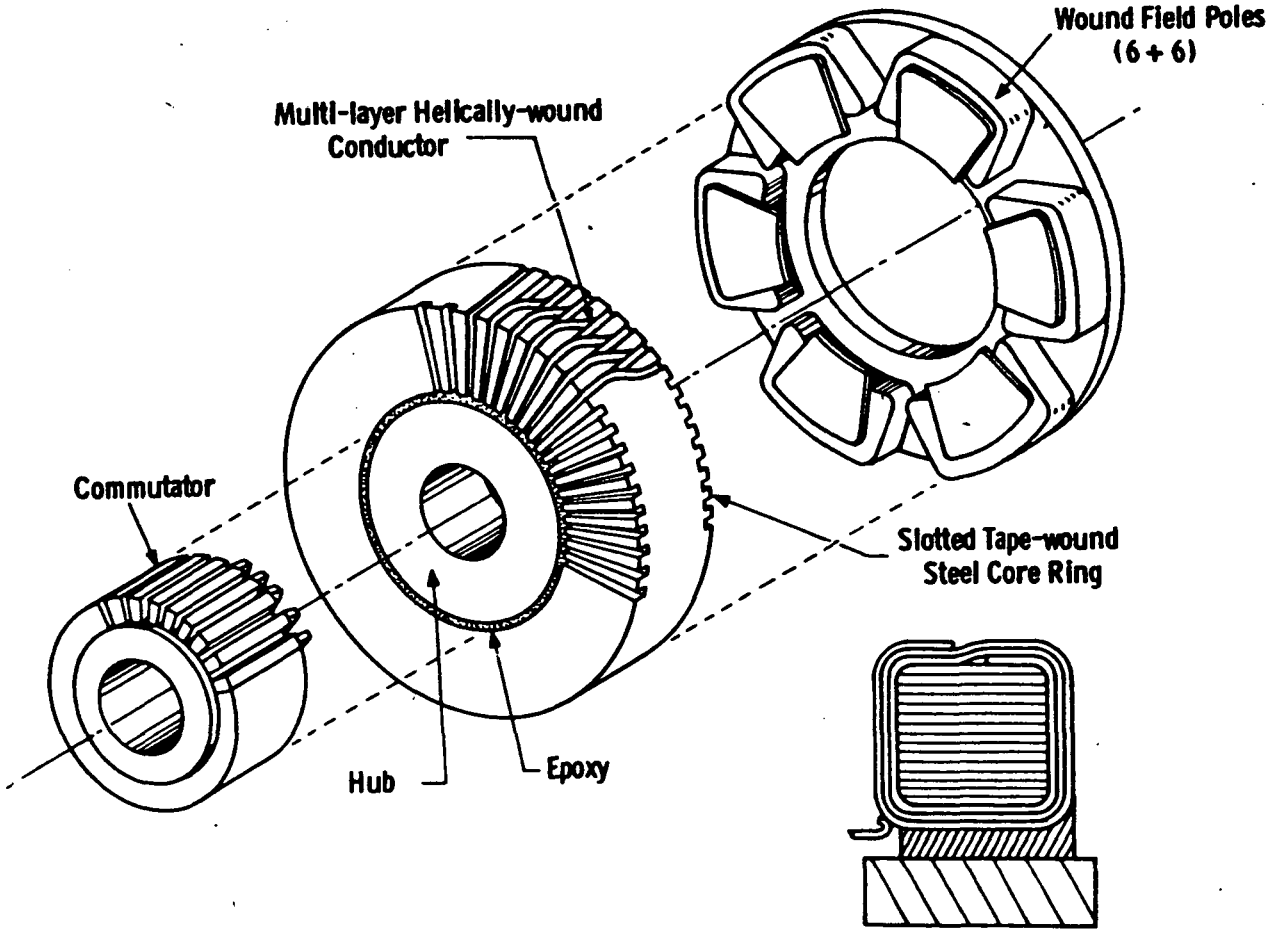

Figure 1 - Axial Field D.C. Machine Concept

The armature is flanked on each face by an assembly of wound field poles attached to a solid steel yoke. The field poles are of alternate polarity and create a flux pattern as illustrated in Figure 2. Notice that no net flux travels axially thru the center plane of the armature; it is sometimes useful to think of the axial field machine as two separate motors, with the two armatures serving as end turns for each other and providing a counter-balancing axial force.

Dwg.7777A16

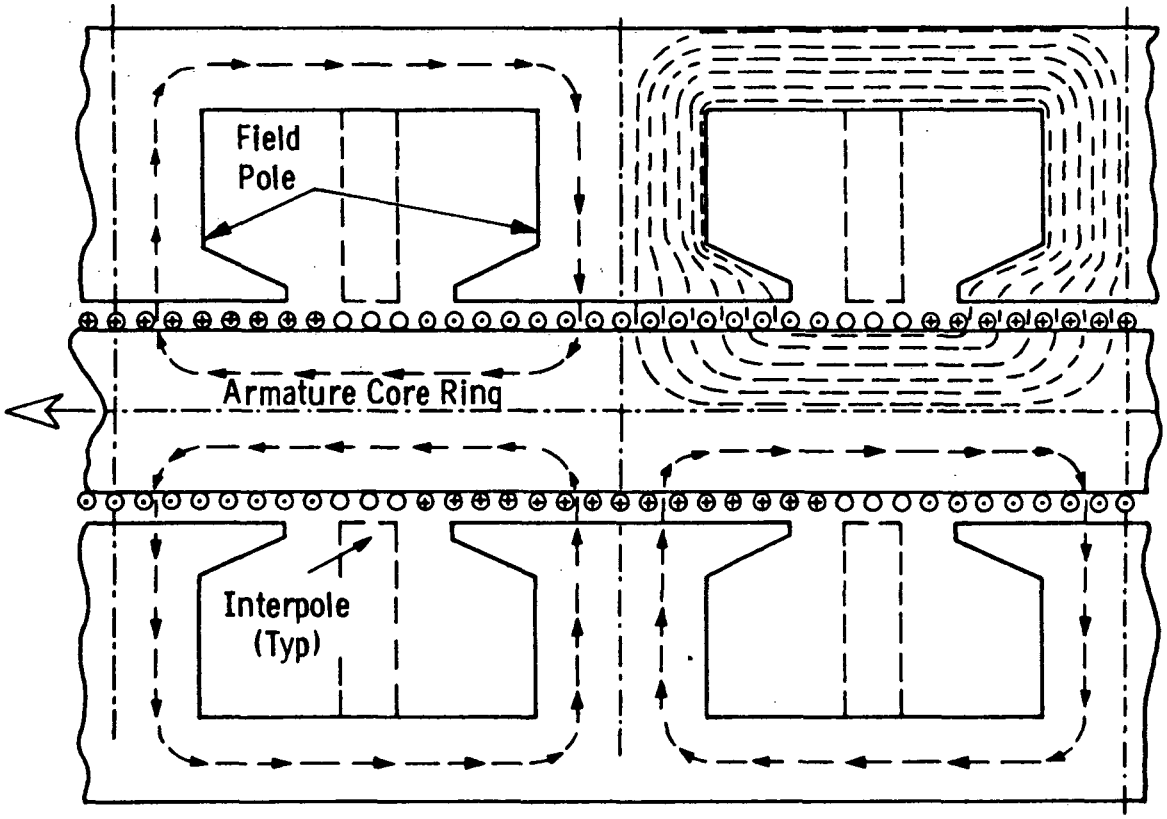

Figure 2 - Magnetic Circuit of Axial Field Machine

A number of design variations of the axial field machine were considered in the investigative phases of the work, including:

- Coreless construction, using circumferential end turns and straight-thru flux
- Airgap (toothless) winding
- External commutation on armature end-turns
- Four, six, and eight pole designs
- Permanent (ceramic) magnet field poles
- Compacted powdered-iron armature teeth
- Interpoles

To minimize developmental risk, a separate commutator and machine-slotted core rings were used to fabricate the models built under this contract. The POP and functional models had six main poles (no interpoles), with the engineering model had four main poles and four interpoles. The design features of the various models will be treated in greater detail in the later sections on each motor model.

4. MOTOR DESIGN AND PERFORMANCE PREDICTION

4.1 General Requirements

The general design requirements prescribed in the contract are listed in Table 1. A two-speed transmission was "available" to meet vehicle performance requirements, if optimum. Air cooling was prescribed and battery voltage between 120-240 VDC was permitted. Motor life of 100,000 SAE J227a (D) cycles (approximately 100,000 miles) was required. The motor design was to be optimized to achieve the lowest initial and life cycle costs, and was to be compatible with the vibration, shock and safety requirements of an electric passenger vehicle application.

Table 1

E.V. MOTOR - GENERAL REQUIREMENTS

- Single or Multiple
- Two-Speed Transmission, if Optimum
- Air-Cooled (Integral or Aux.)
- 120 - 240 VDC Battery Pack
- Life - 100,000 SAE J227a (D) Cycles; 3500 Hours
- Lowest Initial and Life Cycle Cost
- Vehicle Environment - Vibration, Shock, Safety
- Temperature Range (Ambient) - -30°C to +50°C

4.2 Vehicle Performance Requirements

The original vehicle performance requirements established for a 1350 kg (3000 lb.) vehicle are given in Table 2. These original requirements had a rather modest performance specification, particularly in the area of low speed gradeability and acceleration. In order to make a more rational decision regarding the motor controller power requirements and the need for a transmission, the additional performance requirements

of Table 3 were added at the inception of Phase II. These requirements were adapted from the "diesel-equivalent" performance requirements that were later adopted by the Electric and Hybrid Vehicle Program.

Table 2

ORIGINAL PERFORMANCE REQUIREMENTS*

2 hrs. @ constant 89 Km/h (55 mph)

2 hrs. of repeated SAE J227a, Schedule D driving cycles**

Uphill gradeability: 10% grade @ 56 km/h (35 mph) for 5 minutes

Downhill regeneration: 15% grade @ 48 km/h (30 mph) (30 mph) for 2 minutes with no mechanical braking

Table 3

ADDITIONAL PERFORMANCE REQUIREMENTS*

Acceleration:

0-48 km/h (0-30 mph) within 8 seconds
40-88 km/h (25-55 mph) within 16 seconds

Gradeability:

4% grade @ 64 km/h (40 mph), continuous
5% grade @ 80 km/h (50 mph) for 1 minute

Min. passing speed of 104 km/h (65 mph)

*1350 kg (3000 lb.) gross weight vehicle

**See Appendix D

4.3 Vehicle Performance Prediction

Our strategy of motor optimization required that we simulate repetitive operation of the vehicle (and motor) over a predetermined driving cycle (the SAE J227-Schedule D), and calculate the integrated motoring/generating energy consumption and efficiency over this driving cycle. To do this we first developed a computer program to predict the required motor operating speeds and torque over this cycle. This vehicle simulation program is based upon the usual road load power equation, given in Appendix A. The values of the vehicle-dependent parameters (mass, frontal area, and tire rolling resistance coefficient) are specified in the contract. We compiled a computer program in which the required vehicle velocity (and acceleration) profile could be entered, using one second intervals. The required propulsion system output speed, power and torque are then computed by the program.*

Other inputs to the program are also available to simulate the drive system speed ratios and efficiencies at each operating point. In this way, various multi-speed or even variable-speed transmissions can be simulated. The required power, torque and shaft speed are then reflected to the motor as an instantaneous demand.

In addition to the D-cycle capability, the computer simulation can also be used to calculate the required motor inputs at a variety of quasi-steady state vehicle performance conditions as specified by the contract. The road power required from the propulsion system for a number of these performance requirements is illustrated by the points and envelope lines of Figure 3. The required propulsion system performance can thus be specified in terms of a continuous and overload power-speed map. Note that the maximum continuous power rating indicated is approximately 13.5 kW (18 H.P.), with a 2:1 overload capability.

In addition to the ability to prescribe vehicle speed and acceleration (and calculate the required propulsion system inputs), limiting motor armature and field currents can also be specified, available motor torque computed and the resulting vehicle acceleration

*See Appendix

Curve 725755-A

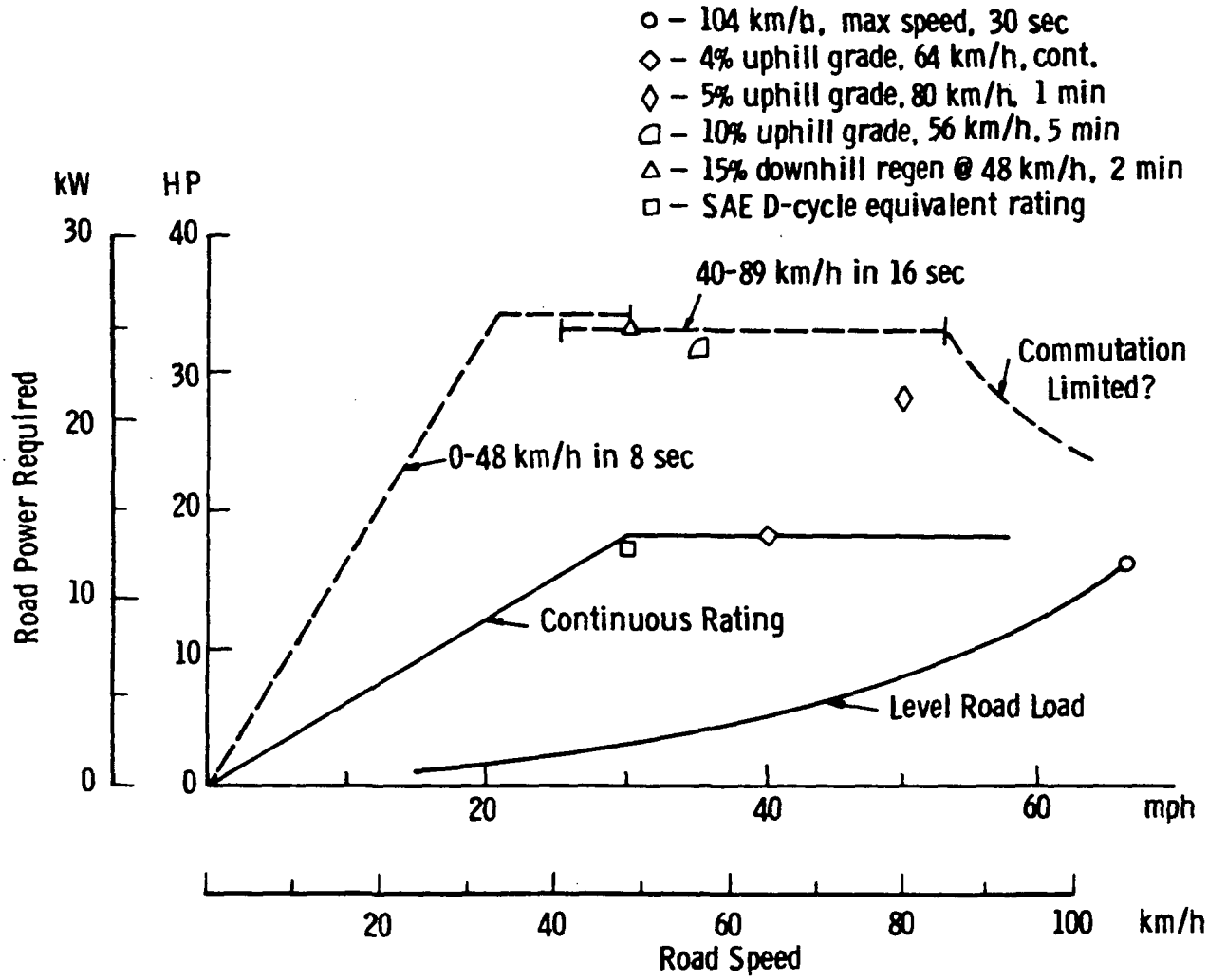

Figure 3 - Required Propulsion System Performance

computed. In this way a maximum vehicle acceleration profile can be generated for any given motor current limits. This is not only useful for predicting the vehicle maximum acceleration performance, but was used at sub-maximum currents to determine a constant armature current speed profile for use in the D-cycle acceleration phase.

4.4 Motor Performance Prediction

Although the axial field D.C. motor is considerably different in mechanical construction than a conventional drum-armature D.C. machine, electromagnetically it is nearly identical, and calculation of "equilibrium" operating conditions and losses use standard methods which are known to the industry. For a detailed treatment of D.C. motor performance prediction, the casual reader is referred to The Design of Small Direct Current Motors, A. F. Puchstein, J. Wiley and Sons, Inc., 1961.

For convenience in making design iterations, we first codified a motor design program for the axial field ring winding machine. There are 32 required user inputs including:

- number of poles
- terminal voltage
- rated armature current
- base speed
- number of armature slots per side
- number of armature conductors per slot
- pole enclosure (main and interpoles)
- rotor active radii, inner and outer
- commutator diameter
- armature and field conductor current densities
- slot and field conductor packing factors
- main pole and interpole airgaps
- magnetic flux densities in the core ring, armature teeth, pole body, and back iron
- brush contact drop, current, density, contact pressure, and friction coefficient

The motor design program then contained design rules and procedures for completely sizing the machine and computing its total weight. A variety of design variables that are uniquely determined by the input parameters are also computed and printed out. A typical computer printout, including the motor design section, is shown in Appendix B.

After the motor and transmission have been completely specified, the vehicle is "exercised" thru a variety of operating conditions including a current-limited vehicle maximum acceleration, D-cycle operation, and "steady-state" operation at various cruise, uphill climb, and downhill regeneration conditions. The motor performance prediction program calculates the required motor inputs/outputs, the losses, efficiency, and commutation voltages at each operating point. In optimizing the design of the motor, its net energy efficiency over the D-cycle driving profile is optimized to minimize energy consumption. The net input energy, output energy, and losses at each of the quasi-steady-state operating points are totaled and an overall cycle energy efficiency is compiled using the expression:

$$\text{Cycle Efficiency} = 1 - \frac{\text{total motor energy losses}}{\text{total motor input energy}}$$

When the vehicle is motoring, the input is electrical, and when it is generating the input is mechanical. Individual motoring and generating efficiencies are also computed. Optimization of the design is accomplished by manual iteration of the design parameters and examining the effect upon motor weight and cycle energy efficiency.

4.5 Motor Design Optimization Guidelines

The optimization of the design of a vehicle propulsion system in general, and the motor in particular, is a complex issue which can only be addressed here in an oversimplified way. The computerized design program gave us a useful tool for characterizing and evaluating the performance of a variety of motor design alternatives. Each of these design alternatives results in a motor of a certain weight which must not only meet the peak performance requirements, but will operate efficiently over the SAE J227a D-cycle. Many of the design alternatives have conflicting effects on motor weight, cost and efficiency. We

therefore needed a simple trade-off guideline whereby any particular motor design that could be characterized by a specific set of cost, weight, and cycle efficiency could be compared on a uniform basis.

The optimization rationale which we developed is that a particular motor (propulsion system) design would be penalized not only for its own cost and weight, but for the cost and weight of the additional required battery capacity due to its inefficiency. We can thus calculate an adjusted weight and cost which includes the battery penalty. Using battery energy density and capacity figures estimated by the EHV program office for commercialized batteries, it was demonstrated that each 1% inefficiency of the propulsion system results in carrying an additional 5.5 kg (12 pounds) of batteries. With this simple rule, the "adjusted" weight (motor weight plus battery penalty) can be calculated and compared for any design iteration, and the overall vehicle weight optimized.

To pursue an optimization of vehicle initial and/or life cycle* cost requires a similar knowledge of the battery costs and the energy required to recharge it. Using D.O.E. goals established for commercialized E.V. batteries of $3.75 per kg and calculating a battery recharging (fuel) cost over the projected life of the vehicle of $3.00 per kg of battery, we get a total life cycle cost for batteries of $6.75 per kg or $37 for each 1% inefficiency of the motor. Using estimated motor costs of $6.75 per kg, we can also calculate optimization criteria for initial cost ($1\% \ \eta \cong 8.6$ kg). Obviously, we cannot simultaneously optimize both initial and life cycle costs. For simplicity, we selected a weight penalty of 5.5 kg per % inefficiency because this criteria simultaneously optimized propulsion system weight and vehicle life cycle cost.

*As used here, component life cycle cost is defined as the sum of the initial cost of the component, its anticipated replacement cost, if required, and the energy costs associated with the inefficiencies in that component when operated over the life of the vehicle, all normalized per pound of component weight.

4.6 Transmission Selection

Translation of the propulsion system power-speed requirements into a motor power-speed curve requires knowledge of the transmission gear ratio(s) and efficiency (-ies). The contract prescribed the availability of separate armature and field choppers; the use of a two-speed transmission was optional, depending upon overall propulsion system optimization. The use of additional low gear ratio(s) has the effect of flattening the power speed curve, or extending the peak power region to lower speeds. It thus improves low speed performance and gradeability. However, the same result can be achieved by increasing the power rating of the armature chopper, assuming the motor can handle the overload. Thus the use of a two-speed transmission may have the effect of reducing the required peak power rating of the armature chopper.

The tradeoff between transmission weight and efficiency and chopper current rating is complex and beyond the scope of our study. We, therefore, chose to arbitrarily limit the chopper power rating to 360 amps at 120 VDC (comparable to the power rating of the ETV-1 chopper), and use the two-speed transmission if required to achieve the desired low speed performance.

Figure 4 illustrates the required motor torque speed curve using a 7.5:1 direct reduction chain drive with a 95% efficiency. The vehicle computer performance model predicted that the peak current required from the chopper to meet the 0-48 km/h in 8 sec acceleration specification was slightly less than 300 amps, using 200% field excitation on the motor. Thus the vehicle performance requirements can be met without a two-speed transmission and a direct reduction chain drive was chosen for our reference design.

It should be noted that the selection of a direct reduction drive for our reference design should not be considered as a blanket endorsement for the use of such drives in electric vehicles. The use of a multi-speed transmission does have a beneficial impact upon the current rating and cost of the required armature controller, and thus may have a favorable

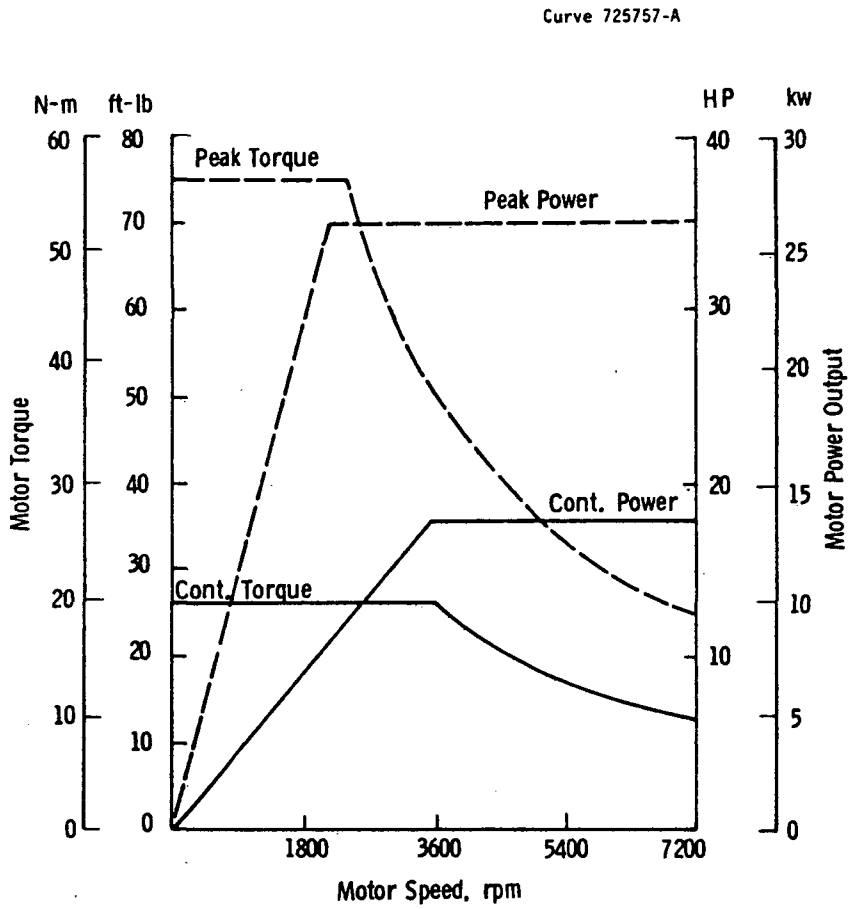

Figure 4 - Required Motor Performance Envelope

impact upon overall propulsion system optimization. Furthermore, to implement a simple D.C. field control scheme (and eliminate the armature chopper entirely) a multi-speed or variable ratio transmission is clearly needed to achieve good efficiency and vehicle controllability in the low-speed range. A brief study of the energy efficiency related design parameters associated with multi-speed shifting transmissions is included in Appendix C. This study supports the conclusion that with a two or three speed transmission, the energy losses incurred by starting the vehicle with a slip clutch or similar dissipative element are insignificant, and the armature chopper could indeed be eliminated without a significant energy penalty.

5. TEST METHODS AND EQUIPMENT

5.1 General Approach

In testing the D.C. machines developed under this contract, a uniform test methodology was utilized and is described in this section. In general, our approach was to first analytically model and predict the expected behavior of the machine in terms of energy conversion and dissipation under various test conditions, to confirm these results with tests, and then to rationalize the differences and upgrade our model.

5.2 No-Load Tests

In order to gain a more complete understanding of the various loss mechanisms in each machine, a complete set of no-load tests were first performed. The shaft of the test machine is connected to that of an auxiliary motor and is driven at controlled speeds under various operating conditions while the input torque, speed, and power (computed) is measured. Without brushes and with no field excitation, the losses attributable to bearing friction and aerodynamic drag on the rotor can be measured by measuring the input torque at various speeds. By placing the brushes on the commutator and noting the incremental torque at each speed the additional loss due to brush friction can be isolated. Next, with the armature circuit open, the field is excited at various currents and at various speeds. The incremental torque required to drive the rotor with field excitation is attributed to the magnetic losses* (hysteresis and eddy currents) in the iron of the armature and pole faces that experience a reversing or cyclic magnetic flux.

---

*In a poorly designed machine, circulating currents in the armature circuit can also occur, and these cannot be distinguished from iron losses without opening the winding.

The open-circuit armature voltage generated during the previous test is also measured. At any fixed speed this curve of open-circuit armature voltage vs field current is called a no-load saturation curve; it gives a quantitative measure of the actual flux produced per pole in the machine for a given field excitation. The effect of saturation in the iron path is indicated by a distinct flattening of the open-circuit voltage as excitation is increased.

The total no-load armature loss can also be measured by operating the machine as a motor with no load on the shaft and measuring the electrical inputs required under various operating conditions. For this data the motor is generally operated over the speed range using a combination of armature and field control. Base speed is defined as the speed at which the motor will operate with full rated voltage applied to both the armature and field. Below base speed full rated field excitation is used and the armature voltage is varied to maintain the pre-selected shaft speed. Above base speed full rated armature voltage is maintained and the field excitation current is reduced to achieve the desired speed. Under these conditions, the motor field, armature and total losses can be measured and plotted vs motor speed.

In simplistic models of a D.C. motor, the only additional load-related losses are those due to the I^2R losses in the armature circuit. Thus, if the no-load saturation curve, no-load losses, and the armature circuit resistance are all known, the motor operation under any loading conditions can be extrapolated, and its losses and efficiency predicted. In our computer models, the additional effects of armature current upon the field flux distribution under the main poles (armature reaction) was also factored into the model as well as additional losses in the interpole faces.

5.3 Load Tests

To obtain motor characteristics under load conditions, generally the motor output shaft speed and torque are pre-determined and the electrical inputs (armature and field voltage and current) required to maintain the pre-selected output are measured. Alternately for convenience in testing, armature electrical input current may be specified and the resultant output torque measured. During load tests the same armature/field control philosophy is used below and above base speed as described for no-load tests. The most important data characterization of the part load and full load tests are the motor efficiency and its thermal performance. In general, the continuous rated load of a motor is defined as the maximum load at which the motor will maintain acceptable operating temperatures for a continuous period of time, usually at base speed. Below base speed it is generally assumed that the motors rated torque is constant, while above base speed it is generally assumed that the machine can operate at constant horsepower (torque-speed product). This torque and power vs speed envelope corresponds to operation of the armature at a constant maximum input current over the entire speed range. Generally, the constant power region of motor operation is limited at some speed by commutator sparking and consequent commutator overheating.

In addition to continuous rated loads, the overload capability of a machine can be characterized by specific power-speed envelopes which the machine will sustain for pre-selected time intervals without excessive overheating. The baseline condition for starting such overload tests can be room temperature, but generally overload capability is based on thermal equilibration at some full or partial load condition, with a pre-determined allowable thermal excursion. Usually the allowable thermal limits during overload tests exceed those for continuous operation.

During overload tests below base speed it is also necessary to specify some aribtrary relationship between armature and field current. To control armature reaction and to achieve maximum efficiency, field current should be increased above full rated value (field "forcing")

when the machine is drawing armature currents above full rated value at speeds below base speed. Such a relationship can be built into the controller logic eventually, but must be done manually in our tests. We arbitrarily decided to maintain the ratio between field and armature current during overload constant, so that during a 2:1 armature current overload, 2:1 field current forcing would be employed.

The allowable temperature excursion during an overload test determines the duration of a particular test condition. We chose allowable temperatures of 220°C for the peak winding temperature, and 150°C for the peak commutator temperature.

5.4 Test Apparatus

The principle pieces of test support equipment utilized to test the various motor models include (1) a hydraulic dynamometer capable of dissipating up to 30 kW (40 H.P.) at speeds up to 4400 rpm; (2) manually variable voltage and current D.C. power supplies for the armature and field; (3) instrumentation suitable for measurement of the voltages, currents, torque, speed and temperatures of the test motor; and (4) a source of cooling air for the motor, approximately 5.66 m^3/min (200 cfm) at 1000 nt/m^2 (4 in. of water) pressure.

The dynamometer was originally equipped with a reaction cradle for torque measurement; two reaction force measuring elements were available with a range of either 68 or 136 nt·m (50 or 100 ft. lbs.). Later, for the tests of the engineering model the reaction cradle was removed and an in-line torque-speed transducer was utilized. This not only permitted automatic data logging, but eliminated a low speed stability problem that was apparently caused by the low natural frequency of the cradle.

The motor output shaft is connected through a flexible coupling (and through the in-line torque-speed transducer when utilized) to a hydraulic pump. The pump circuit includes a manual throttling valve, pressure gauges, flowmeter reservoir, and oil-to-water heat exchanger.

For tests of the POP and functional model, armature current was supplied from a 0-200 VDC, 0-150 A D.C. current-controlled power supply. For tests of the engineering model, this current rating was inadequate and armature power was derived from a large motor-generator set that supplied essentially armature voltage control by controlling the D.C. generator field. In both cases, the D.C. output was relatively free of distortion, and the power delivered is accurately calculatable from the D.C. voltage and current. The field power supply for all tests was a rectified and filtered AC/DC converter with passive voltage control.

5.5 Instrumentation

The test instrumentation used and data taken vary with the different models and will be addressed in detail in the later sections describing the test results.

6. PROOF OF PRINCIPLE MODEL MOTOR

6.1 Description

The proof of principle (POP) model was built to demonstrate the basic design principles embodied in the axial field D.C. machine. No attempt was made to optimize the design or to scale it to meet specific vehicle performance requirements. For these reasons, the quantitative description of the POP model and its test results are quite brief in this report. The more advanced models are described in greater quantitative detail in later sections.

To facilitate the completion of a POP model, an existing stator from an experimental axial-field D.C. machine was utilized intact, and only a new rotor embodying the ring winding armature concept had to be fabricated. The existing stator, illustrated in Figures 5 and 6 had six poles on each side with flat solid steel pole faces. One end bell supported the outboard commutator housing and pilot bearing, while the other end bell supported the main radial/thrust bearing. The two field pole assemblies were separated by an aluminum barrel.

The new armature was constructed from a 3% silicon-steel tape wound core ring into which slots were machined on each face (see Figure 7). The core inner and outer diameters were made to match those of the existing field pole faces, and the core axial width was made to fit into the existing machine frame. This core ring was then wound helically with a continuous length of an insulated rectangular copper conductor (Figure 8). Slot liners were used, and on the last turn of each coil at the inner diameter of the core a lead was soldered to the main conductor to serve as the lead to the commutator. An armature winding diagram is illustrated in Figure 9. The six pole lap winding had four turns per slot and one slot per bar. Important details of the electrical and electromagnetic design are given in Table 4.

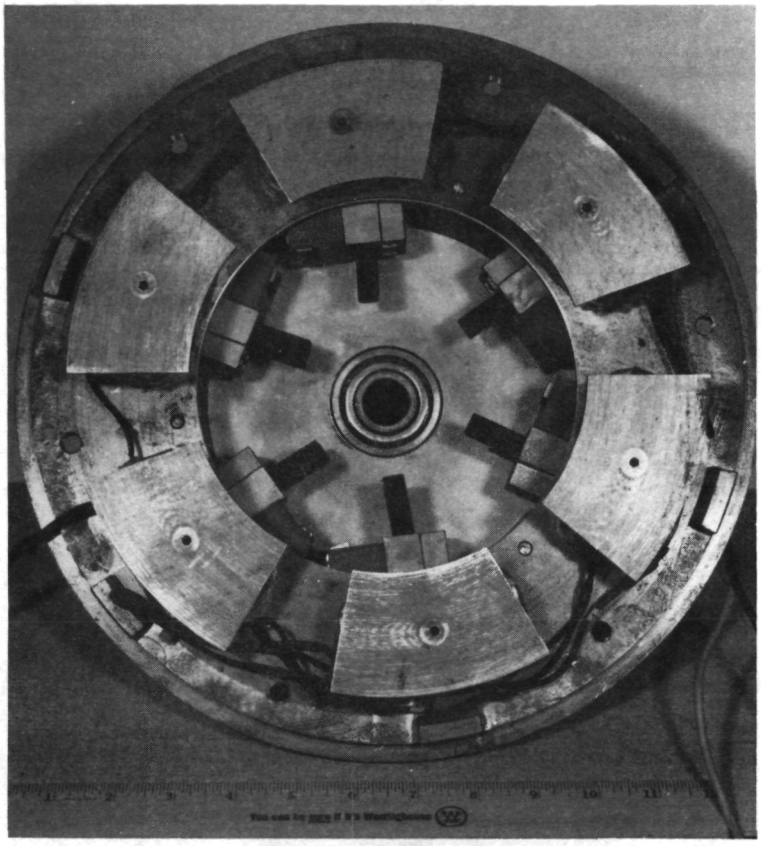

Figure 5 - POP Model Stator - Brush End

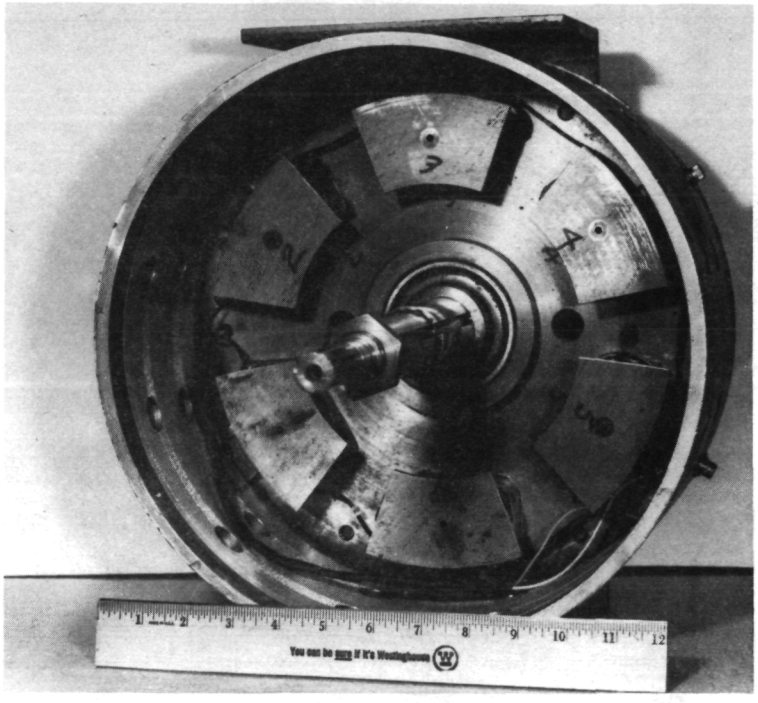

Figure 6 - POP Model Stator - Shaft End

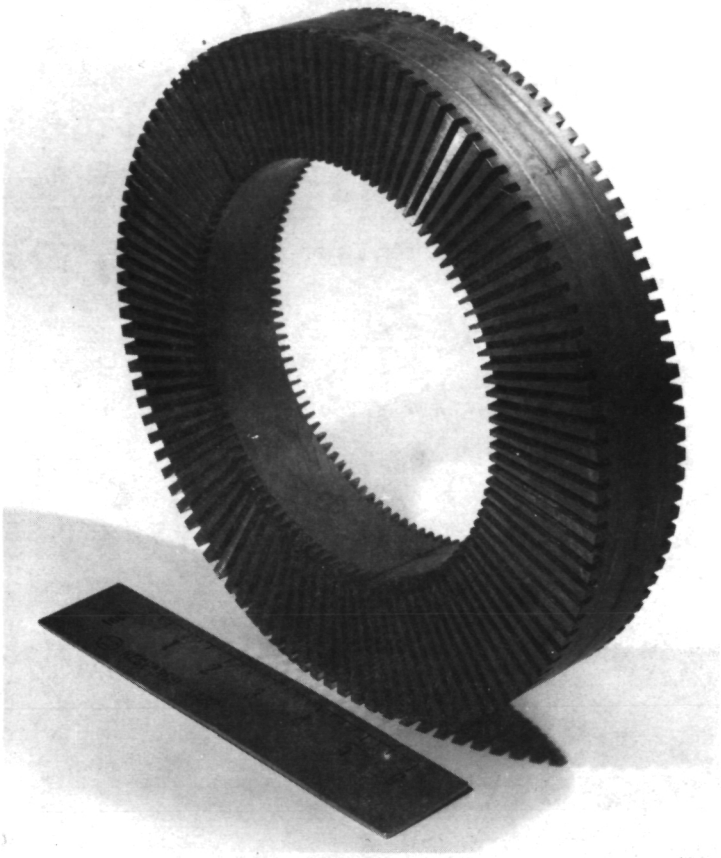

Figure 7 - POP Model Slotted Core Ring

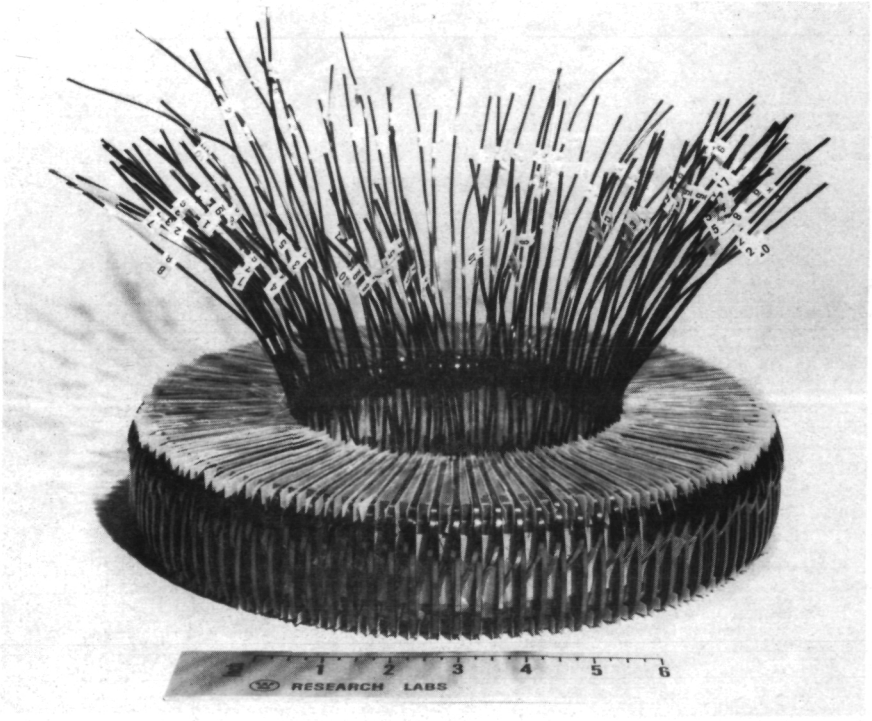

Figure 8 - POP Model Wound Core Assembly

Table 4

DESIGN DATA FOR POP MODEL

General

Nominal Armature Voltage	110 VDC
Rated Armature Current	100 amps
Continuous Rated Power Output	10.0 kw
Base Speed	3600 rpm
Nominal Field Excitation	5 amps @ 85 volts
Poles	6
Slots	108
Bars	108
Turns per Bar	4
Pole Embrace	65%

Dimensions (cm)

Outside Diameter	32.4
Length, excluding shaft	28.1
Rotor Diameter	29.8
Airgap Length	0.15
Core Ring Outside Radius	13.3
Core Ring Inside Radius	8.3
Core Ring Length	5.1
Slot Width	0.32
Slot Depth	0.63
Commutator Diameter	12.0

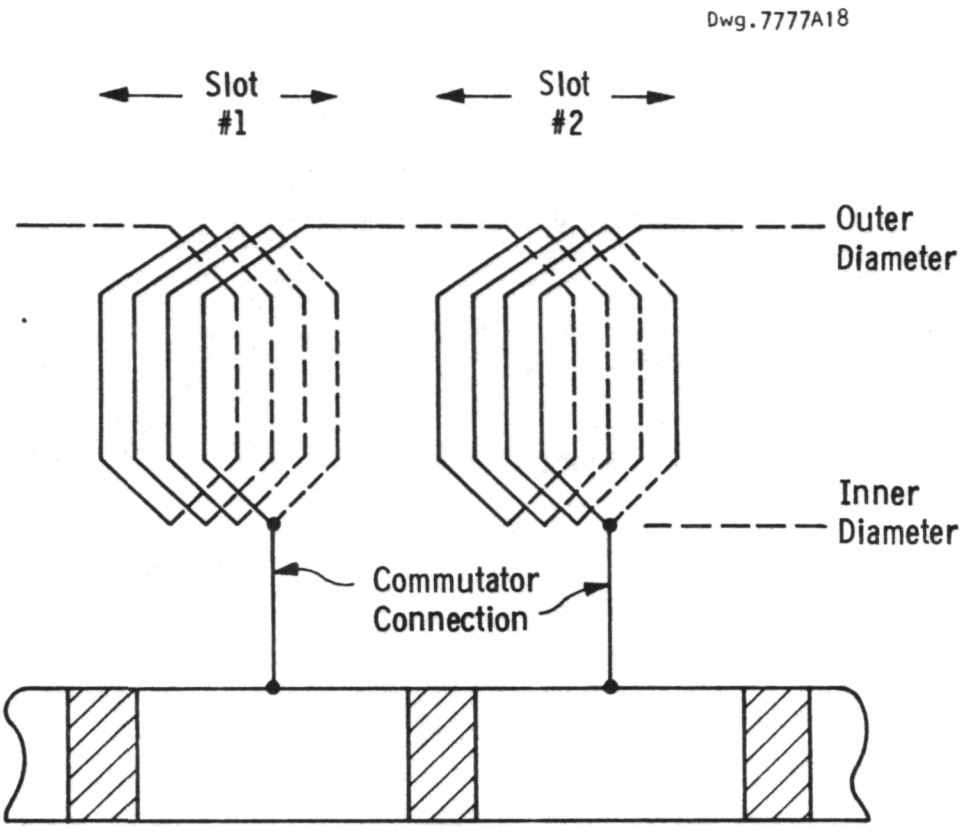

Figure 9 - POP Model Winding Diagram

After completion of the armature winding, the wound core was clamped into a casting fixture with a central hub, and a silica-filled epoxy* was cast onto the inner and outer end-turn regions of the winding. This assembly was then placed on the shaft with the commutator and the individual leads soft-soldered to the risers. As a final step the rotor assembly was placed in a lathe between centers, the commutator turned, and excess epoxy trimmed from the periphery (see Figures 10, 11).

A large annular contact ball-bearing was fixed on the output end of the motor shaft to support any axial load on the rotor due to

*Shell EPON 815 (100 PPHR), Shell Curing Agent Z (20 PPHR), Fused Silica (310 PPHR).

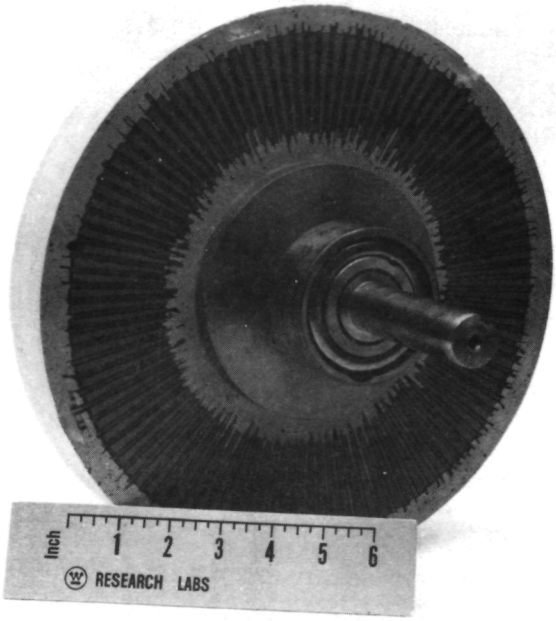

Figure 10 - POP Model Rotor - Shaft End

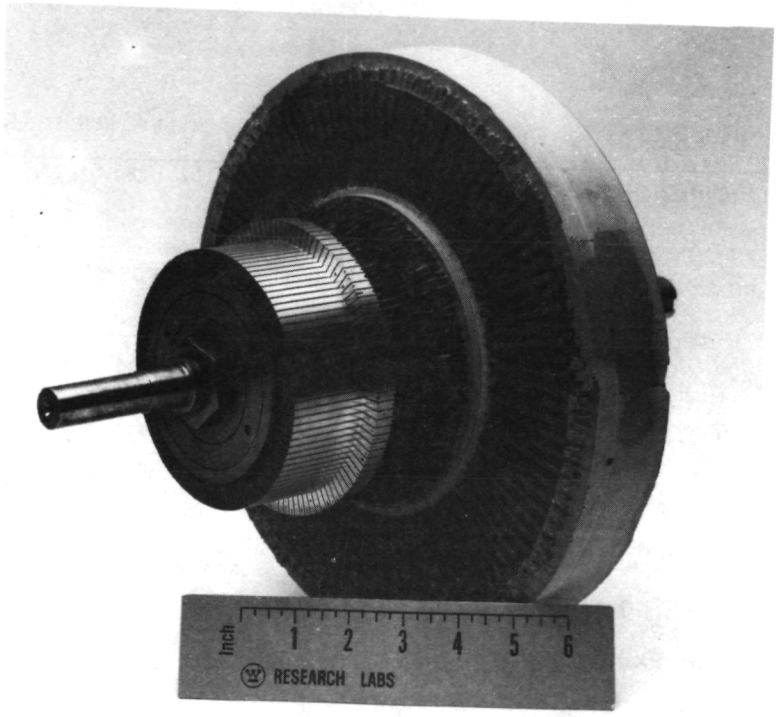

Figure 11 - POP Model Rotor - Commutator End

any non-uniformity of the airgap fluxes (see Figure 12). Shims were used to adjust the axial position of the rotor between the two field pole assemblies to achieve proper force equalization. The other end of the shaft was allowed to float axially in a smaller bearing retained in the commutator housing. The completed POP model was an open-frame naturally-ventilated machine (see Figure 13).

6.2 Test Results

The POP model was tested in the hydraulic absorption dynamometer (see Section 5). Figure 14 illustrates the POP model mounted in the reaction cradle and connected to an auxiliary D.C. motor for measuring no-load losses. Figure 15 illustrates the load tests with the motor connected directly to the hydraulic pump. A summary of the test results is illustrated in Figures 16, 17 and 18.

6.3 Conclusions

The POP model testing was, in general, quite successful. The motor produced a continuous output of 10 kW at 3600 rpm with an overall efficiency of 88%, and was tested at a maximum power of 14.7 kW at 3600 rpm and 84% efficiency. Although we had no thermal instrumentation on the rotor, spot measurements of armature temperature during interrupted steady state tests agreed well with our calculations of armature total thermal conductance.

The major deficiencies pointed out by our experience in building and testing the POP model were:

(1) Machining (grinding) the slots in the armature core was very laborious. We experimented briefly with electrochemical machining of the core slots but had difficulty with process controls. We concluded that an adequate solution to this problem was a key to successful volume production.

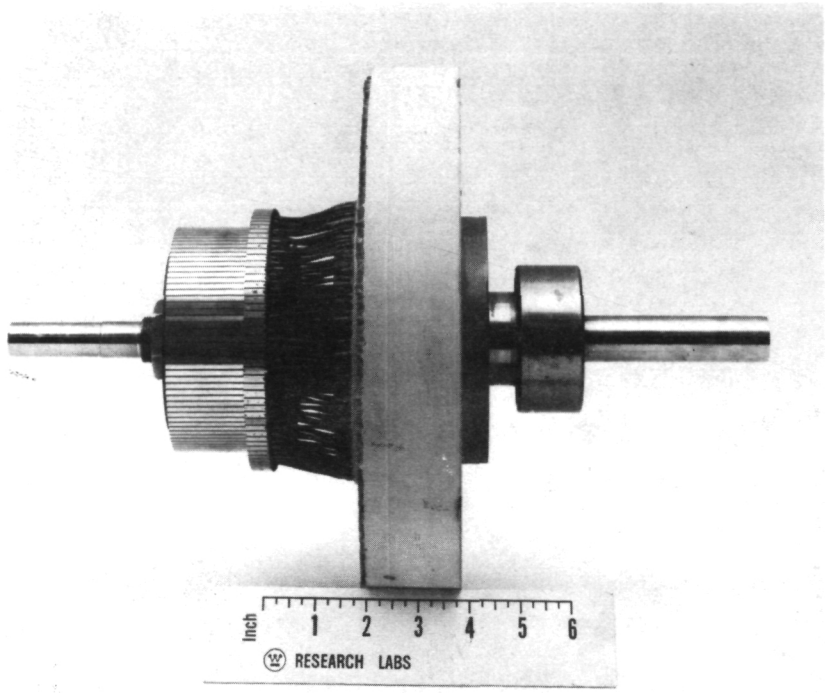

Figure 12 - POP Model Rotor Assembly

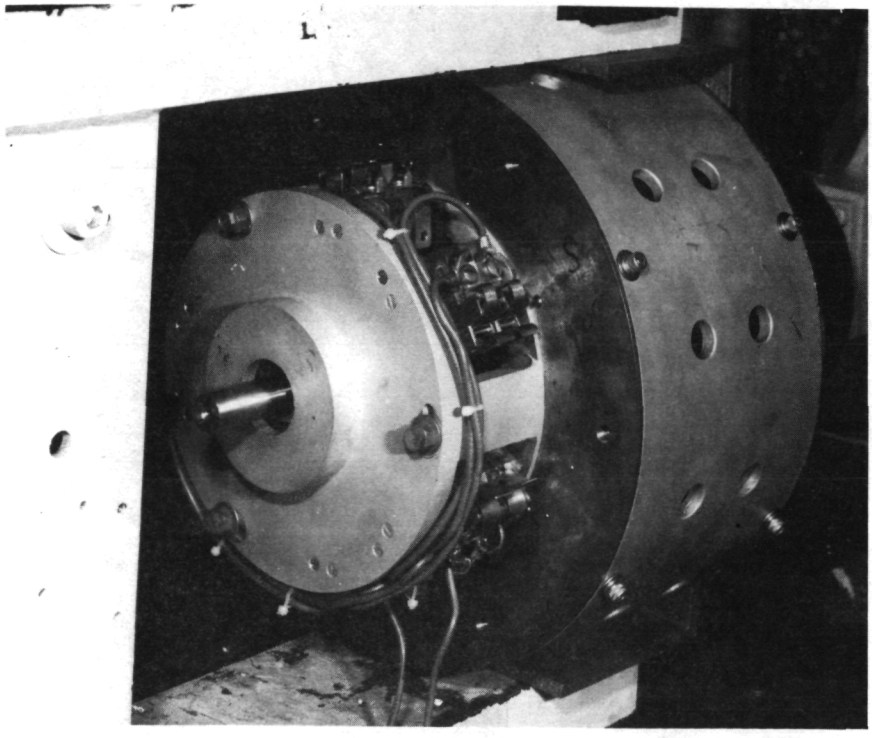

Figure 13 - POP Model Motor Assembly

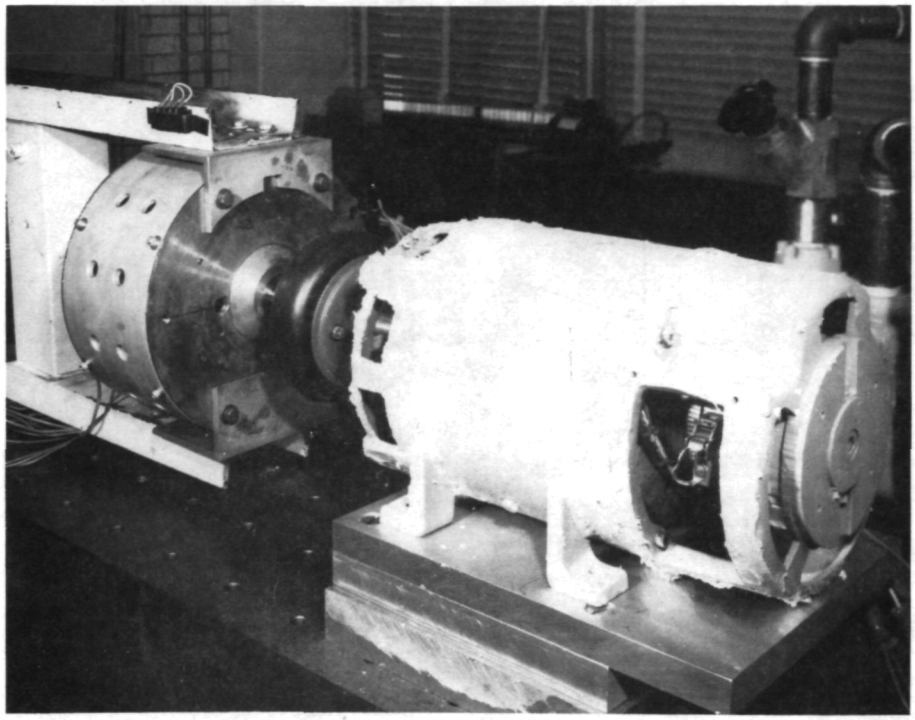

Figure 14 - No-Load Tests of POP Model

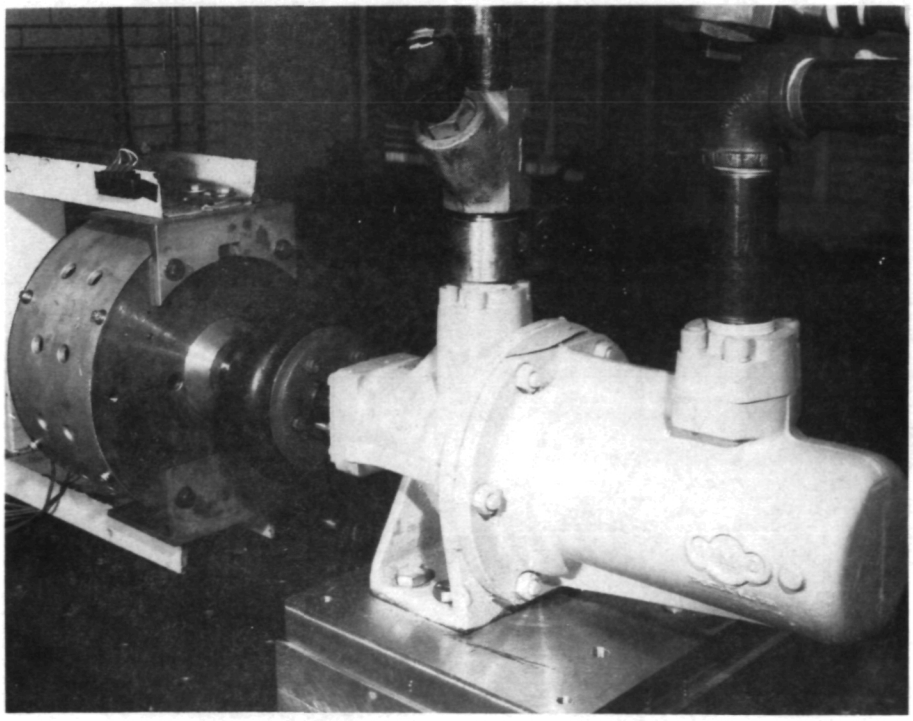

Figure 15 - Load Tests of POP Model

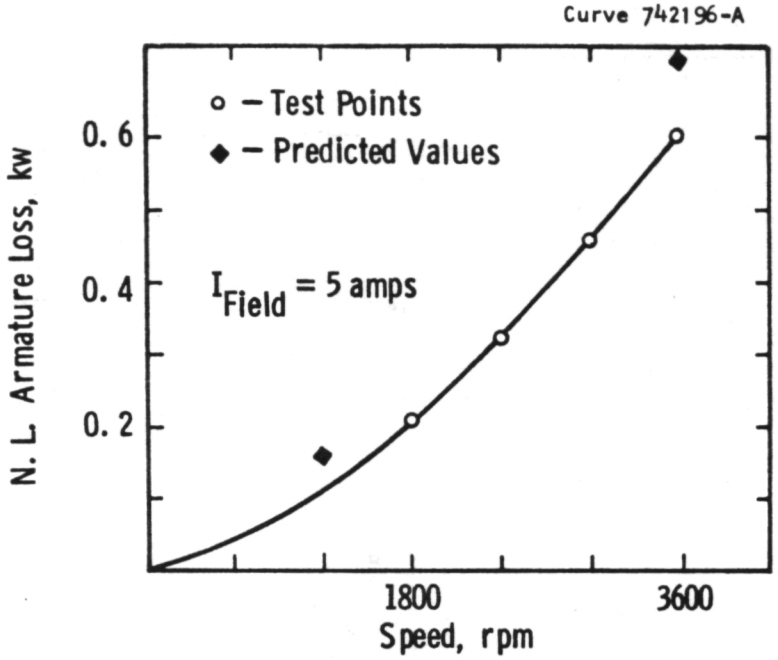

Figure 16 - POP Model N.L. Armature Losses

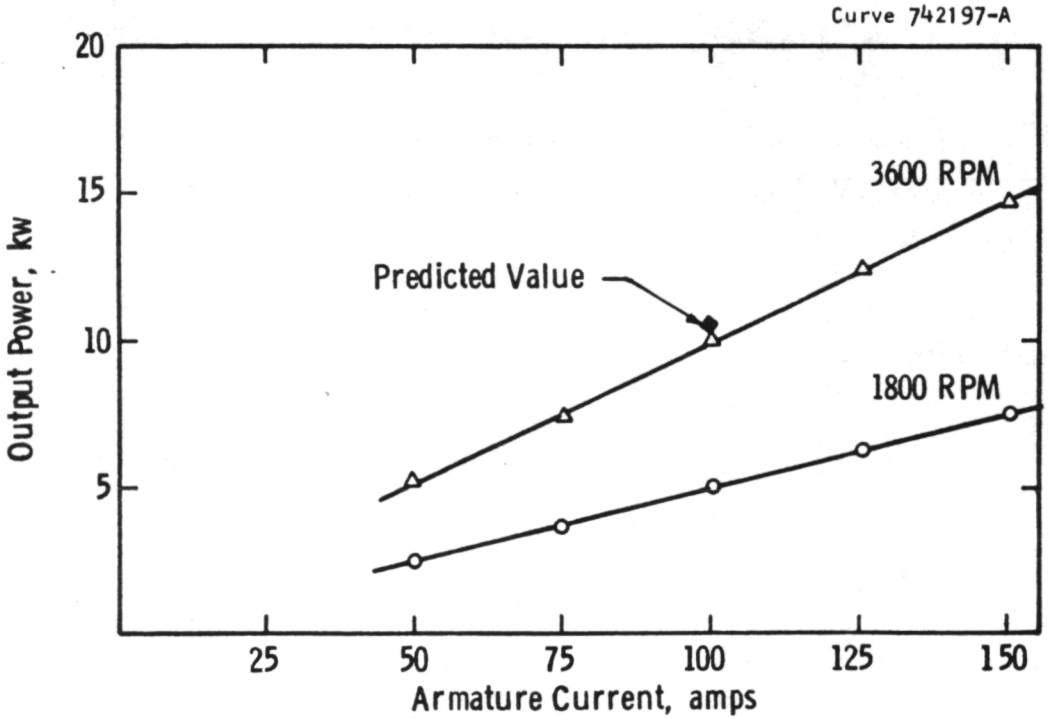

Figure 17 - POP Model Power Output

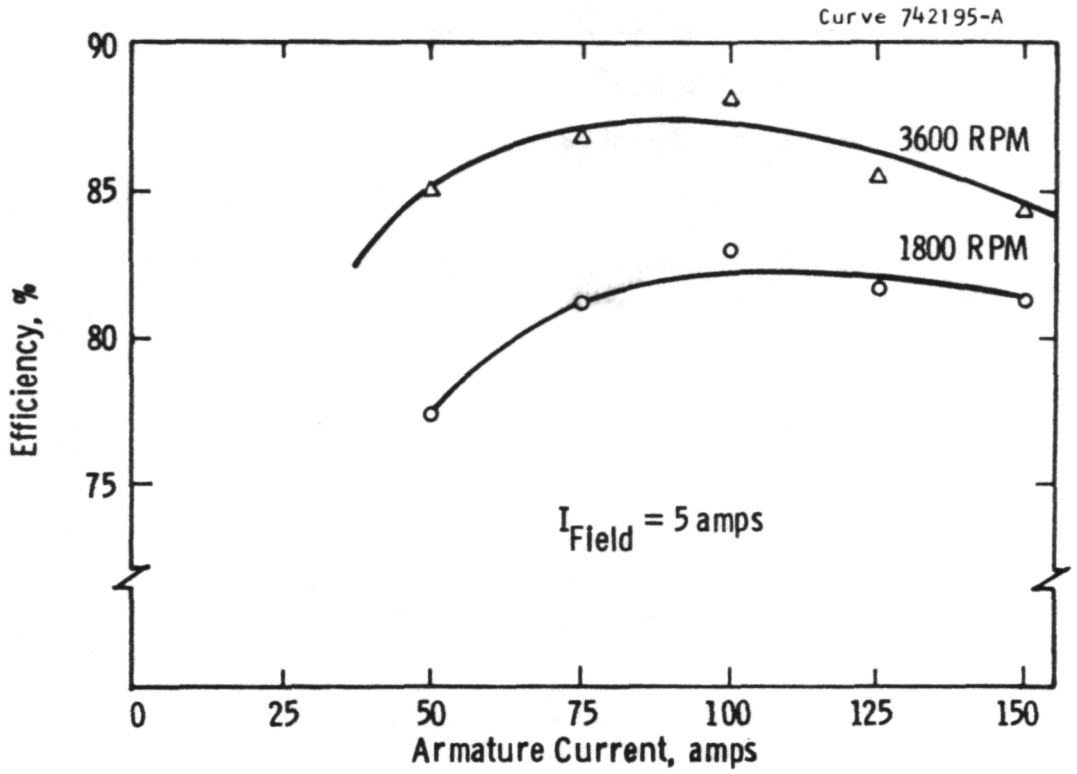

Figure 18 - POP Model Efficiency

(2) Non-uniformities in the axial airgap can cause circulating currents in parallel (lap) windings unless equalizer connections are used on the commutator.

(3) Axial force balance on the rotor is difficult to achieve with small airgaps.

7. FUNCTIONAL MODEL MOTOR

7.1 Description

The Functional Model machine was quite similar in design and construction to the POP model. It used the same basic airgap dimensions; however, larger area field pole bodies and a wider core ring were utilized in order to take full advantage of the flux-carrying capacity of the armature teeth. The iron area in the end bells (yokes) was also increased to handle the additional flux. The voltage rating and electrical loading on the armature were also increased somewhat by increasing the slot depth and the number of turns per slot to six. A summary of the principle design parameters of the functional model are given in Table 5.

The core ring was slotted by grinding the individual slots in the faces using an indexing fixture; the top, inner, and outer corners of the slots were broken manually to avoid sharp edges. The slotted core ring was then epoxy-powder coated by electrostatic spray to obviate the need for individual slot liners (see Figure 19). A new commutator housing was fabricated; the brush gear was supported on an insulated support ring so that the brush area could be closed for purposes of forced ventilation. The main pole faces were laminated by fabricating them from a thin tape wound core held in a hollow steel shell (see Figure 20). Initially the laminations were adhesive bonded in place; later retaining pins were added after a bonding failure occurred. The pole faces were also contoured to achieve a tapered airgap.

The core was wound with six turns per slot of rectangular insulated copper conductor. The toroidal winding was continuous, with commutator leads soldered to the last layer at the inner end turns as with the POP model (Figure 9). The conductor was pre-wrapped on a long "spool" for winding (see Figure 21). Figure 22 shows a close-up of the method by which the last (outer) turn in a filled slot becomes the first (inner) turn in the next slot. The resulting winding had 108 slots and bars, and used a six pole parallel (lap) winding.

Dwg. 4259B99

TABLE 5—FUNCTIONAL MODEL DESIGN PARAMETERS

General	
Base Speed, rpm	2160
Max. Speed, rpm	4800
Rated Output Power, kw	16.9
Peak/Rated Output	1.5
Total Weight, kg	88.5
D-Cycle Efficiency, %	88
Poles	6
Interpoles	0
Slots	108
Bars	108
Turns per Bar	6
Main Pole Enclosure, %	70
Dimensions (cm)	
Outside Diameter	31.2
Length (not incl. Shaft)	24.1
Air Gap Length (min/max)	.075/.150
Core Ring Outside Radius	13.3
Core Ring Inside Radius	8.25
Armature Length	8.83
Slot Width	0.317
Slot Depth	0.825
Commutator Diameter	12.1
Field Poleface Area, Each of 12 (cm^2)	41.3
Armature Winding	
Rated Voltage, volts	180
Rated Current, amps	100
Conductor Size, cm × cm	0.13 × 0.26
Terminal Resistance, ohms	0.028
Amp. Turns per Pole	1800
Field Winding	
Rated Voltage, volts	120
Rated Current, amps	6.0
Wire Size, AWG	17
Turns per Coil	275
Resistance (12 Coils), ohms	20.0
Amp Turns per Pole	1650
Flux Densities (Tesla)	
Main Pole Air Gap, AWG	1.03
Core Ring, max.	1.50
Armature Teeth, max.	1.80
Pole Body	1.70
Yoke	1.60
Brush Parameters	
Contact Drop, volts	1.1
Current Density, amp/cm^2	15.5
Brush Pressure, $10^3 N/m^2$	20.7
Friction Coefficient	0.15
Max. Sliding Velocity, m/sec	30.3
Brush Arc, Rad	0.16

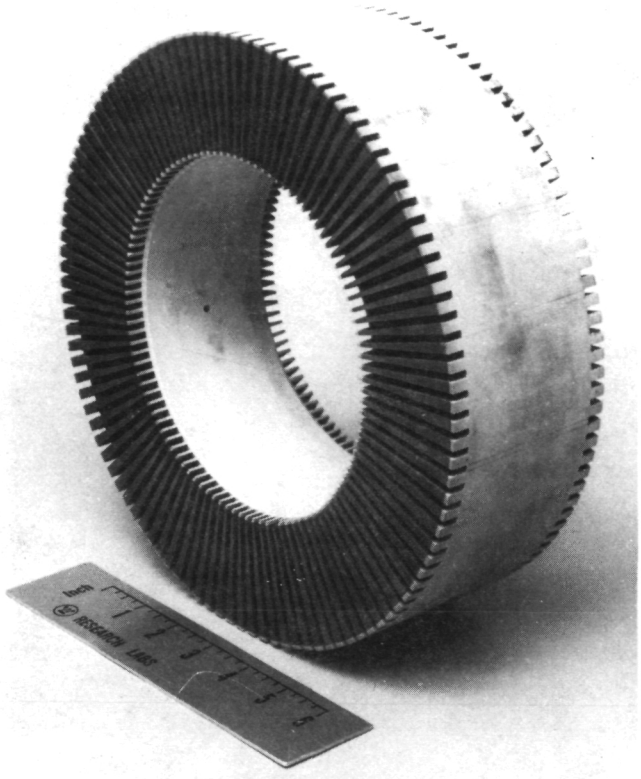

Figure 19 - Functional Model Slotted Core

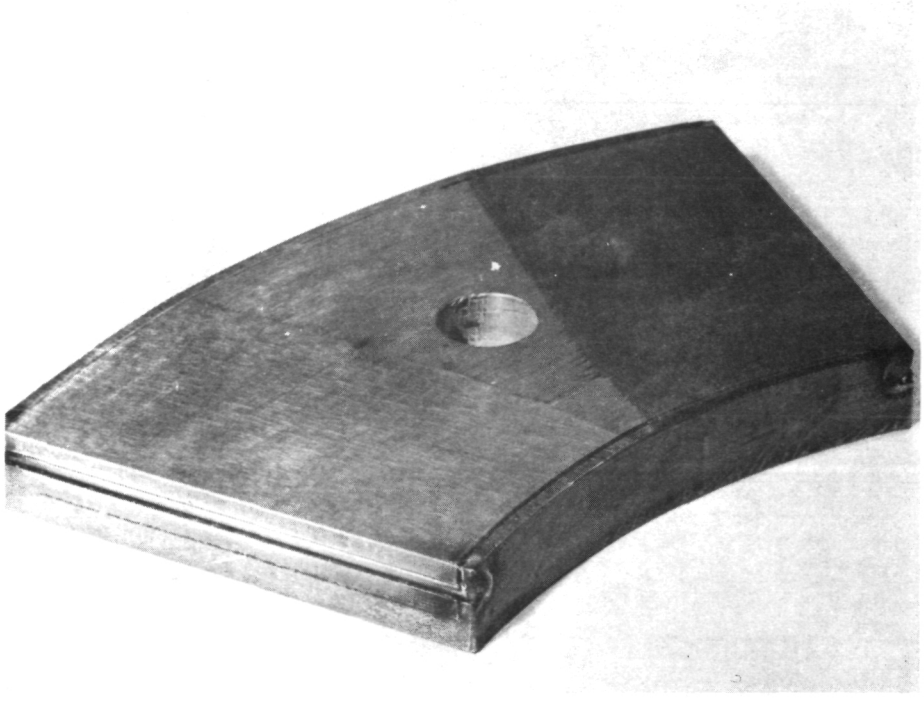

Figure 20 - Functional Model Laminated Pole Face

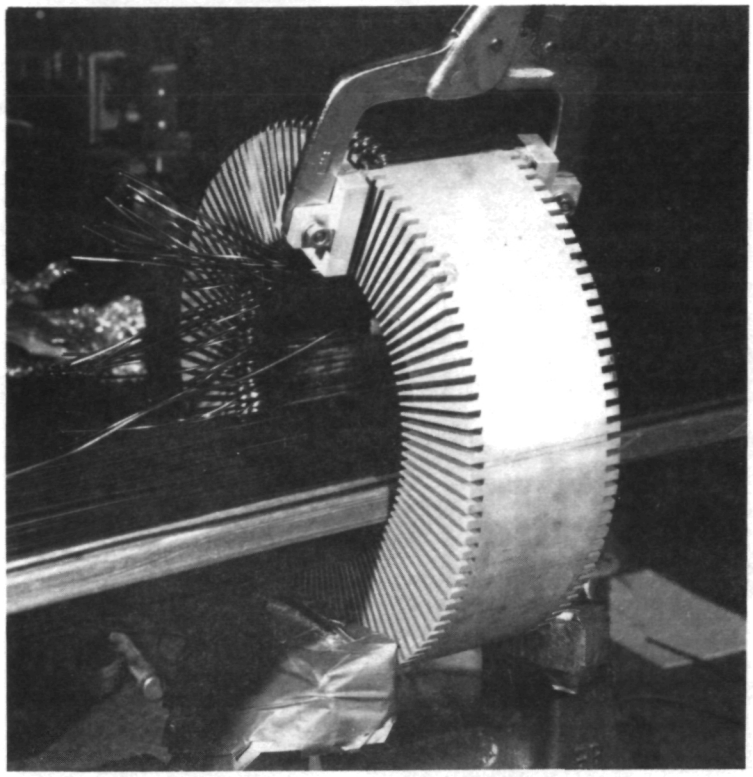

Figure 21 - Winding the Functional Model Armature

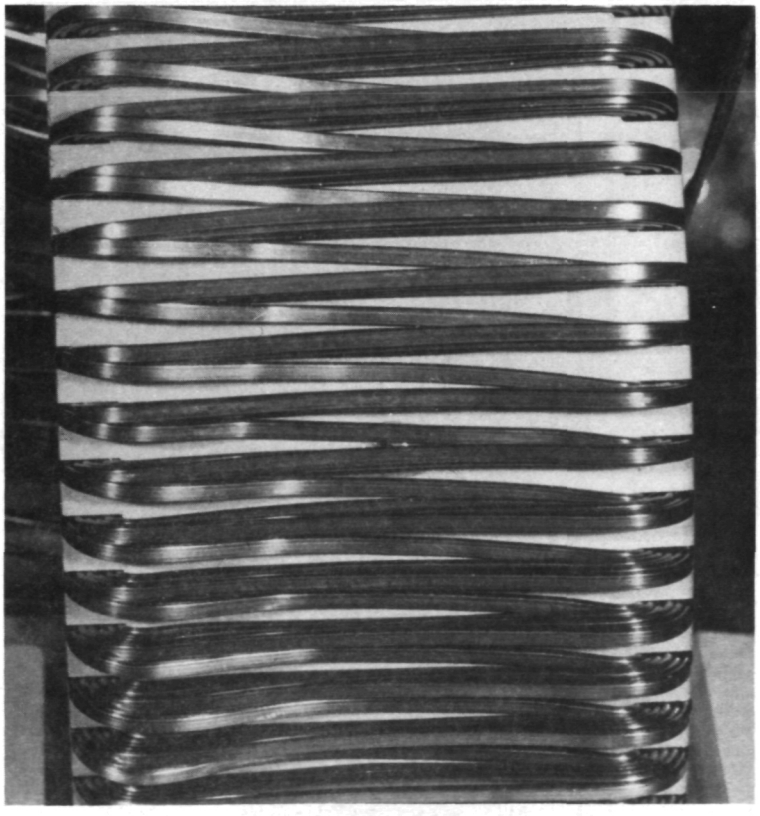

Figure 22 - Crossover of Outer End-Turns-Functional Model

7.2 Test Results

A summary of the test results obtained on the functional model are given in Table 6 and Figures 23 thru 32. The major performance goals for continuous motoring were met. We were, however, unable to perform the two-minute 25 kw generation test at 2400 rpm because we had no suitable drive motor on hand. It was reasoned that the five-minute, 24 kw motoring test at 2800 rpm was actually a more severe test for a D.C. motor with no brush lead. The motoring performance of the machine was quite satisfactory in most respects. The outputs and efficiencies measured agreed quite well with the predicted results, as seen by the curves, and we developed considerable confidence in our ability to predict the losses and performance in such a motor with our computer model.

Thermally the results were also satisfactory. The armature acted as a nearly isothermal mass as predicted, with less than a 5°C temperature difference between the core and the highest measured temperature. The armature temperature rises above ambient observed (post steady state) were 48°C on the D-cycle equivalent test (vs. 40°C predicted) and 68°C on the 5 min. uphill climb simulation (vs. 65°C predicted). The armature had a 20 min. time constant on thermal transients.

The temperature rise of the armature was correlated with its heat dissipation rates (losses) and an overall thermal conductance calculated as a function of rotor speed. The agreement between the experimental results and the predicted results was good as illustrated in Figure 33.

7.3 Conclusions

The principal deficiency in the performance of the functional model was marginal commutation. Sparking under overload conditions created excessive commutator temperatures which limited the duration of the tests. The commutator leads had been soft-soldered to the risers, and as the commutator temperature approached 150°C, the soldered

Table 6

FUNCTIONAL MODEL TEST DATA SUMMARY

MOTOR OUTPUT			MOTOR INPUTS									
			Armature			Field					Temperatures (°C)	
Speed (RPM)	Torque (N·m)	Power (KW)	RMS Volts	RMS Amps	KW	Volts	Amps	KW	Total KW	Eff. (%)	Arm.	Comm.
600	35.3	2.22	55.5	50.6	2.75	115	6.0	0.69	3.44	64.5	57°	63
"	53.9	3.40	56.7	76.2	4.28	115	6.0	0.69	4.98	68.3	66	76
"	72.1	4.53	58.0	100.0	5.77	115	6.0	0.69	6.46	70.1	80	94
1200	34.2	4.29	92.1	50.1	4.51	113	6.0	0.68	5.19	82.7	56°	66
"	52.9	6.65	94.2	74.7	6.96	113	6.0	0.68	7.64	87.0	68	84
"	72.3	9.08	96.2	100.7	9.62	117	6.0	0.70	10.32	88.0	88	113
"	83.4	10.48	88.6	126.2	11.11	113	6.0	0.68	11.79	88.8	-	-
"	97.6	12.27	91.2	149.1*	13.42	114	6.0	0.68	14.10	87.0	-	-
1800	33.8	6.36	137.5	50.0	6.76	112	6.0	0.67	7.43	85.6	61	71
"	53.3	10.04	139.2	75.8	10.48	115	6.0	0.69	11.17	89.9	76	95
"	71.5	13.47	138.2	100.9*	13.92	117	6.0	0.70	14.61	92.2	91	126*
"	80.7	15.21	131.0	124.6*	16.18	115	6.0	0.69	16.87	90.1	-	-
"	96.4	18.33	133.3	150.0*	19.69	115	6.0	0.69	20.38	89.9	-	-
2400	31.3	7.87	169.1	50.0	8.42	93	5.1	0.48	8.90	88.4	67	91
"	49.2	12.37	174.1	74.8	12.97	106	5.7	0.60	13.57	91.1	76	89
"	66.2	16.63	180.6	96.6*	17.48	107	5.75	0.61	18.06	92.1	81	123*
"	81.4	20.45	172.9	125.9*	21.55	112.5	6.0	0.68	22.23	92.0	-	-
"	97.0	24.37	176.4	147.0*	26.00	112.5	6.0	0.68	26.68	91.3	-	-
3000	26.0	8.18	177.8	50.7	8.96	87.5	5.0	0.44	9.40	87.0	63	86
"	39.7	12.48	174.6	75.3	13.10	78	4.50	0.35	13.45	92.8	71	83
"	52.0	16.27	171.4	99.8*	17.10	76	4.4	0.33	17.43	93.4	86	122*
"	71.9	22.58	168	150.0	25.25	75	4.4	0.33	25.58	88.3	-	-
3600	13.4	5.06	177.8	33.3	5.93	52	3.25	0.17	6.10	82.9	54	68
"	21.3	8.03	177.2	50.5	8.89	66	4.0	0.26	9.15	87.7	63	77
"	31.3	11.81	174.0	74.5	12.90	59	3.6	0.21	13.11	90.1	64	86
"	43.4	16.36	175.0	100.8	17.60	82	5.0	0.41	18.01	90.8	-	-
4200	18.2	7.99	177.3	50.1	8.81	50	3.25	0.16	8.97	89.1	58	69
"	26.4	11.63	172.3	75.3	12.92	45	2.9	0.13	13.05	89.1	73	110*
"	36.6	16.10	174.0	101.6	17.68	57	3.5	0.20	17.88	90.0	-	-

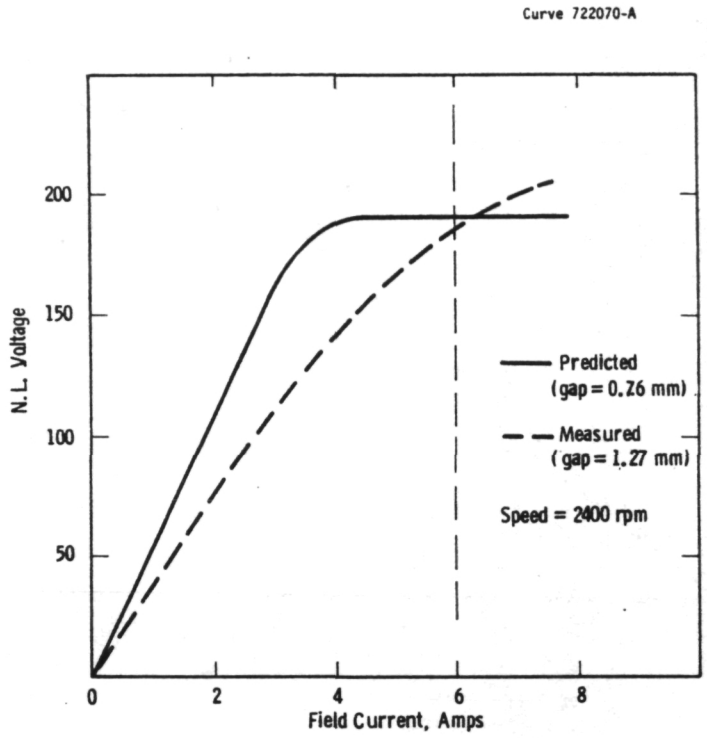

Figure 23 - Functional Model N.L. Saturation Curve

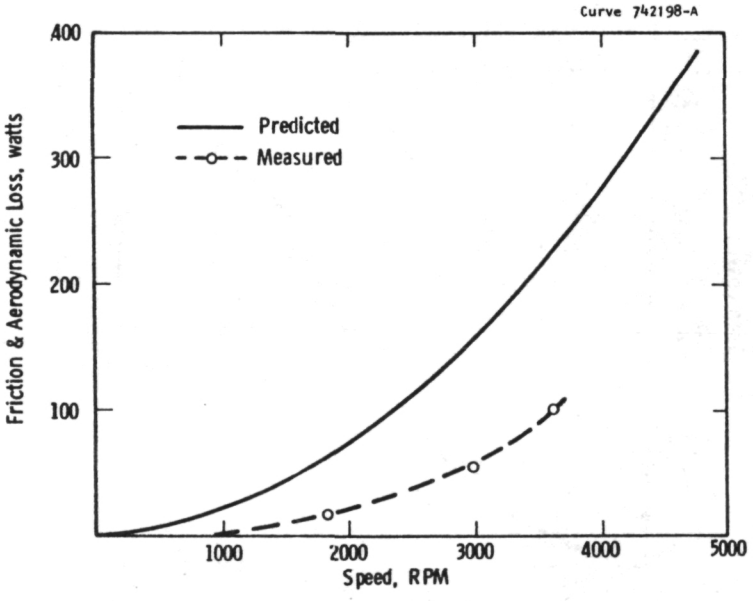

Figure 24 - Functional Model Friction and Aerodynamic Losses

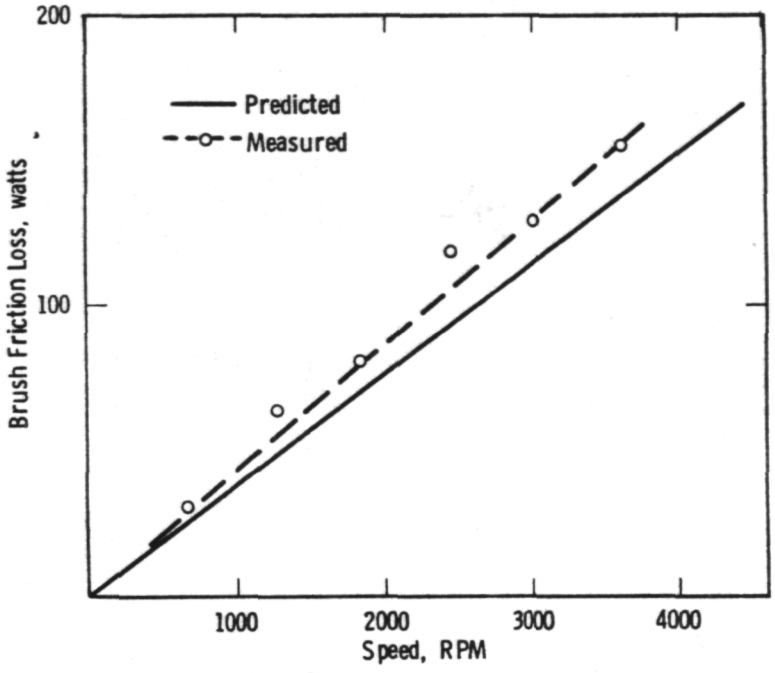

Figure 25 - Functional Model Brush Friction Losses

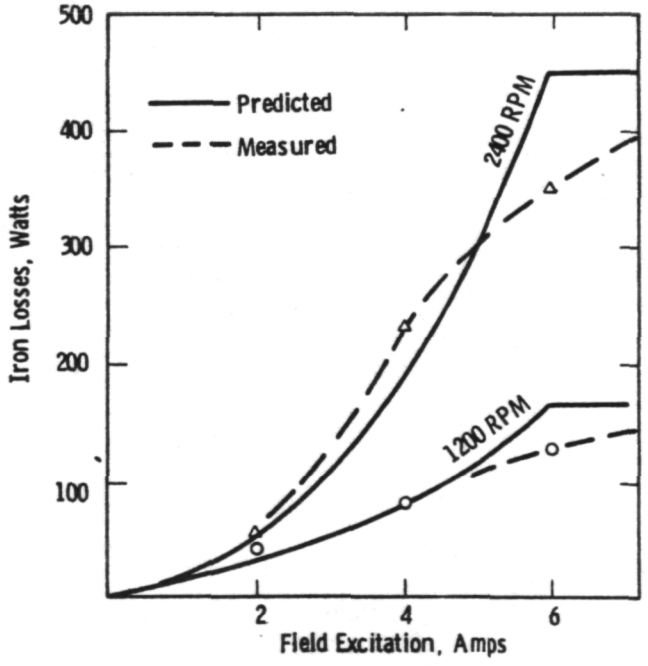

Figure 26 - Functional Model Iron Losses

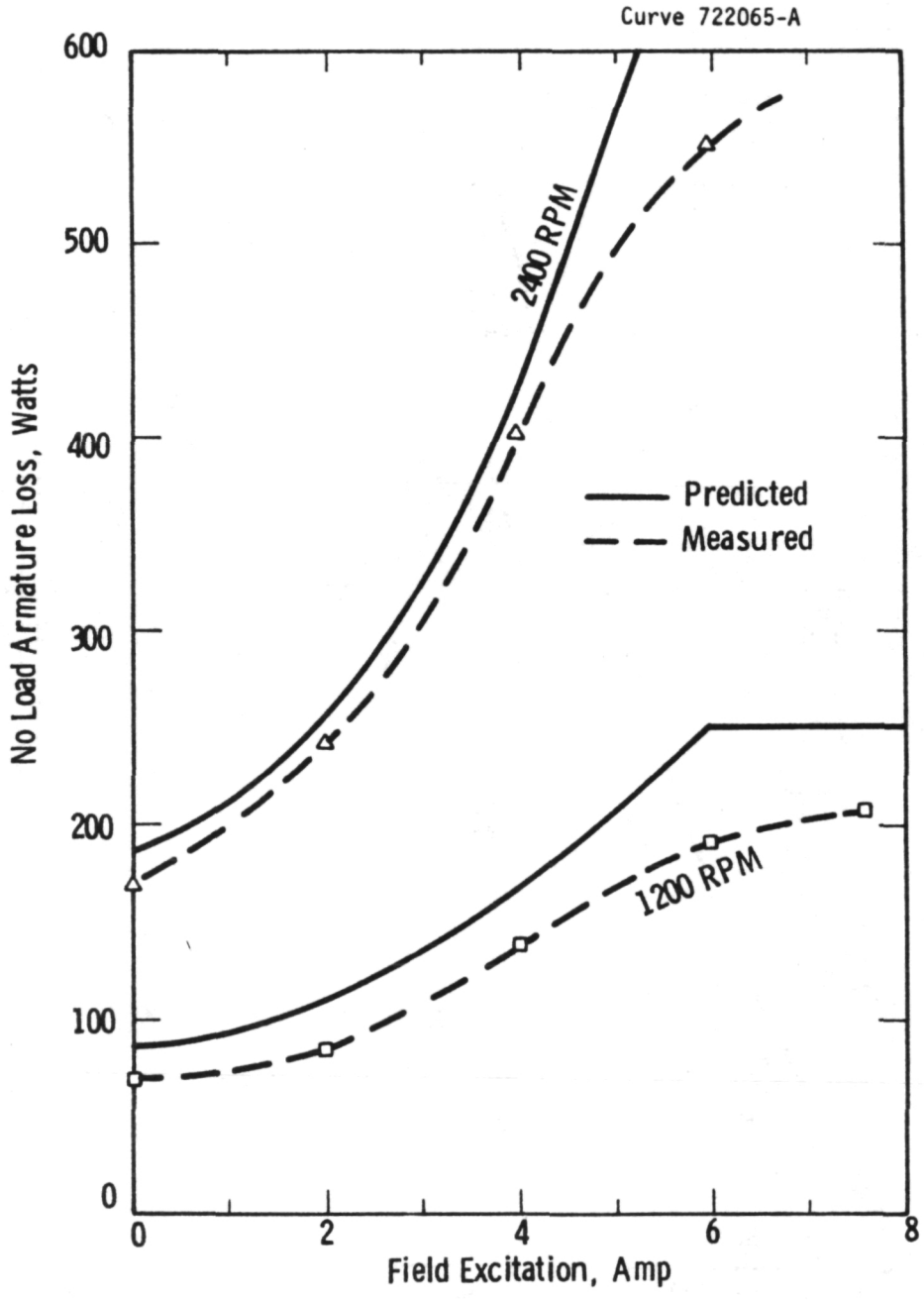

Figure 27 - Functional Model N.L. Armature Losses vs Field Current

Curve 722071-A

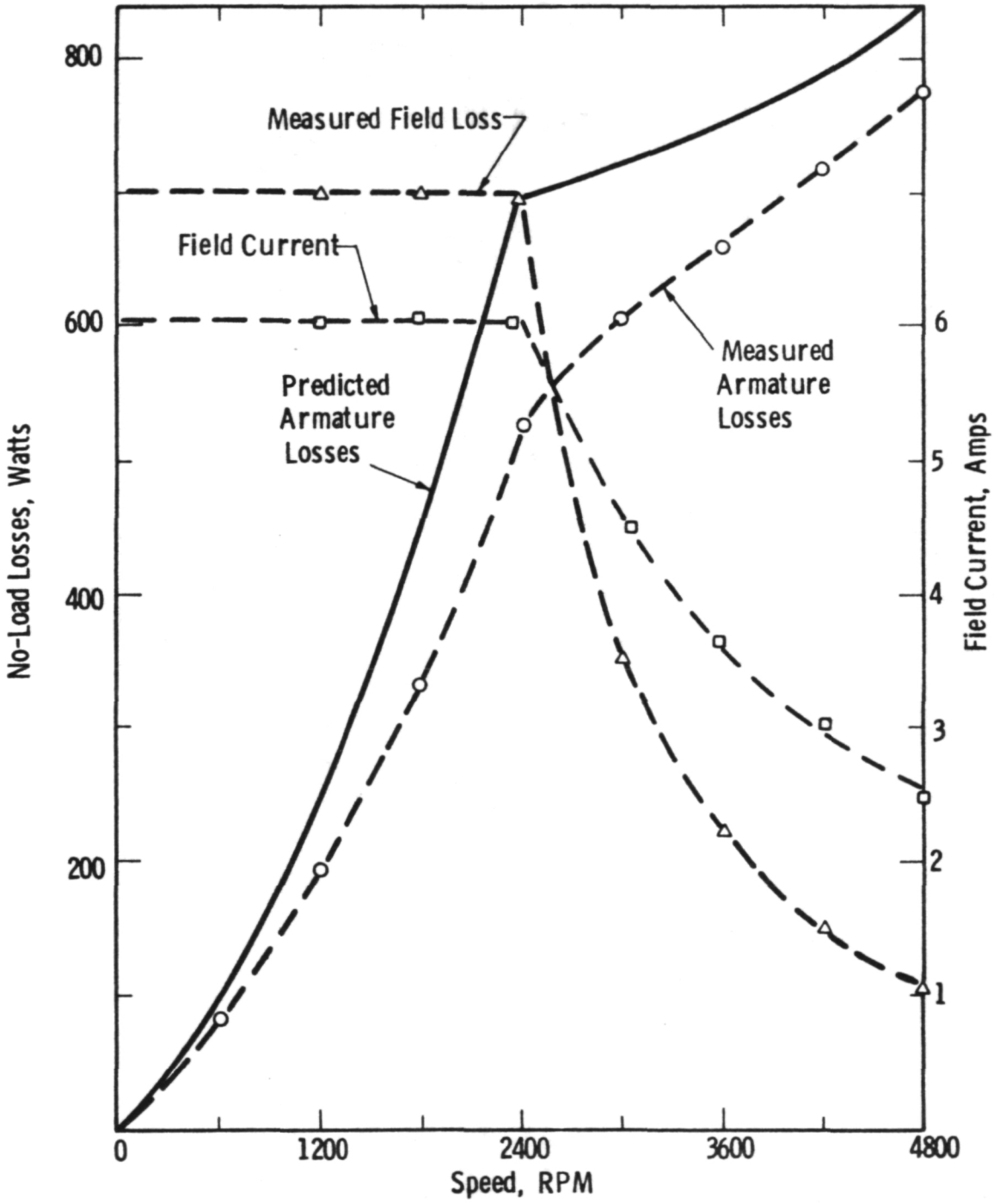

Figure 28 - Functional Model N.L. Losses vs Speed

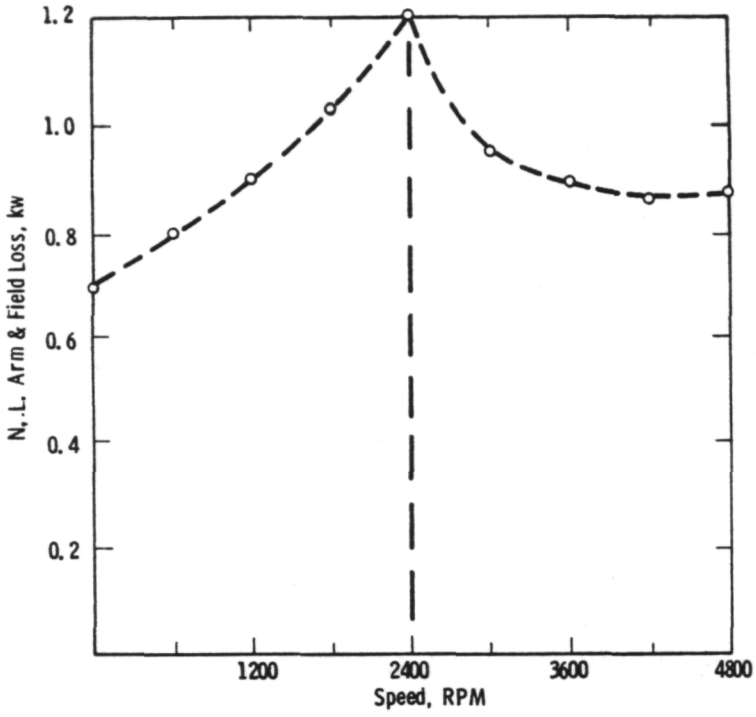

Figure 29 - Functional Model Total N.L. Losses vs Speed

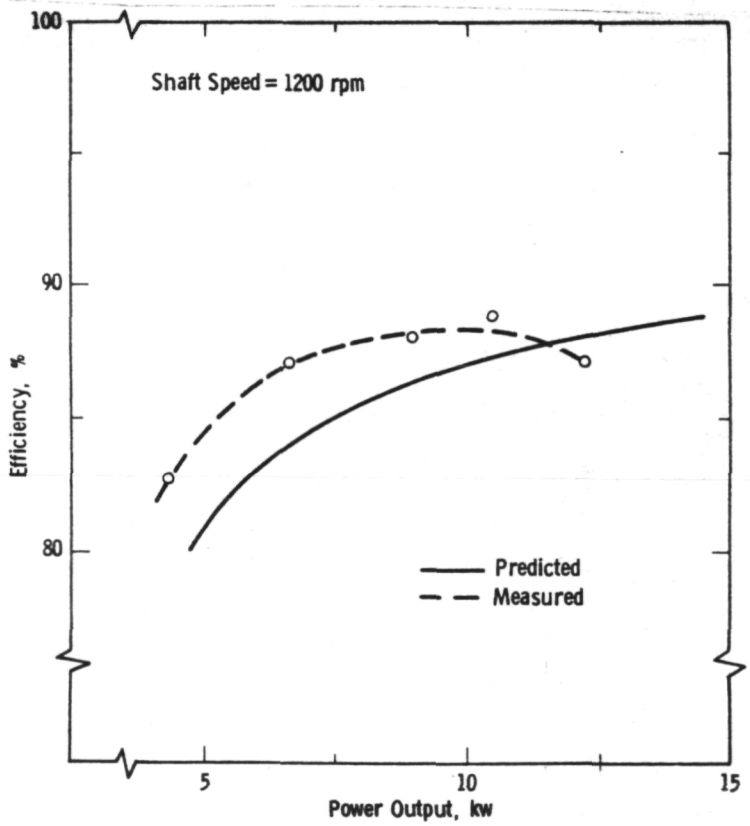

Figure 30 - Functional Model Efficiency at 1200 RPM

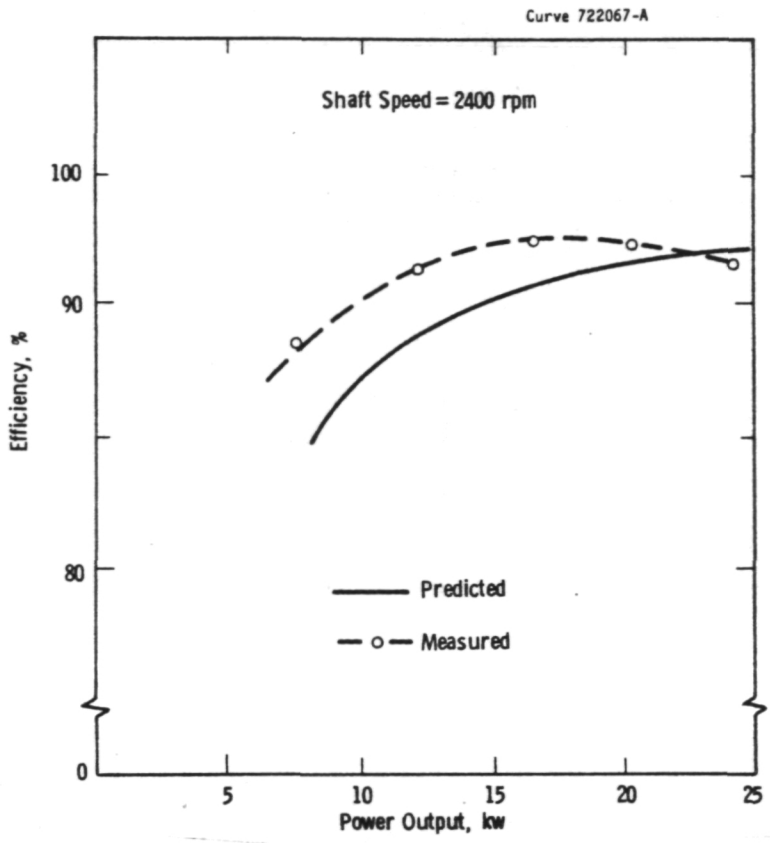

Figure 31 - Functional Model Efficiency at 2400 RPM

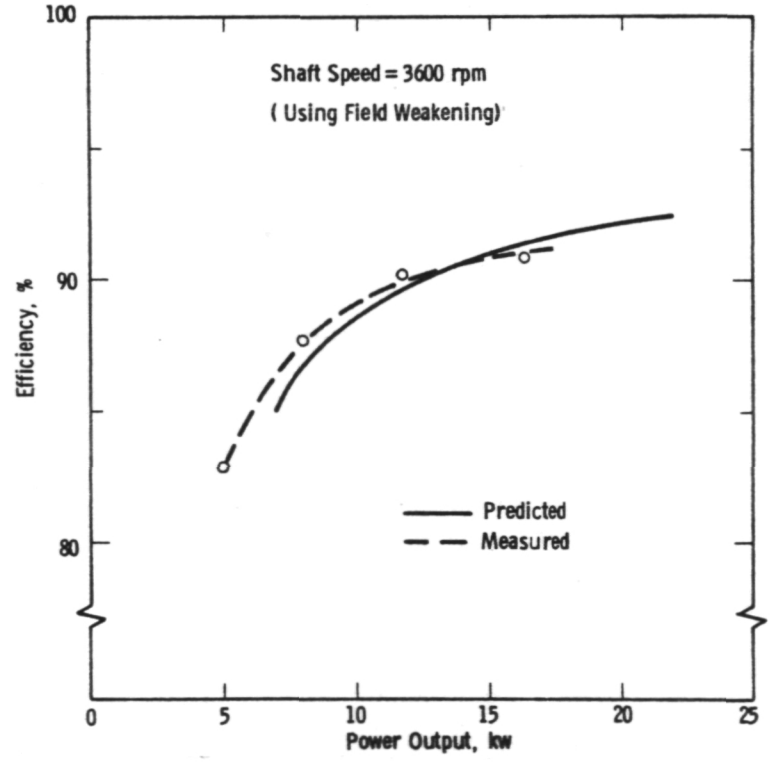

Figure 32 - Functional Model Efficiency at 3600 RPM

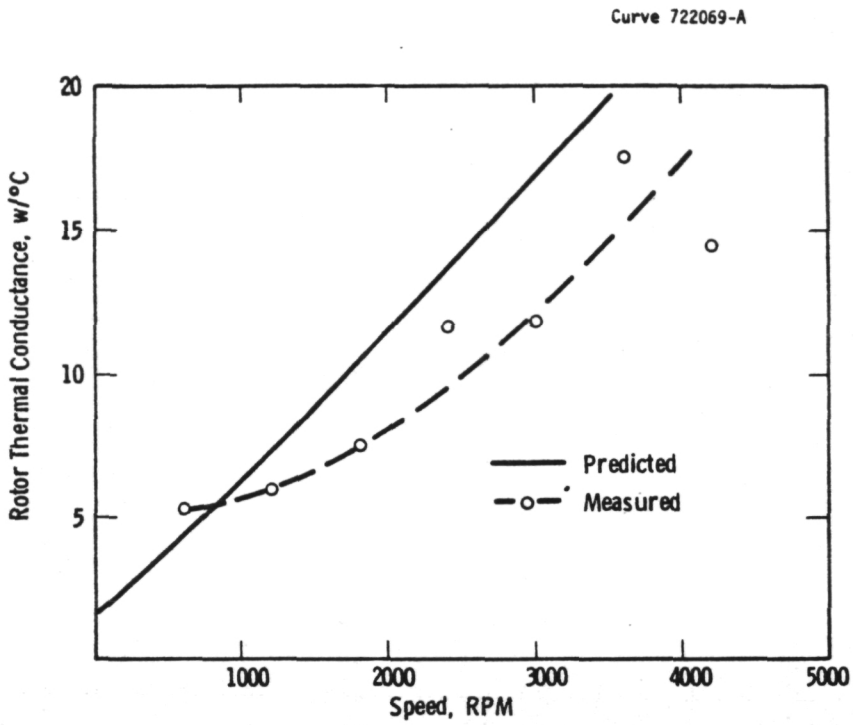

Figure 33 - Functional Model Rotor Thermal Conductance

connections softened and started to "throw" solder. Although we were able to complete the required overload tests without damage, commutator overheating was clearly the weak link in this machine's performance.

A comparison of the functional model of the Westinghouse Axial Field D.C. Motor to the current state-of-the-art is illustrated in Table 7, which compares it to the D.C. motor developed by General Electric for the Electric Test Vehicle (ETV-1). The two machines are quite similar in size, weight and full-load efficiency. The major performance difference appears to be that the axial field motor maintains its efficiency over a much broader operating range, and therefore attains (in computer simulations) a higher cycle efficiency, which results in a significantly lower "adjusted" weight (after battery weight penalty). Since these cycle efficiencies are predicted, not measured, and come from entirely different computer simulation programs, it is not clear how much reliance can be placed upon this cycle efficiency comparison.

Table 7

COMPARISON OF FUNCTIONAL MODEL TO ETV-1 MOTOR

	Axial Field	ETV-1
H.P. Cont.	22	20
H.P. Max.	35	45
Base/Max. Speed (rpm)	2400/4800	2500/5000
F.L. Efficiency, %	92	91
Cycle Efficiency, %	88	81
Compoles	No	Yes
Weight, kg (lbs.)	88.5 (195)	98.5 (217)
Armature Inertia, kgm^2 (in·lb)	1.74 (8·5)	0.45 (2·2)

*Adjusted Weight, Lbs.

Another major difference between the two motors is in the rotor inertia, the inertia of the Axial Field Machine being 3 to 4 times higher than the ETV-1. The importance of rotor inertia depends upon the type of transmission utilized. With a direct reduction drive (or a continuously variable transmission) rotor inertia is of relatively little importance. But with a shifting transmission, high rotor inertia can be a significant disadvantage. The implications of motor rotor inertia are discussed more fully in Appendix C.

The functional model of axial field D.C. motor was judged to have demonstrated sufficient technical merit to proceed into Phase II of the contract. However, because the axial field machine incorporates a number of new manufacturing technologies with certain associated risks, and because of advances demonstrated in competing motor technologies, it was concluded that the engineering model must demonstrate a significant reduction in weight to be a viable option for advanced electric vehicles. Therefore, a design study was initiated to investigate methods of

achieving significant weight reduction. The result of this investigation was that to achieve a significant weight reduction, the motor must incorporate commutating poles (interpoles) to permit both higher armature electrical loading and higher speeds.

8. ENGINEERING MODEL MOTOR

8.1 Objectives

The design objective of the engineering model was to address two major concerns, weight and manufacturability. The major functional limitations of the machines had been identified as excess weight and marginal commutation under overload conditions. Our design goal was to reduce the motor dead weight to approximately 45 k g. (100 lbs.), while improving commutation and with minimal sacrifice in efficiency. In the area of manufacturability, we felt that the new design must also address some concerns we had regarding core slotting, core winding and commutator interconnection, and airgap uniformity.

8.2 Design Modifications

The major design modification that was utilized in the engineering model was the inclusion of commutating poles (interpoles). Historically, the advent of interpoles permitted a significant size and weight reduction in D.C. motors by permitting higher armature electrical loadings and higher speeds. We found that our functional motor had three times more active iron than copper, and that by doubling the electrical loading (copper) and halving the magnetic loading (iron) we could achieve an 18 k g. (40 pound) weight reduction alone. This change, however, increased the commutation reaction voltage (already marginal) and required the use of interpoles. Once interpoles were included, however, we found that we could make other desirable design changes, including increased speed (to reduce weight), and wider and deeper slots to improve manufacturability. It seems clear that the addition of interpoles to the machine design was a desirable step, even though it involved some fundamental design changes rather than just an iteration toward manufacturability. A comparison of the principal design parameters is given in Table 8.

Table 8

COMPARISON OF FUNCTIONAL AND ENGINEERING MODELS

	Functional Model	Engineering Model
Base Speed, rpm	2400	3000
Max. Speed, rpm	4800	7200
Rotor Diameter, cm	30	25.4
Rotor Length, cm	7.92	9.65
Rotor Inertia, kg m^2	1.74	1.12
Total No-Load Flux, weber**	0.046	0.023
Armature Amp-Turns	10,800	12,960
Poles	6	4
Interpoles	0	4
Slots	108	36
Slot Depth, cm	0.82	1.77
Slot Width, cm	0.32	0.65
Commutator Diameter, cm	12.1	8.9
Max. Comm. Peripheral Speed, m/sec	30.3	33.5
Terminal Voltage	180	114
Full Load Current, amps	100	120
Rated Power Output, kw	16.9	13.2
Peak/Rated Output	1.5	2.0
Armature Thermal T.C., min.	20	18
Armature Temp-Rise, °C	48	70
D-Cycle Efficiency, %	88	88
Motor Weight, kg	89	47
Adjusted Weight,* kg	155	113

*See Section 4.5 for definition.

**1 weber = 10^8 Maxwells = 10^8 lines

8.3 Description of Engineering Model

The design of the engineering model represents the evolution of a series of computer design iterations in which we attempted to optimize the motor adjusted weight, and thus strike a balance between weight and efficiency. The principle design parameters which resulted from the computer design are given in Table 9. Several of the design changes we made actually were counterproductive to motor weight and performance, but were adopted because of overriding system or manufacturability considerations. The selection of a battery voltage of 120 VDC, for example, was driven by battery optimization considerations, and was in fact deleterious to the required brush size and associated brush losses. The reduced number of slots (from 108 to 36) was dictated by eventual manufacturability considerations, although it increased magnetic losses and commutation reactance voltage.

The engineering model is a four pole machine with a base speed of 3000 rpm at full load and rated full field excitation. With field forcing (200% field excitation) and at a maximum armature current of 240 amps (200% f.l.), the transition to field control actually occurs at approximately 1700 rpm, partially because of battery voltage drop. The motor has a full set of interpoles (4), but they are arranged on one side only (commutator side). This facilitates interconnection, but results in a small axial force imbalance on the rotor which is variable in magnitude (with armature current). The rotor diameter is reduced from 30 cm (12.0 inches) to 25.5 cm (10.0 inches). The overall weight is reduced from 89 kg (195 lbs.) to 47 kg (104 lbs.). The predicted D-cycle efficiency is unchanged @ 88%. Thus the adjusted weight is reduced by about 42 kg (93 lbs.) compared to the functional model.

Dwg. 4260B00

TABLE 9—ENGINEERING MODEL DESIGN PARAMETERS

General	
Base Speed, rpm	3000
Max. Speed, rpm	7200
Rated Output Power, kw	13.2
Peak/Rated Output	2.0
Total Weight, kg	47
D-Cycle Efficiency, %	88
Poles (per Side)	4
Interpoles (one Side)	4
Slots	36
Bars	72
Turns per Bar	6
Dimensions (cm)	
Outside Diameter (including fins)	33
Motor Length (excl. Shaft)	33
Core Ring Outside Radius	11.4
Core Ring Inside Radius	7.6
Armature Length	7.9
Slot Width	0.65
Slot Depth	1.77
Commutator Diameter	8.9
Main Pole Air Gap (min/max)	0.07/0.15
Interpole Air Gap (min/max)	0.15/0.40
Main Poleface Area Each of 8 (cm^2)	45.1
Interpole Poleface Area Each of 4 (cm^2)	18.0
Flux Densities, (Tesla)	
Main Field Air Gap, Avg.	.79
Core Ring, Max.	1.50
Armature Teeth, max	1.50
Pole Body	1.50
Yoke	1.50
Armature Winding	
Terminal Voltage, volts	114
Rated Current, amps	120
Conductor Size, AWG	10
Terminal Resistance, ohms	.022
Amp. Turns per Pole	3240
Field Winding	
Rated Voltage, volts	60
Rated Current, amps	6.0
Turns per Coil	260
Conductor Size, AWG	17
Resistance (8 Coils), ohms	10.0
Amp. Turns per Pole	1560
Interpole Winding	
Rated Current, amps	120
Conductor Size, cm × cm	0.11 × 2.5
Resistance (4 Coils), ohms	.011
Turns	18
Brush Parameters	
Contact Drop, volts	1.1
Current Density, $amps/cm^2$	9.3
Brush Pressure 10^3 N/m^2	20.7
Friction Coefficient	0.15
Brush Arc, Radians	0.35
Max. Sliding Velocity, m/sec	33.5
Peak Bar to Bar Volts	20

8.4 Fabrication of Engineering Model

In the initial design of the engineering model, we proposed to fabricate the armature teeth out of an epoxy-bonded powdered iron material that was being developed on a support technology development task. This was consistent with the recommendations of our manufacturing engineers who identified this process as a feasible method for making slotted cores in volume production. However, because of the added risks involved by this change, it was ultimately decided to fabricate the cores by machining slots in a tape wound core ring similar to the previous models. This time the machining was done in a numerically-controlled milling machine and generous radii were added to all sharp corners to facilitate core winding without slot liners. Prior to machining the core, a mandrel which would allow the core ring to be mechanically mounted directly to the hub but slotted to permit space for the inner end turns was first installed in the center of the ring. Although the proposed production design utilized an aluminum die-cast mandrel, a laminated mandrel built up from a stack of coated aluminum laminations that resembled the stator core of an A.C. induction motor (see Figure 34) was used to reduce eddy current losses in the mandrel. After assembly and pinning of the mandrel into the core ring, the slots were machined and the entire assembly was epoxy powder coated by electrostatic spray.

The armature was then wound using round insulated copper conductor. Round wire was utilized for reasons of manufacturability. Our manufacturing engineers felt that for the armature winding to be accomplished with automatic winding machines, it must use round wire. We recognized the accompanying disadvantages in terms of slot fill factor and thermal conductivity, but felt that the manufacturing advantages of round wire were an overriding consideration.

Initially we had planned to avoid the use of separate slot liners by using the epoxy powder coating for the primary groundwall insulation. However, we soon found that the coating was not tough enough to avoid damage during winding, particularly during repetitive winding operations

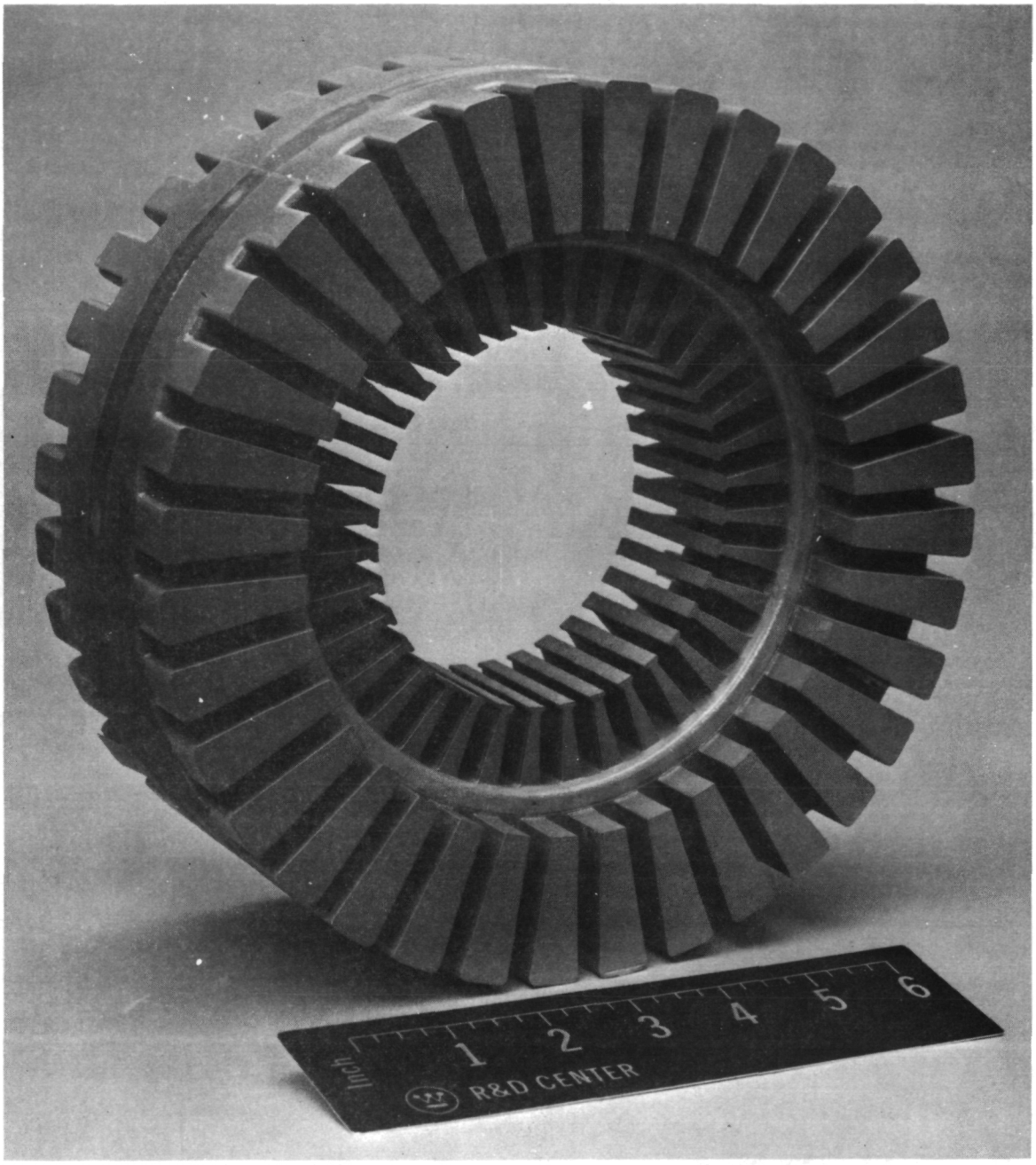

Figure 34 - Engineering Model Slotted Core Assembly

in the same slot. We were finally forced to use discrete slot liners to achieve a reliable winding free of ground faults. Since the slot width had not been designed to accept the slot liners, we have to reduce the wire diameter by one size (from #9 AWG to #10 AWG) to accommodate the slot liners.

The armature coils consisted of six turns per bar; two coils were wound simultaneously in each slot and connected in series at the commutator (see Figure 35). Instead of using a continuous armature winding with soldered taps for the commutator connections, the coils pairs in each slot were wound individually, leaving leads for subsequent connection to the commutator risers. After completion of the armature winding, the hub was inserted in the mandrel and the assembly was clamped in a specially designed fixture for epoxy impregnation. The periphery of the armature was banded with a fiberglass cloth belt for strength, and a filled epoxy was molded to cover the outer end turns for reduced aerodynamic losses. The inner end turns of the winding in the mandrel were also epoxy-filled inadvertently due to capillary interconnections with the periphery.

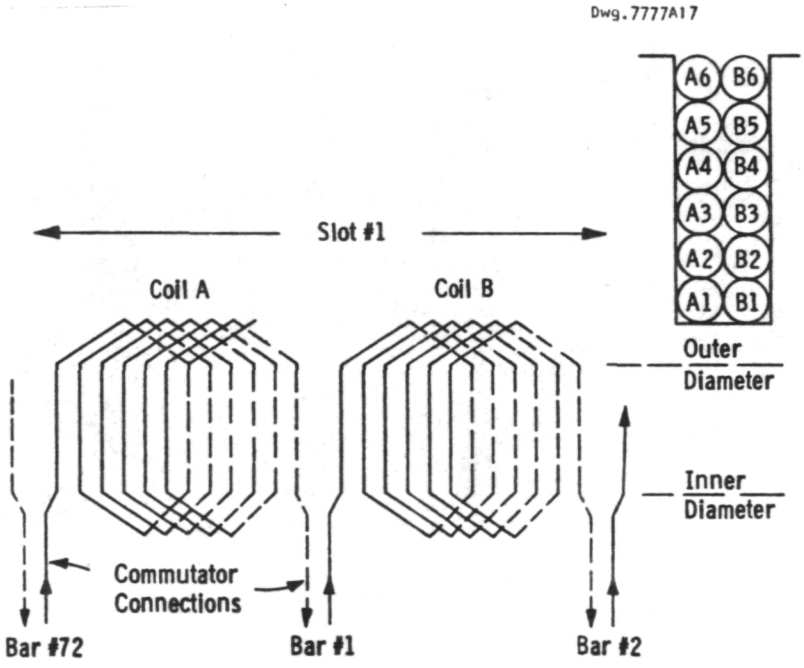

Figure 35 - Engineering Model Armature Winding Diagram

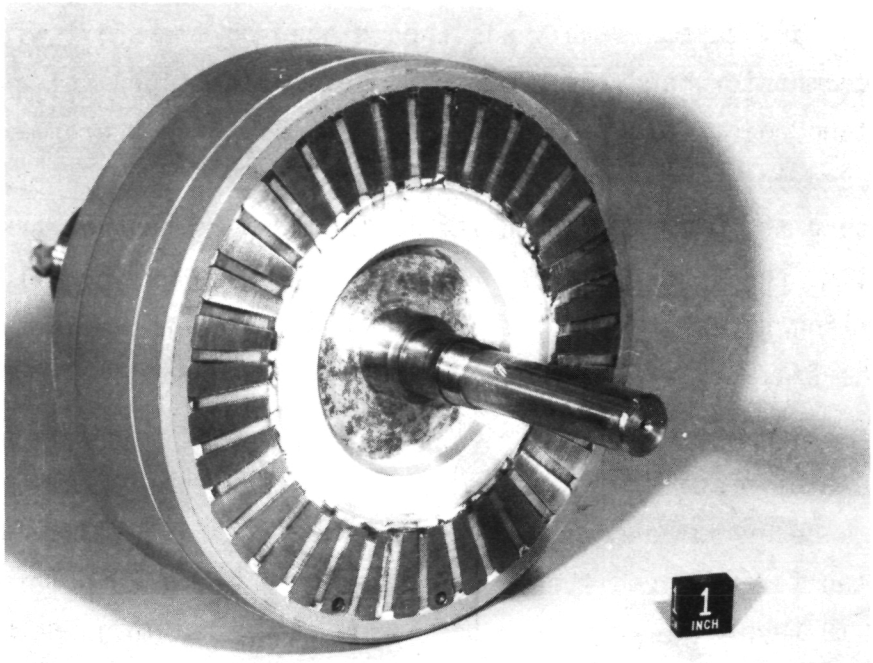

Figure 36 - Engineering Model Rotor Assembly - Shaft End

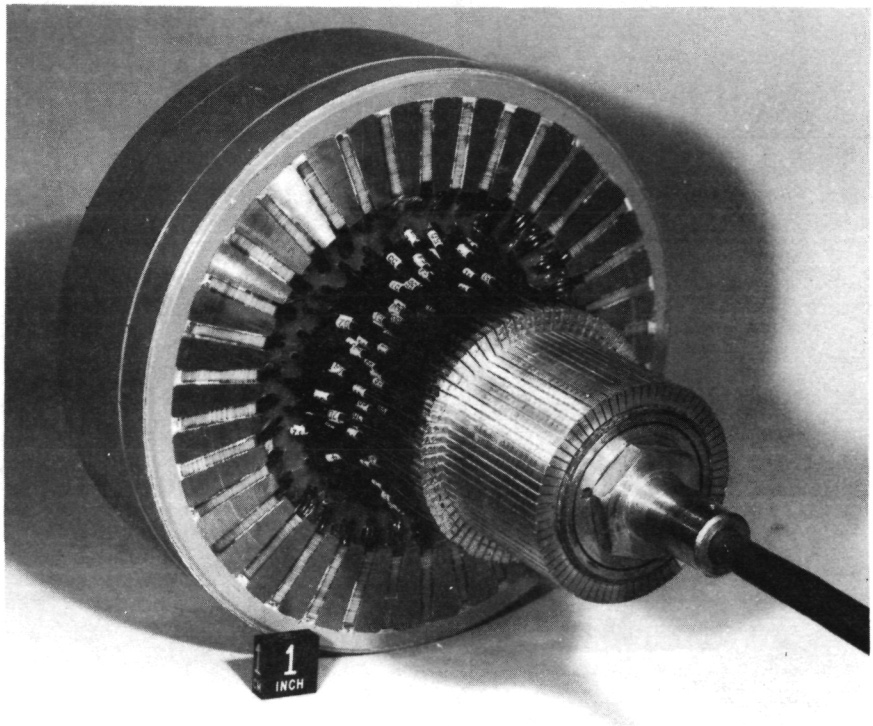

Figure 37 - Engineering Model Rotor Assembly - Commutator End

The cast armature assembly was then placed on the shaft with a spacer and the commutator, and the commutator interconnections soldered with a high melting point lead-tin (95-5) solder. Finally, the armature assembly was placed in a lathe between centers and all critical surfaces machined, including the commutator and the faces and periphery of the armature. Finally, the rotor assembly was statically and dynamically balanced by drilling holes in the face of the armature teeth at their widest part. The finished armature assembly is illustrated in Figures 36 and 37.

The main pole coils were wound using 260 turns of #17 AWG enameled copper wire on solid center steel bobbins (see Figure 38) and vacuum impregnated for improved thermal performance. The interpoles were fabricated from 19 turns of .12 cm x 2.5 cm (.05 in. x 1.0 in.) rectangular copper strip conductor which was laminated to 2.5 cm (1.0 in.) wide polyimide film tape. Two adjacent interpole coils were connected in series; each pair of coils were then series connected with the brushes and armature. The field coils are, of course, separately excited.

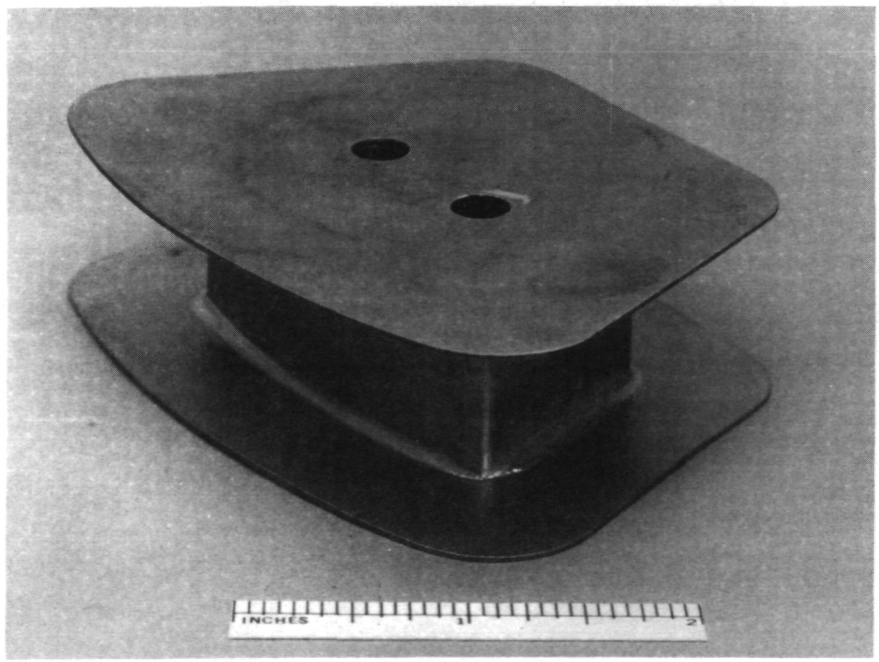

Figure 38 - Engineering Model Main Pole Coil Bobbins

A photograph of the completed commutator-side stator assembly with its four field pole assemblies and four interpole coil assemblies is shown in Figure 39. The brush rigging can also be seen beyond the yoke ring. On the other (output) end, the main field pole assemblies are identical, but the interpoles are omitted and replaced with ventilation air access holes (see Figure 40). The complete motor assembly is illustrated in Figure 41. Removal of the sheet metal cover gives access to the brushes (Figure 42). A ventilation air collection ring is provided on the commutator end for connection to an auxiliary blower which is required for proper motor cooling.

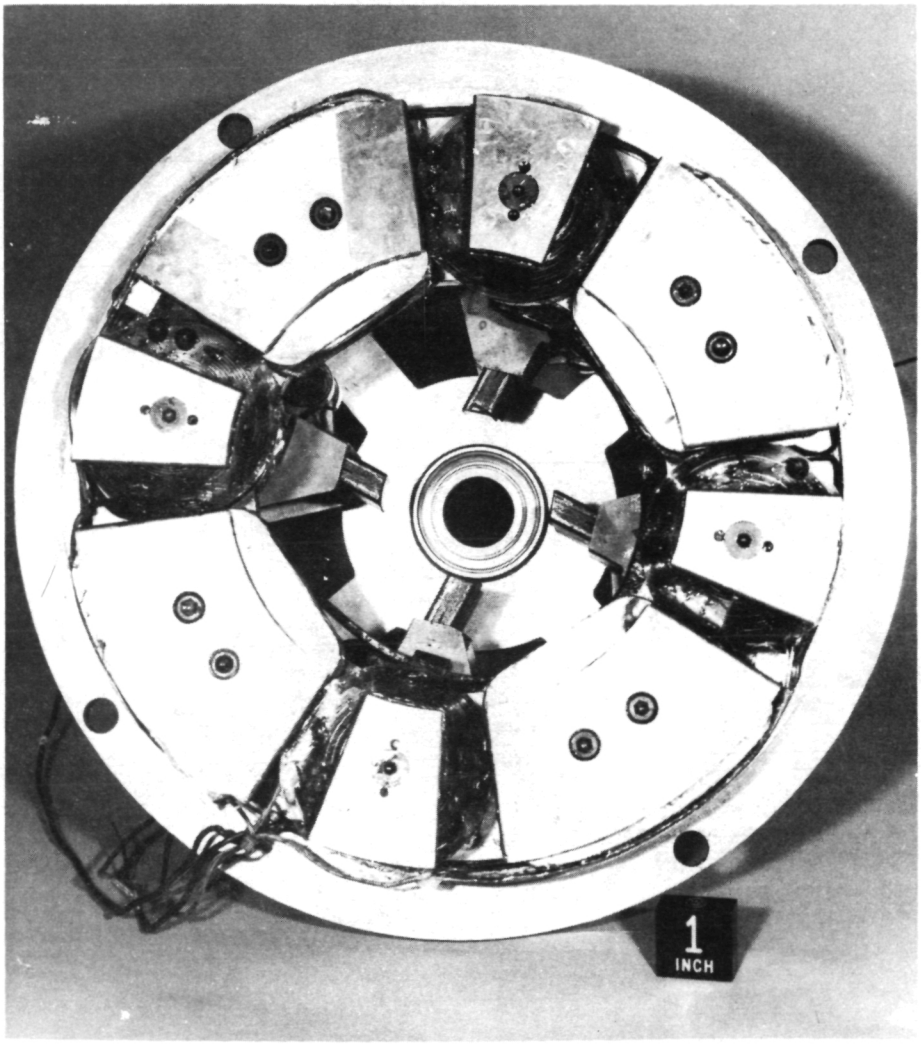

Figure 39 - Engineering Model Stator Assembly - Commutator Side

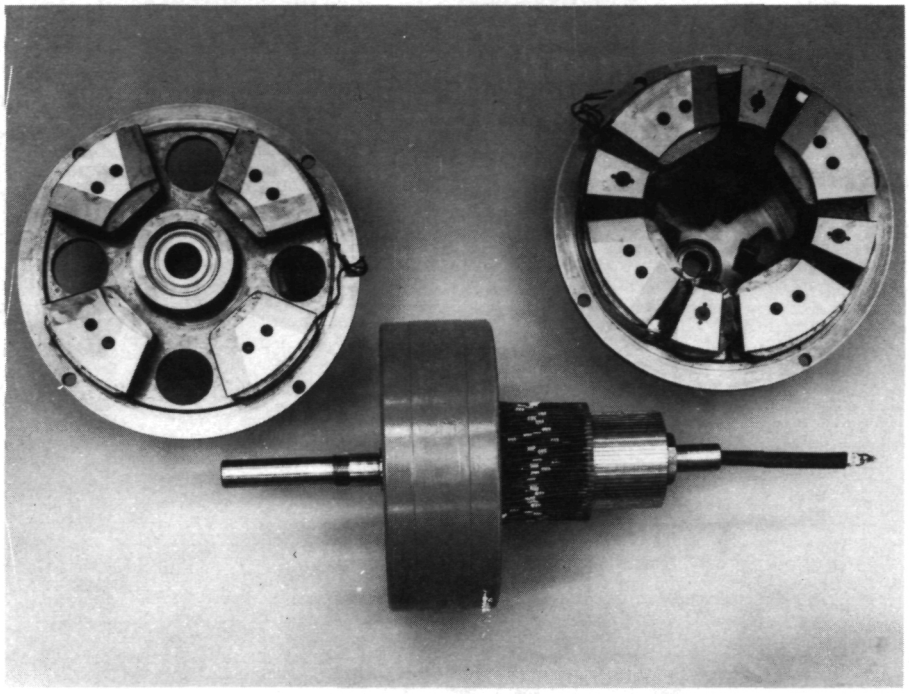

Figure 40 - Engineering Model Main Subassemblies

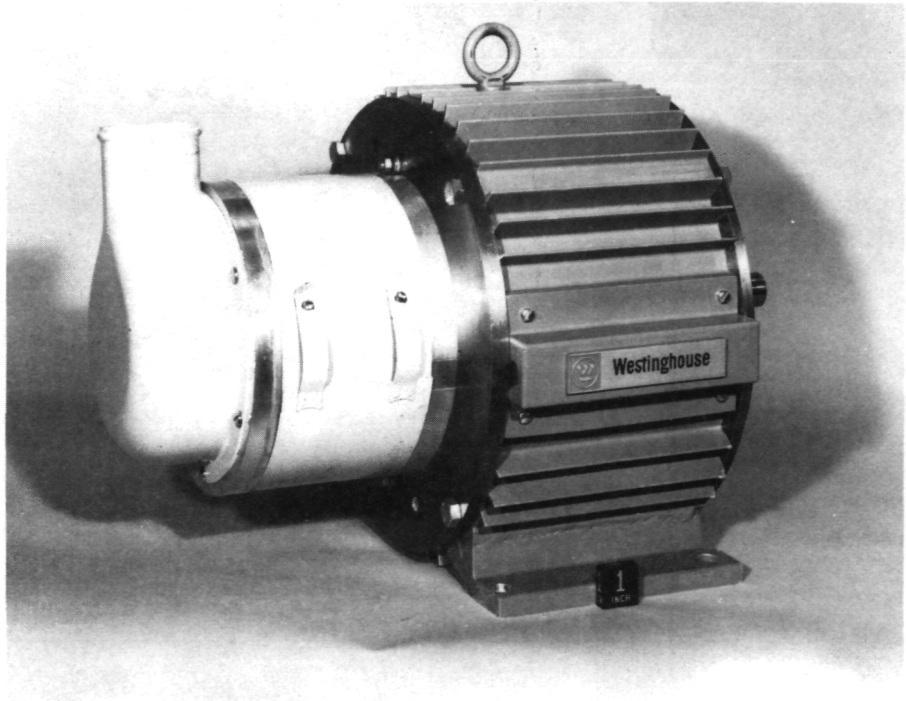

Figure 41 - Engineering Model Motor Assembly

Figure 42 - Engineering Model, Brush Cover Removed

8.5 Test Equipment

For test purposes, the engineering model was equipped with an extension housing (see Figure 43) to accommodate a rotary slip ring assembly which was used to bring out temperature and electrical data from the rotor to the instrumentation harness. A summary of the parameters measured during the test runs is given in Table 10. The dynamometer was modified to use fixed-base mounting of the test motor with an inline rotary torque-speed sensor (see Figure 44). For low-speed tests (below 4000 rpm) direct drive to the hydraulic pump was used; for high speed tests a belt drive with a 2:1 step down ratio was used to avoid overspeeding the pump. The instrumentation harness was connected to an automatic data logger, and the test parameters were recorded on a minute-by-minute basis during all test runs.

8.6 Test Results

Because of cost overruns incurred in the fabrication of the engineering model, we had limited funding available to test the engineering model. We first completed a series of no-load tests, and the results are illustrated in Figures 45 thru 49. The no-load losses were somewhat higher than expected; the extra losses were related to armature excitation and were, therefore, presumed to be either core losses or losses due to circulating currents. Insufficient time was available to investigate the added loss mechanism in any more detail.

Before initiation of the load test sequence, the commutation of the machine was investigated. Poor commutation was observed under full load at base speed, with sparking at the trailing edges of the brushes and blackening of the commutator. Several days were spent trying to correct the commutation problem prior to initiation of the test sequence. The position of the brushes was reset to the neutral position. Brush potential curves under load were taken and indicated the machine was under-commutated. But shimming of the interpoles to reduce the interpole

Table 10

TEST PARAMETERS

Parameter	Range	Accuracy	Sensor
Arm. Voltage	0-120 VDC	± 1.0% F.S.	Volt. Divider; DVM
Arm. Current	0-250 A	± 1.0% F.S.	Shunt; DVM
Field Voltage	0-120 VDC	± 1.0% F.S.	Volt. Divider; DVM
Field Current	0-10 A	± 1.0% F.S.	Shunt, DVM
Shaft Torque	0-2000 in-lb.	± 1% F.S.	Rot. Torque Transducer
Shaft Speed	0-7500 RPM	± 1%	Freq. Pickup
Temperatures:			
Arm. Core	25-150°C	± 2°C	Cu. Const. T.C.
Arm. Winding	25-150°C	± 2°C	Cu. Const. T.C.
Commutator	25-150°C	± 2°C	Cu. Const. T.C.
Main Pole Coil	25-150°C	± 2°C	Cu. Const. T.C.
Main Pole Face	25-150°C	± 2°C	Cu. Const. T.C.
Interpole Coil	25-150°C	± 2°C	Cu. Const. T.C.
Cooling Air Inlet	25-150°C	± 2°C	Cu. Const. T.C.
Cooling Air Exit	25-150°C	± 2°C	Cu. Const. T.C.
Cooling Air Flow	150 cfm	± 5%	Orifice Plate

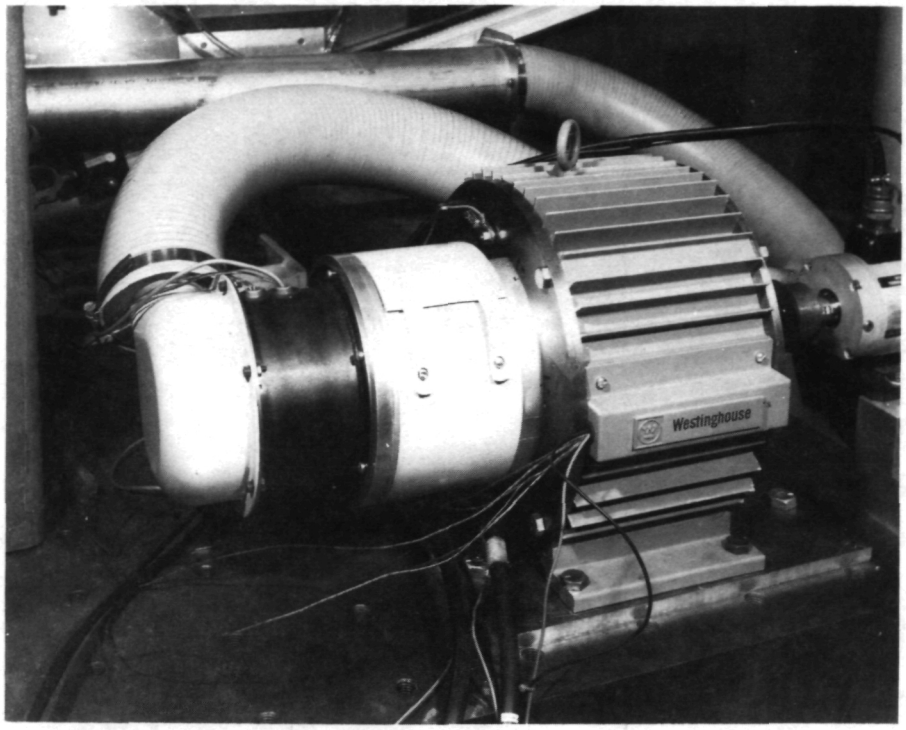

Figure 43 - Engineering Model with Test Extension

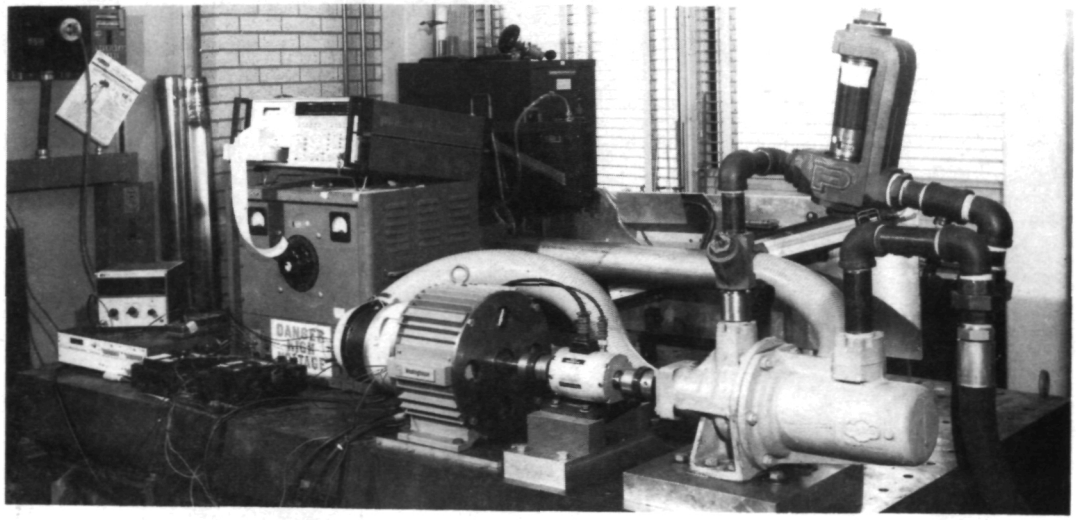

Figure 44 - Engineering Model on Test Stand

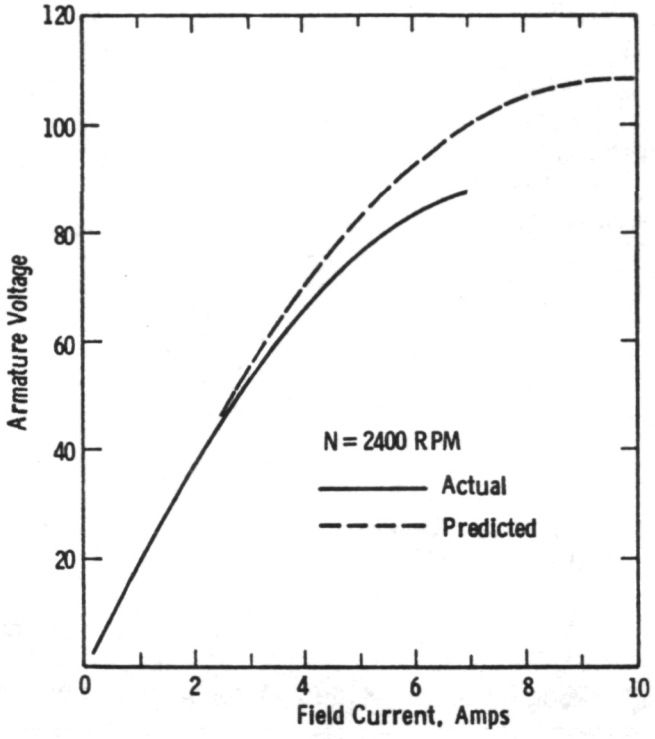

Figure 45 - Engineering Model N.L. Saturation Curve

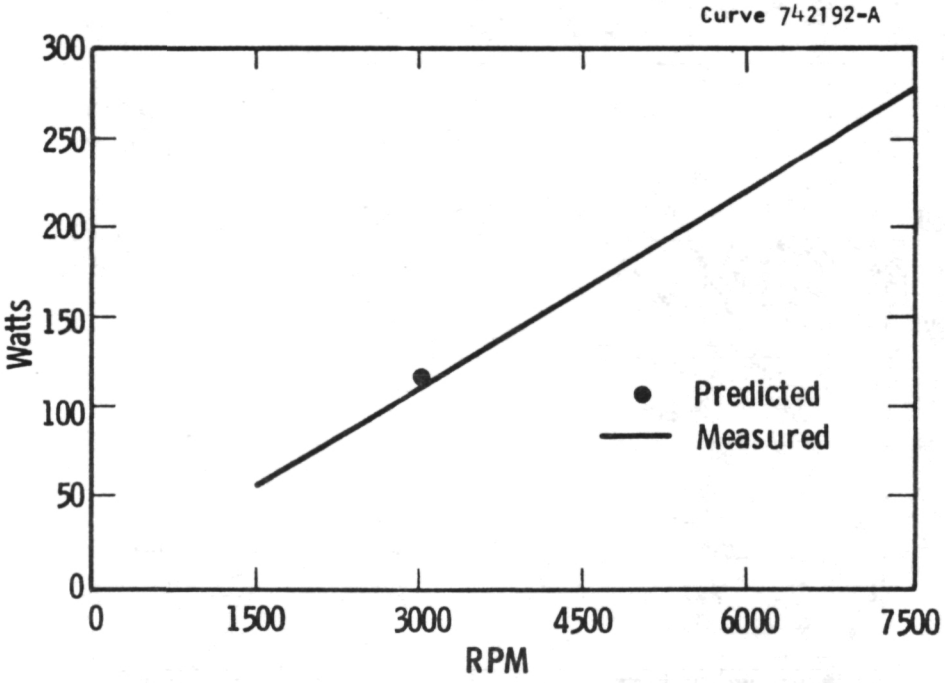

Figure 46 - Engineering Model Brush Friction Losses

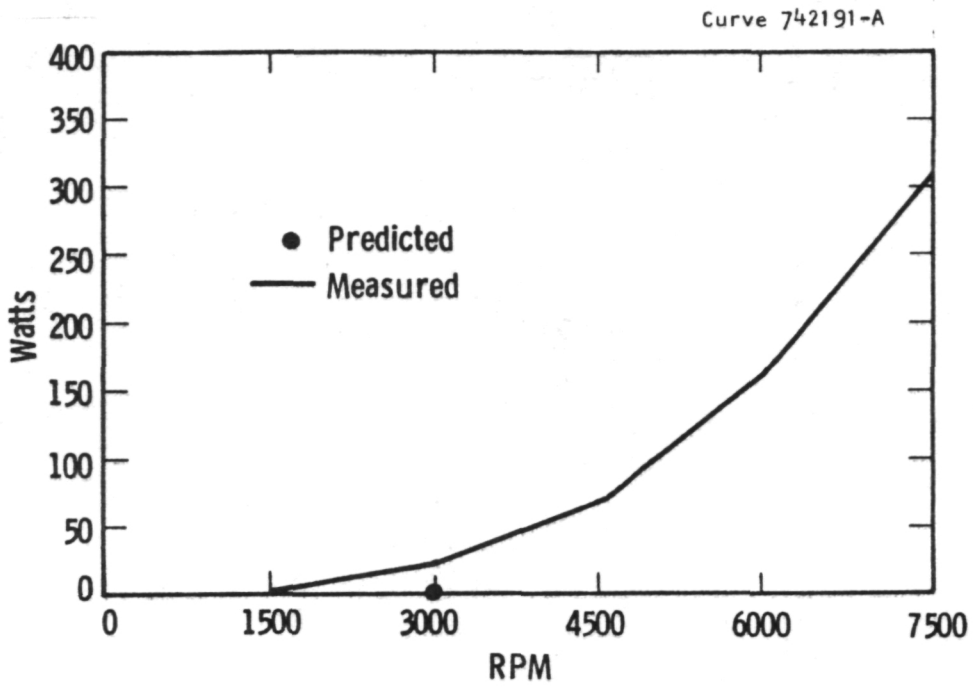

Figure 47 - Engineering Model Aerodynamic Losses

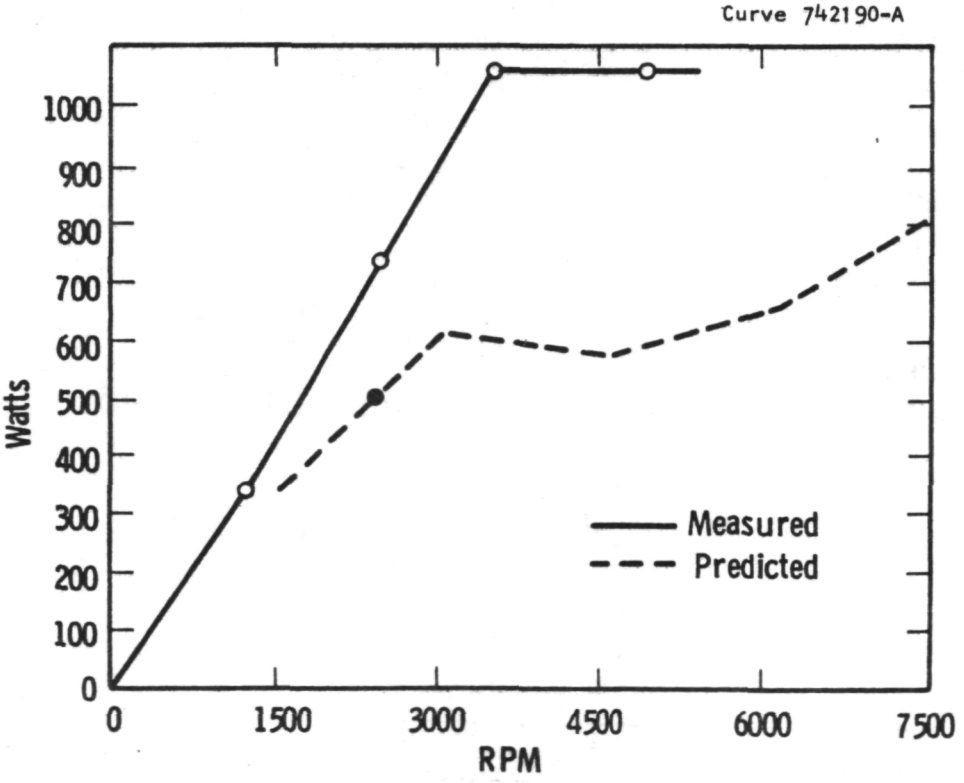

Figure 48 - Engineering Model N.L. Armature Losses

Curve 739735-A

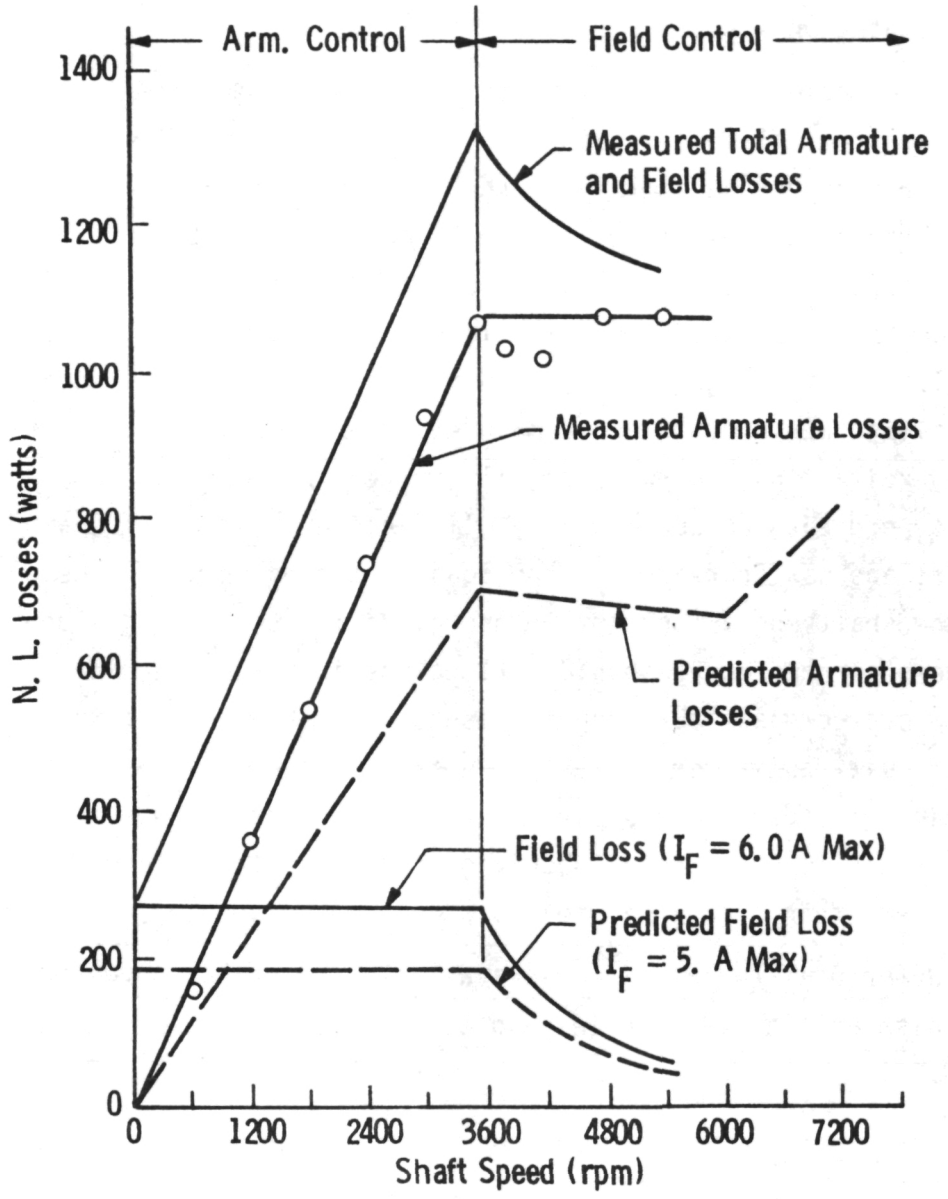

Figure 49 - Engineering Model Total N.L. Losses

airgap failed to improve the commutation. A "boost-buck" test on the interpole circuit was not run because the interpole-armature connections were not easily separated. With time running out, we decided to move onto the load test sequence and get whatever data was possible with the existing commutation limitation.

A series of low-speed motoring tests were completed. The proposed motor test plan is illustrated in Figure 50; the tests actually completed are circled. A summary of the test results are given in Table 11. In general, the tests results were very disappointing with efficiencies well below those expected. In some cases, the losses under load were almost twice those expected. Examination of the output torque vs. armature current relationship (Figure 51) showed nothing unusual. But when the armature voltage was plotted vs. armature current for a series of fixed speeds and excitations, the results illustrated in Figure 52 were observed. These tests were each conducted with full field excitation (6.0 amps); the armature voltage was increased as the load on the motor was increased to maintain the shaft speed constant. Theoretically, the rising slope of the voltage - current curve should reflect the increased terminal voltage required to overcome armature copper losses, and should equal the static armature circuit resistance (.028 Ω). Although the relationship was linear at any one speed, the apparent armature resistance was speed sensitive. This is very unusual behavior and indicates a load-sensitive loss mechanism other than armature resistance is present.

Unfortunately, no time was available to further investigate this loss mechanism and the test series had to be terminated with these questions unanswered.

Table 11

ENGINEERING MODEL TEST RESULTS

Speed (rpm)	Torque (N·M)	Output Power (kw)	Field			Armature			Efficiency		Comments
			Volts	Amps	Watts	Volts	Amps	Watts	Meas.	Pred.	
600	63.9	4.01	51.0	6.06	0.30	31.6	217.6	6.88	.558		
600	66.9	4.20	70.4	7.75	0.55	33.6	204.7	6.88	.565		CONT (TARM=117°C)
600	76.6	4.82	67.9	7.63	0.52	35.5	236.7	8.40	.540		CONT (TCOM=114°C)
600	55.6	3.52	49.5	5.98	0.30	29.6	173.4	5.13	.648		CONT (TARM= 86°C)
1200	60.0	7.54	49.8	5.92	0.29	54.7	196.5	10.75	.683		t=15 min.(TCOM=127°C)
1200	63.6	8.00	53.2	6.20	0.33	54.0	214.0	11.56	.673		t=15 min.(TCOM=127°C)
2400	23.2	5.82	50.0	6.04	0.30	86.8	78.1	6.78	.822		CONT
3000	12.0	3.76	50.1	6.01	0.30	103.0	43.0	4.43	.795		CONT
3000	22.7	7.14	50.1	5.97	0.30	108.0	81.1	8.76	.788		CONT (TCOM=84°C)
3000	24.5	7.71	N.A.	5.88	0.29*	111.2	82.2	9.14	.818		CONT (TCOM=83°C)
2400	11.2	2.81	48.6	5.93	0.29	82.4	41.1	3.39	.764		CONT
1800	22.9	4.33	48.6	5.97	0.29	65.9	77.2	5.09	.805		CONT
1800	11.4	2.15	48.5	5.99	0.29	62.8	42.2	2.65	.731		CONT
1200	23.3	2.93	48.2	6.00	0.29	45.0	78.0	3.51	.771		CONT
1200	11.8	1.48	48.1	6.03	0.29	42.5	43.5	1.85	.692		CONT
600	22.7	1.43	48.0	6.05	0.29	24.1	76.9	1.85	.668		CONT
600	11.5	0.72	46.5	5.91	0.27	22.4	43.1	0.965	.583		CONT
3600	22.8	8.60	N.A.	4.20	0.15*	119.0	87.2	10.4	.815		CONT
1800	46.1	8.68	50.5	5.99	.30	73.9	149.5	11.04	.765		CONT
1200	48.3	6.07	50.2	6.02	.30	51.5	157.0	8.08	.720	.850	CONT
600	46.0	2.89	49.9	6.01	.30	28.2	147.4	4.16	.649		CONT
3000	32.1	10.09	50.2	5.93	.30	115.8	108.6	12.58	.783		CONT
2400	32.4	8.16	49.2	5.91	.29	92.6	109.3	10.13	.783	.875	CONT
1800	33.8	6.37	49.0	6.00	.29	71.2	110.6	7.88	.779		CONT
1200	33.2	4.17	47.8	5.96	.29	49.1	106.0	5.21	.760	.82	CONT
600	31.8	1.99	47.4	5.91	0.28	25.5	104.3	2.66	.679		CONT

*est.

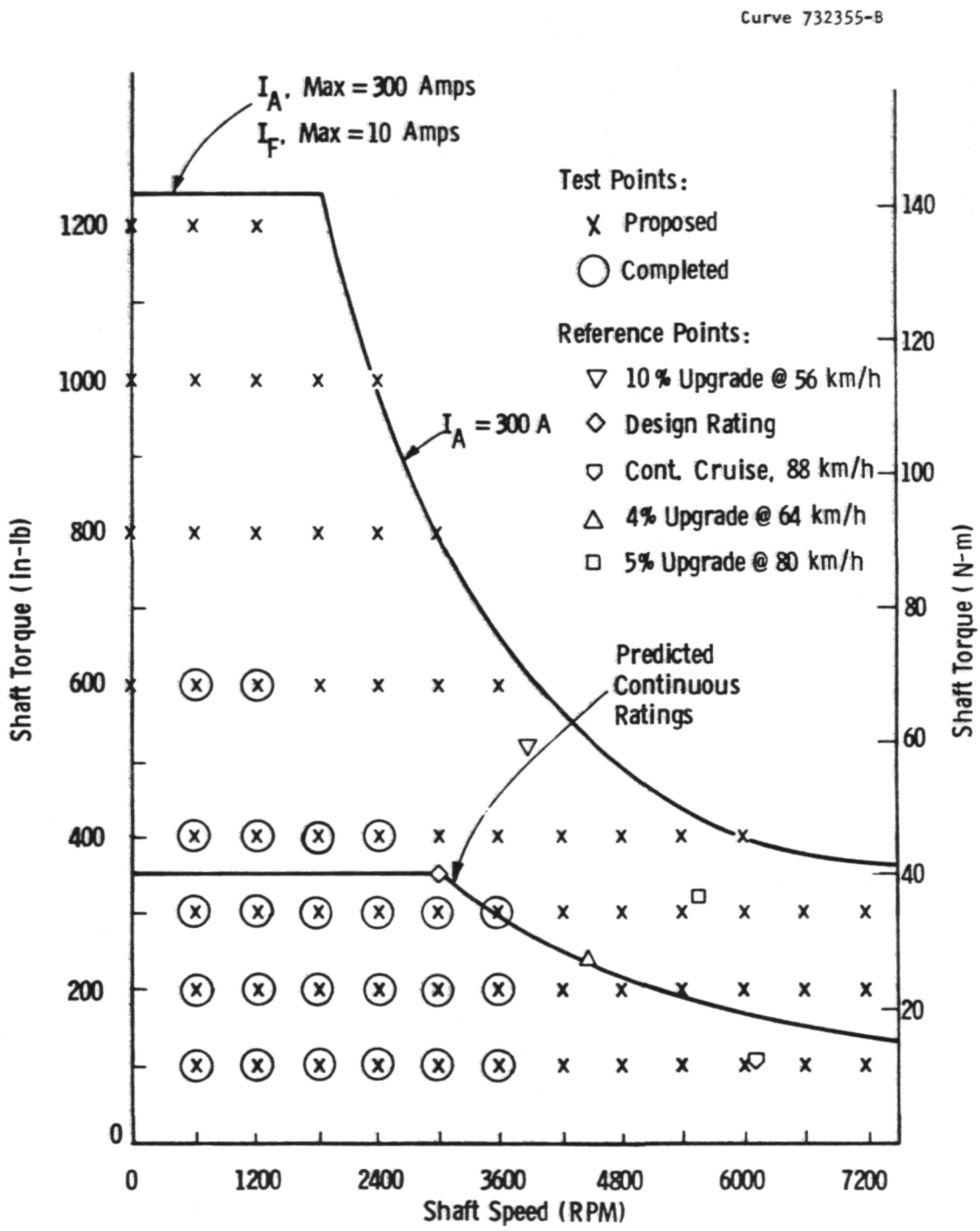

Figure 50 - Engineering Model Test Plan

Curve 739733-A

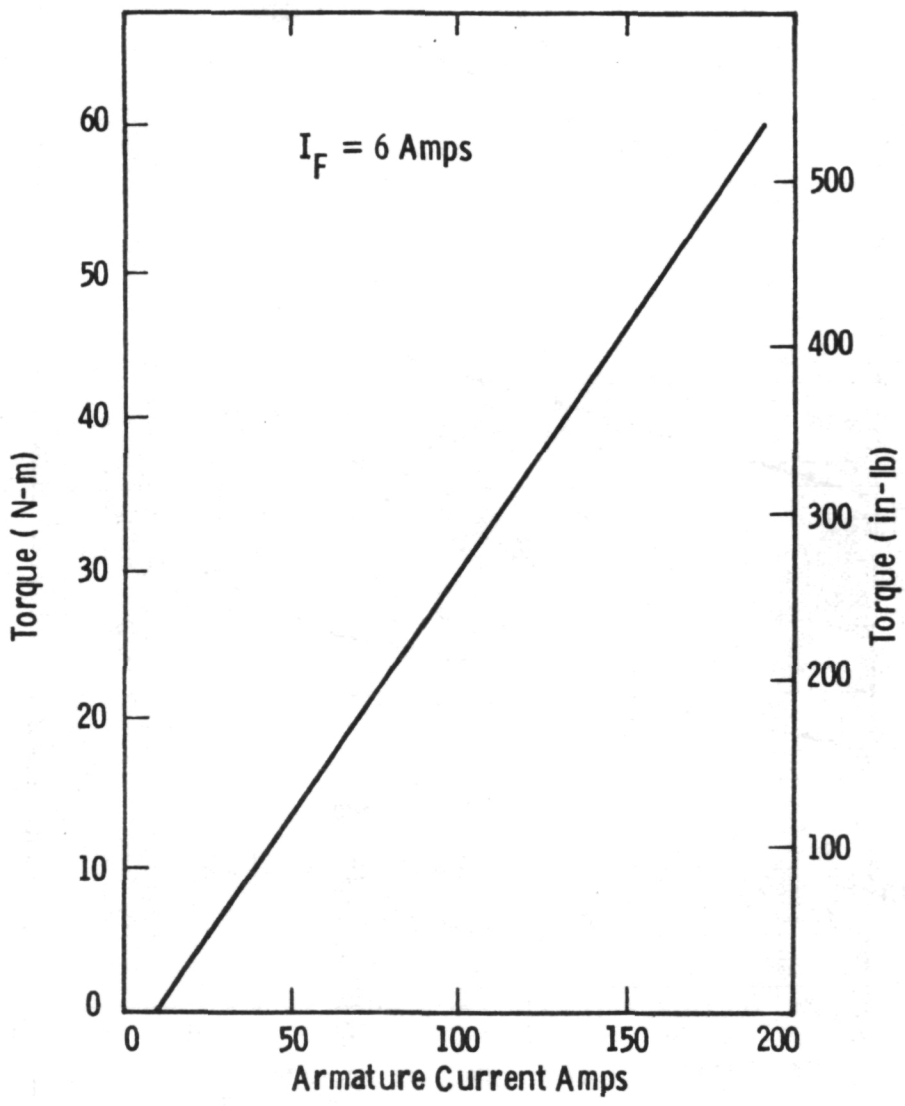

Figure 51 - Engineering Model Torque vs Current

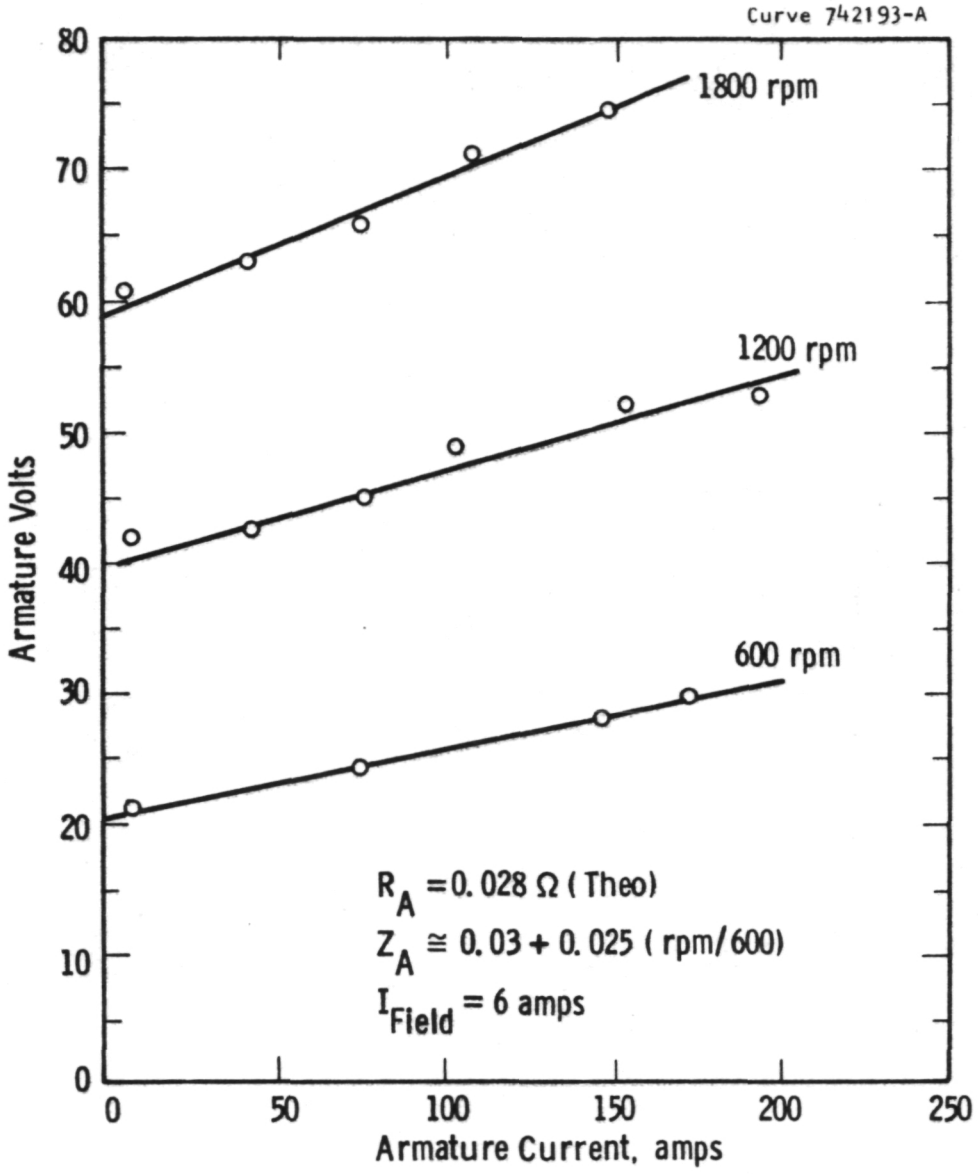

Figure 52 - Engineering Model Voltage-Load Curve

9. MANUFACTURING TECHNOLOGY ASSESSMENT

9.1 Introduction

One of the fundamental considerations in the development of the axial field D.C. motor was its adaptability to low cost volume production. We reasoned from experience that in volume production the motor would be materials cost intensive. Our primary thrust, therefore, was towards reduction of material costs and weight. Since no costly materials are used in this machine, our thrust was basically toward reducing the weight of the machine, while recognizing the need to keep efficiency high to avoid battery weight (and cost) penalties.

However, we also recognized that certain fabrication and assembly procedures associated with the proposed axial field motor presented unusual production problems and needed special attention to assess their possible impact upon its design and performance. The major problem areas identified included slotted core production and automated armature winding and commutator interconnection.

9.2 Slotted Core Production Methods

Our manufacturing engineers agreed that machining of slots in tape wound core rings was too slow and costly for high volume production, and some alternate production method must be developed. Initially we considered electrochemical machining as an alternative production method. With a multi-toothed electrode, one full side of the core could be machined at once, and the resulting product should be free of interlaminar welds and generously radiused. Early in the program, we attempted to fabricate a slotted core for one of our prototypes using a single slot electrode and an indexing fixture (Figures 53 and 54); however, development of the tooling and process controls to attain acceptable dimensional control on the slots proved difficult and this effort was soon abandoned in favor of conventional machining and deburring. We ultimately concluded that electrochemical machining was not competitive with alternative processes as a production slot forming process.

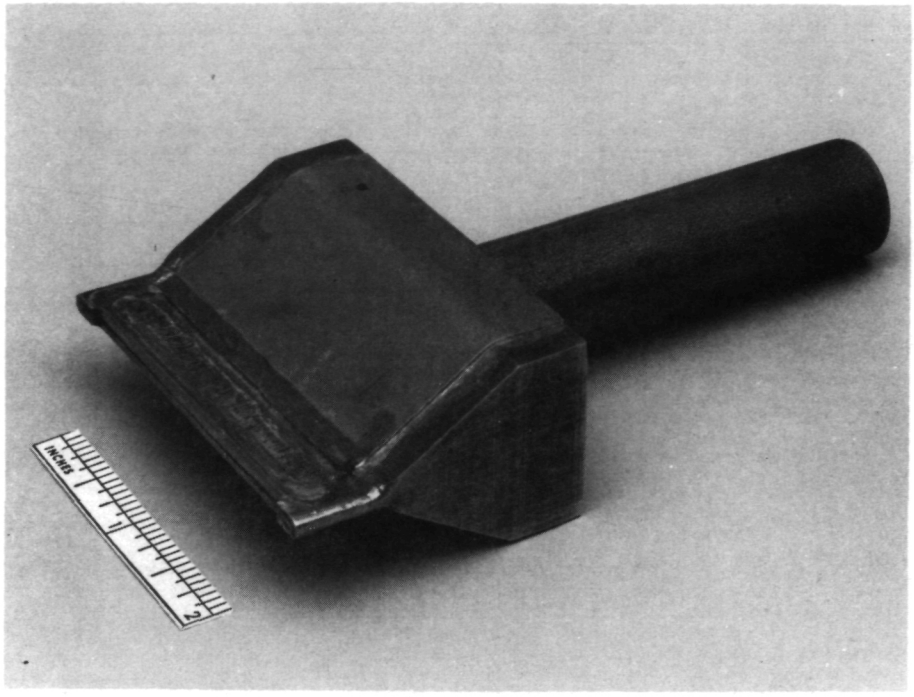

Figure 53 - Electrochemical Machining Electrode

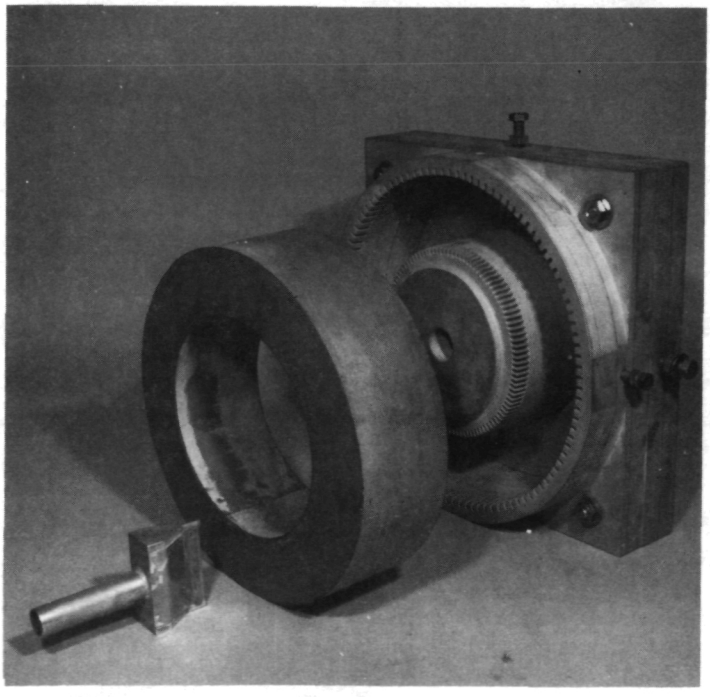

Figure 54 - Core Slotting Fixture

Another core-slotting alternative which received considerable attention was the punch-and-wrap technique wherein a strip of core material was passed through a reciprocating slot punch as it was wrapped on the mandrel. By proper synchronization of the mandrel and die speeds, a core slotted on both sides can be produced directly from strip stock. However, it was estimated that operating at maximum punch repetition rate of 10 Hz, cores of the type used in the engineering model would require about 10 minutes to fabricate. For anticipated production rates this would require several machines operating continuously to satisfy the production requirements. It was also anticipated that alinement of the successive slot layers on the wrapped core may be quite difficult to achieve, and a deburring operation may have to be interposed between the punch and mandrel to assure a tight wrap. Overall it was felt that sufficient uncertainty existed with regard to this method of production to justify investigation of alternate production methods.

A method of building slotted cores by adding teeth to a core ring rather than removing slots was conceived in Phase 2 of the program. It was appreciated that the armature teeth need not have the very high relative permeability characteristic of solid steel sheet ($\mu_r \cong 1000$), but could in fact use tooth materials of significantly lower permeability ($\mu_r \cong 100$), as long as its saturation flux density was not significantly lower, and iron losses could be controlled. A materials evaluation indicated that a matrix of compacted soft iron particles would have suitable properties. It was anticipated that a complete powdered iron core, or preferably a compression molded slot and tooth array bonded to a central wound core ring would give adequate performance and could be produced inexpensively in large volumes (see Figure 55). We planned to demonstrate this technology in one of our Phase 2 prototypes, and some samples were prepared and evaluated on the support technology development task.

Dwg. 7735A81

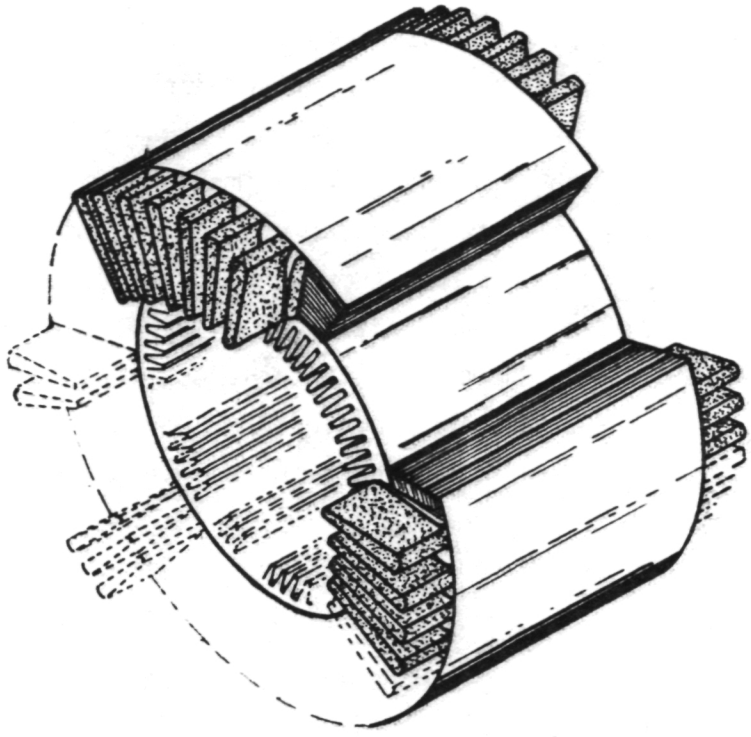

Figure 55 - Design Concept for Powdered Iron Toothed Core

9.3 Powdered Iron Compacts Technology Development

Several investigators have reported in the literature on magnetic properties attainable in powdered iron compacts.[1] However, there was no available data on the mechanical and thermal properties of such materials, nor optimum composition and processing variables. We determined that if we were going to utilize such materials in one of our prototypes we must develop such information ourselves. We selected an atomized iron powder and an electrolytic iron powder for experimental evaluation. We also decided to investigate several minor admixtures of binders (epoxy),

[1] Compressed Iron Powder Core for Electric Motors, K. Fukui, et al., IEEE Trans. on Magnetics, Sept. 1972, p. 682-684.

lubricants (talc), and coatings (magnesium metholate) as adjuncts to the process. Since the pressing pressures required (and the powder densities attained) affected the production press requirements, we also used a variety of pressing pressures from 50 to 100 kpsi. A total of 17 samples were prepared and pressed in an existing die to make ring samples 4.4 cm (1.75 in.) O.D. by 2.5 cm (1.00 in.) I.D. x approximately 1.3 cm (0.5 in.) thick. The samples were all evaluated for magnetic properties and then selected samples were evaluated for thermal and mechanical properties.

Preliminary experimental results with heat treatment (to stress relieve) compacted powders convinced us that such treatment promoted sintering and resulted in unacceptably high eddy current losses. Thus our main test series was performed with unsintered compacts. The magnetic properties of the electrolytic iron powders were much more directional than the atomized iron powders, with better properties in the plane perpendicular to pressing. Because this directionality was a disadvantage the way we anticipated using the material, and because the electrolytic powders were significantly more expensive, further consideration was limited to atomized iron powders.

None of the admixtures (epoxy powders, talc powder, or magnesium methalate coatings) seemed to significantly effect the magnetic properties of the resulting compacts. Since the epoxy powder binder was anticipated to add significantly to the strength of the unsintered compacts, we further focused our attention upon atomized iron compacts with 2% by volume epoxy powder.

The variation in magnetic properties of several such materials pressed at three different pressures is given in Table 12. In general, the higher the pressing pressures, the greater the density and permeability; however, the losses on a weight or volumetric basis were not significantly affected. Since our design goal was to attain an effective A.C. permeability of 150 (relative to air), we concluded that pressing pressures of approximately 80 kpsi and theoretical densities between 85-90% that of solid steel would be necessary to attain the desired magnetic properties in such unsintered compacts.

Table 12

TEST RESULTS ON POWDERED IRON COMPACTS

Sample No.	Pressing Pressure $10^6 N/m^2$ (kpsi)	Density (% THEO)	AC Perm*	Losses* (w/kg)	Thermal Conductivity (w/m·°C)	Tensile Strength $10^6 N/m^2$ (kspi)
15	600 (87)	90	257	15.0	-	-
16	510 (74)	85	122	15.0	0.38	8.89 (1.29)
17	345 (50)	78	N.A.	15.8	0.24	4.27 (0.62)
Design Goals	-	-	150	-	0.13	13.8 (2.00)

NOTE - All samples contained 2% by volume of epoxy powder

*@ 1.0 Tesla, 60 Hz

Following the magnetic tests, two samples containing epoxy powder binders were subjected to further testing of their thermal and mechanical properties. These results are also given in Table 12. Even the lowest density compact had a thermal conductivity which exceeded the design goal, so that thermal conductivity was judged to be no problem.

Finally, the same two selected ring samples were subjected to a tensile pull test in a specially constructed saddle fixture. The results of these tests are also given in Table 12. The apparent tensile strengths of the two samples tested was 620 and 1290 psi, well below the 2000 psi established as a minimum design goal. This was difficult to understand because the information available from the supplier for this material* indicates a "green" strength of the unsintered compacts of approximately 2000-4000 psi in this range of pressing pressures, and we expected that the epoxy binder would increase this value. However, we found that the densities achieved were also considerably lower than published data, probably because of failure to lubricate the die. Also the heat cycle used to cure the parts (10 minutes @ 200°C) appeared to be inadequate to allow full penetration of heat into the ring section.

There are a number of possible explanations for the low strength observed in the tested samples, and we feel confident that we would have no difficulty attaining the requisite tensile strength in properly processed parts. However, by this time it was clear that we would not be utilizing such materials in the construction of a prototype armature. Because of anticipated overruns in the program, it was decided to conclude this technology development effort and put our available funds into other more critical tasks.

*Anchorsteel 1000B, Hoganaes Corp.

9.4 Armature Winding

One of the most difficult manufacturing problems we anticipate is the development of suitable automated production equipment to wind the slotted core armatures and make the appropriate commutator connections. Conventional automatic winding machines are capable of incredibly complex motions but they are basically limited to placing a continuous wire into a slot on the outside of a drum-type armature. Interconnection of the commutator can be accomplished at the same time by providing appropriate hooks in place of armature risers. However, the axial field motor armature requires toroidal winding, which requires passing the spool of wire through the center of the core ring for each turn applied. Toroidal winding machines are commercially available; however, placing the wire in discrete slots (as opposed to on the surface of a plain core) would require considerable equipment development. Even more difficult is the problem of commutator interconnection. Since the hub cannot be inserted until the toroidal winding is completed, the armature core cannot be placed on the rotor shaft with the commutator and the commutator connections integrated with the coil winding process. One initial concept for post-connection of the commutator was a turning operation to expose the bare copper conductor on the outer turn of each completed coil; these exposed areas would then be precisely aligned with a multitude of fingers extending from the commutator and laser-welded. Later the evolution of the design to two coils per slot (with two commutator connections per slot) made this technique considerably less attractive. This remained an unresolved problem until late in the program when a new winding concept was conceived that obviated several of the winding-related problems simultaneously. The basic idea is to eliminate the toroidal winding process, in favor of a totally external winding in which no turn is required to pass through the center of the core ring. Such a winding concept is illustrated in Figure 56, in which the core ring and commutator are premounted on the shaft in the conventional manner. In this winding, the inner (axial) end turns are replaced with circumferential end turns of one pole pitch which then permits the winding to start another turn of

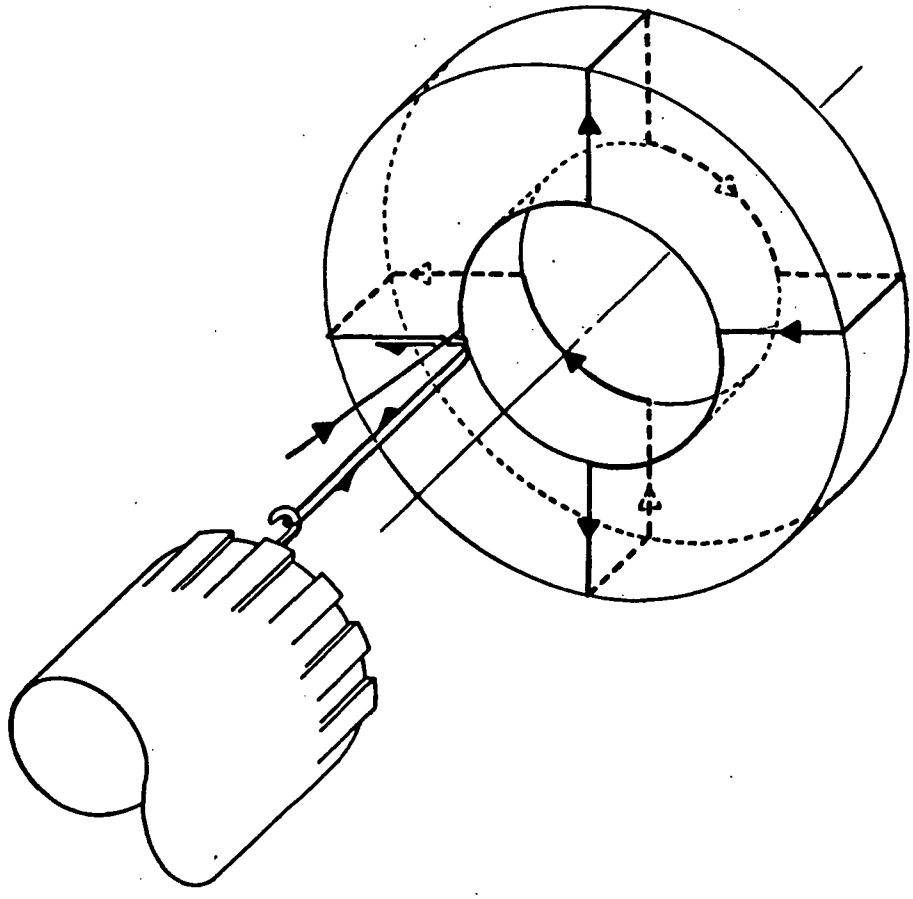

Figure 56 - External Winding Concept

similar polarity under the adjacent pole. By continuing this progression around the armature before returning to the commutator, each complete four-turn coil has eight series coil sides under all eight pole faces. Besides being a totally external winding and thus compatible with conventional automated winding equipment, the winding is completely equalized and requires no separate equalizer connections. Although the design details need to be worked out, we feel strongly that such an external winding method would almost certainly be required to make volume production of this motor feasible.

9.5 Other Problem Areas

Although we were not successful in demonstrating the feasibility of utilizing an epoxy powder coating on the slots and teeth to eliminate the need for additional groundwall insulation (slot liners), we feel quite strongly that a tough, adherent coating can almost certainly be developed. If the molded powdered iron epoxy-matrix tooth construction is developed, this second coating may not even be required, because the major cause of wire insulation failures (sharp corners at the top and exit ends of the slots) can be totally eliminated.

We did successfully demonstrate the utility of unsintered powdered iron compacts in minimizing pole face losses in the experimental model. Slugs of "green" compacts were first vacuum impregnated with a liquid epoxy resin and then machined to final form. Using the pre-blended epoxy powders with post-cure, a pressed to shape part could certainly be developed for production.

One area that will require some additional process development to minimize the labor content is the banding and epoxy casting operation used on the periphery of the rotor. A separate banding operation using a pre-preg fiberglass band and a conveyor oven, followed by a separate molding operation using a thermoset resin in an injection mold might be preferable. Alternately we may be able to eliminate the aerodynamic fairing material entirely since aeordynamic losses were almost negligible in the engineering model. Tests with and without the fairing would be required to make such a determination.

10. CONCLUSIONS AND RECOMMENDATIONS

The axial-field D.C. machine was shown to be a technically feasible machine that is capable of efficiencies and power densities comparable with the best state-of-the-art D.C. motors. The functional model machine was comparable in size, weight, and efficiency with the D.C. motor used in the Electric Test Vehicle (ETV-1), which was specially designed for this application. The fact that this was accomplished without compoles, and in a machine which was the very first embodiment of this principle, may be considered a significant achievement.

A more advanced version of this motor utilizing higher speed and compoles was designed and built which demonstrated a 40% additional weight reduction. Preliminary testing of this machine was unsatisfactory, evidencing both unexpectedly high losses and commutation difficulties. Unfortunately, the program was concluded without successful resolution of these problems. Despite the poor experimental results on the engineering model, we feel that the electromagnetic design is fundamentally sound, and feel that given further effort the nature of the performance problem with the engineering model could be discovered and remedied, and that the performance predicted for this model could be achieved.

Our experience in building and testing the three axial-field motor models has given us an insight into several problems that must be faced in the further development and commercialization of this technology. Manufacturing problems include principally the development of production methods for producing slotted cores, winding and interconnecting the armature. Performance problems include the control of axial forces on the rotor due to airgap unbalance and one-sided commutating poles.

A problem inherent to the axial-field machine concept appears to be the high rotor inertia relative to conventional motor technologies. This could be a significant detriment if the motor was to be used with a shifting transmission as is currently anticipated.

In conclusion, the axial-field motor did demonstrate reasonable power density and good efficiency and held promise for even better power density. However, it also demonstrated some serious manufacturing problems requiring significant production process development, and a potentially serious problem with rotor inertia that appears inherent to the concept. Because of these demonstrated difficulties, and the lack of a significant potential advantage in power density compared to other advanced motor technologies, further development of the axial-field D.C. motor is not recommended.

APPENDIX A

ROAD LOAD POWER REQUIREMENTS

The instantaneous power (Pr) that must be delivered to the road by the vehicle is given by:

$$P_{road} = mv[(R_r + \sin\alpha)\, g + a] + 1/2\rho C_D A v^3$$

where:

P_r = Instantaneous road load power, watts

m = Vehicle mass* = 1350 kg

v = Vehicle velocity, m/sec

R_r = Tire rolling resistance coefficient = 0.008

α = Road grade

g = Gravitational constant - 9.81 m/sec^2

a = Vehicle acceleration, m/sec^2

ρ = Air density = 1.20 kg/m^3

C_D = Aerodynamic drag coefficient = 0.30

A = Vehicle frontal area = 1.86 m^2

Assuming the equivalent mass of the rotary elements in the vehicle drive train is insignificant compared to the mass of the vehicle itself, the road power required to meet any of the prescribed vehicle performance requirements can be calculated. Typical results are given in Table A1.

---

*including equivalent linear mass of rotary elements. See Appendix C.

Table A1

VEHICLE ROAD LOAD POWER REQUIREMENTS

10% Uphill Grade @ 35 mph	24.0 kw
15% Downhill Grade @ 30 mph	24.8 kw
4% Uphill Grade @ 40 mph	13.5 kw
5% Uphill Grade @ 50 mph	21.0 kw
65 mph Max Speed, Level	11.2 kw
55 mph Cruise	7.5 kw
25-55 mph in 16 sec	24.8 kw
0-30 mph in 8 sec	28.5 kw

The required motor instantaneous power output requirement can then be calculated knowing the efficiency of the various drive train elements. Alternately, if the available motor power is known, the instantaneous vehicle acceleration at any speed can be calculated and a vehicle velocity time profile calculated.

APPENDIX B

TYPICAL MOTOR DESIGN/PERFORMANCE PREDICTION PRINTOUT

4. POLE DISC DC MACHINE WITH GRAMME RING ARMATURE

TERMINAL VOLTAGE = 114.0 VOLTS
RATED CURRENT= 120.0 AMPERES
SPEED = 3000.0 RPM
OUTPUT POWER = 12548.6 WATTS

36. ARMATURE SLOTS PER SIDE WITH 12. CONDUCTORS IN SERIES PER SLOT

DIMENSIONS

OUTSIDE DIAMETER	10.117	INCHES NOT INCLUDING FRAME
OVERALL LENGTH	7.987	INCHES NOT INCLUDING COMMUTATOR
TOTAL WEIGHT	109.	POUNDS
CORE RING OUTSIDE RADIUS	4.500	INCHES
CORE RING INSIDE RADIUS	3.002	INCHES
ARMATURE THICKNESS	3.123	INCHES
SLOT WIDTH	.255	INCHES
SLOT DEPTH	.696	INCHES
TOOTH WIDTH - MAX	.530	INCHES
- MIN	.269	INCHES
AIR GAP LENGTH	.0300	INCHES MINIMUM
MAIN POLE ENCLOSURE	.5555	
POLE FACE WIDTH - MAX	3.927	INCHES
- MIN	2.619	INCHES
POLE BODY WIDTH - MAX	2.909	INCHES
- MIN	1.535	INCHES
POLE TIP THICKNESS	.250	INCHES
BACK IRON THICKNESS	.961	INCHES
FIELD COIL DEPTH	1.190	INCHES
FIELD COIL WIDTH	.558	INCHES
GAP BETWEEN FIELD COILS	.100	INCHES
COMMUTATOR DIAMETER	3.500	INCHES
BRUSH ARC LENGTH	.611	INCHES
BRUSH WIDTH	1.637	INCHES

ARMATURE WINDING

MEAN TURN LENGTH	8.815	INCHES
CONDUCTOR RESISTIVITY	.0210	MICROHM-M
CURRENT DENSITY	3000.0	AMPS/SQ.INCH
ARMATURE RESISTANCE	.01771	OHMS
PACKING FACTOR	.7000	

FIELD WINDING

AMPERE-TURNS/POLE	1296.0	AMP-TURNS
FIELD MMF FACTOR	.8000	
MEAN TURN LENGTH	9.196	INCHES
CONDUCTOR RESISTIVITY	.0210	MICROHM-M
PACKING FACTOR	.6500	
CURRENT DENSITY	3000.0	AMPS/SQ.INCH
COIL RESISTANCE	1.182126	OHMS
TURNS PER COIL	259.2	

INTERPOLE WINDING

AMPERE-TURNS/POLE	2187.0	AMP-TURNS
MEAN TURN LENGTH	7.084	INCHES
CONDUCTOR RESISTIVITY	.0210	MICROHM-M
PACKING FACTOR	.8500	
CURRENT DENSITY	3000.0	AMPS/SQ.INCH
COIL RESISTANCE	.002668	OHMS
EFFECTIVE GAP LENGTH	.0754	INCHES
TURNS PER COIL	18.2	

Case 34: Two-Speed Transmission with Clutch

Gear	Ratio	Efficiency
1	2.0	.90
2	1.0	.94

Max. Armature Current = 280 amps

FLUX DENSITIES

GAP	.7930 TESLA
CORE RING	1.5000 TESLA
ARMATURE TEETH	1.3000 TESLA
POLE	1.5000 TESLA
BACK IRON	1.5000 TESLA
CROSS SLOT	.0698 TESLA
FRINGING FACTOR	.9000

BRUSH PARAMETERS

CONTACT DROP	1.100 VOLTS
CURRENT DENSITY	60.0 AMPS/SQ.INCH
COEFFICIENT OF FRICTION	.1500
OPERATING PRESSURE	3.0000 P.S.I.
SLIDING VELOCITY	45.815 FEET/SECOND
ARMATURE I2R	255.0 WATTS
FIELD I2R	236.4 WATTS
FIELD POLE FACE	117.1 WATTS
CONDUCTOR EDDY LOSS	1.2 WATTS
CORE RING	61.5 WATTS
INTERPOLE I2R	153.7 WATTS
ARMATURE TEETH	140.4 WATTS
BRUSH FRICTION	111.9 WATTS
BRUSH CONTACT	264.0 WATTS
FRICTION AND WINDAGE	26.8 WATTS

MAXIMUM ACCELERATION

TIME SEC	SPEED MPH	MOTOR SPEED RPM	MOTOR POWER OUT WATTS	MOTOR POWER LOSS WATTS	ARM. CURRENT AMPS	FIELD P.U.	MOTOR EFF. PERCENT	FIELD CURRENT P.U.	TERMINAL VOLTS	CLUTCH LOSS WATTS	GEAR
ZERO SPEED GRADEABILITY= 43.36 %											
COMMUTATING VOLTAGE = -.0092 VOLTS											
OUTPUT TORQUE= 185.95 FT-LBS											
1.	9.5	1583.	26479.	4022.	[redacted]	1.289	86.8	1.858	106.00	0.	1
COMMUTATING VOLTAGE = -.0096 VOLTS											
OUTPUT TORQUE= 176.81 FT-LBS											

LOSSES

ARMATURE I2R	1388.2 WATTS
FIELD I2R	945.7 WATTS
FIELD POLE FACE	119.1 WATTS
CONDUCTOR EDDY LOSS	2.8 WATTS
CORE RING	58.8 WATTS
INTERPOLE I2R	836.6 WATTS
ARMATURE TEETH	94.0 WATTS
BRUSH FRICTION	74.9 WATTS
BRUSH CONTACT	616.0 WATTS
FRICTION AND WINDAGE	8.0 WATTS

LOSSES

ARMATURE I2R	1388.2 WATTS
FIELD I2R	696.7 WATTS
FIELD POLE FACE	114.7 WATTS
CONDUCTOR EDDY LOSS	3.1 WATTS
CORE RING	57.3 WATTS
INTERPOLE I2R	836.6 WATTS
ARMATURE TEETH	98.8 WATTS
BRUSH FRICTION	78.7 WATTS
BRUSH CONTACT	616.0 WATTS
FRICTION AND WINDAGE	9.3 WATTS

2.	18.6	3086.	26389.	3680.	280.	.951	87.8	1.154	106.00	0.	1

COMMUTATING VOLTAGE = -.0188 VOLTS

OUTPUT TORQUE= 90.15 FT-LBS

LOSSES

ARMATURE I2R	1388.2 WATTS
FIELD I2R	82.6 WATTS
FIELD POLE FACE	69.8 WATTS
CONDUCTOR EDDY LOSS	12.0 WATTS
CORE RING	41.1 WATTS
INTERPOLE I2R	836.6 WATTS
ARMATURE TEETH	192.6 WATTS
BRUSH FRICTION	153.4 WATTS
BRUSH CONTACT	616.0 WATTS
FRICTION AND WINDAGE	69.1 WATTS

3.	23.0	3832.	26232.	3514.	280.	.582	88.2	.526	106.00	0.	1

COMMUTATING VOLTAGE = -.0233 VOLTS

OUTPUT TORQUE= 72.23 FT-LBS

LOSSES

ARMATURE I2R	1388.2 WATTS
FIELD I2R	50.0 WATTS
FIELD POLE FACE	59.4 WATTS
CONDUCTOR EDDY LOSS	18.4 WATTS
CORE RING	36.9 WATTS
INTERPOLE I2R	836.6 WATTS
ARMATURE TEETH	239.1 WATTS
BRUSH FRICTION	190.5 WATTS
BRUSH CONTACT	616.0 WATTS
FRICTION AND WINDAGE	132.3 WATTS

4.	26.6	4419.	26096.	3628.	280.	.485	87.8	.427	106.00	0.	1

COMMUTATING VOLTAGE = -.0269 VOLTS

OUTPUT TORQUE= 62.33 FT-LBS

LOSSES

ARMATURE I2R	1388.2 WATTS
FIELD I2R	36.6 WATTS
FIELD POLE FACE	53.4 WATTS
CONDUCTOR EDDY LOSS	24.5 WATTS
CORE RING	34.3 WATTS
INTERPOLE I2R	836.6 WATTS
ARMATURE TEETH	275.8 WATTS
BRUSH FRICTION	219.7 WATTS
BRUSH CONTACT	616.0 WATTS
FRICTION AND WINDAGE	202.9 WATTS

5.	29.6	4918.	25962.	3751.	280.	.427	87.4	.373	106.00	0.	1

COMMUTATING VOLTAGE = -.0300 VOLTS

OUTPUT TORQUE= 55.74 FT-LBS

LOSSES

ARMATURE I2R	1388.2 WATTS
FIELD I2R	29.2 WATTS
FIELD POLE FACE	49.3 WATTS
CONDUCTOR EDDY LOSS	30.4 WATTS
CORE RING	32.5 WATTS
INTERPOLE I2R	836.6 WATTS
ARMATURE TEETH	306.9 WATTS
BRUSH FRICTION	244.5 WATTS
BRUSH CONTACT	616.0 WATTS
FRICTION AND WINDAGE	279.5 WATTS

6.	32.2	3570.	26130.	3624.	280.	.574	87.8	.528	106.00	0.	2

COMMUTATING VOLTAGE = -.0163 VOLTS

OUTPUT TORQUE= 52.06 FT-LBS

LOSSES

ARMATURE I2R	1388.2 WATTS
FIELD I2R	117.6 WATTS
FIELD POLE FACE	77.5 WATTS
CONDUCTOR EDDY LOSS	9.0 WATTS
CORE RING	44.1 WATTS
INTERPOLE I2R	836.6 WATTS
ARMATURE TEETH	167.1 WATTS
BRUSH FRICTION	133.1 WATTS
BRUSH CONTACT	616.0 WATTS
FRICTION AND WINDAGE	45.1 WATTS

7.	34.7	3852.	26348.	3440.	280.	.716	88.5	.673	106.00	0.	2

COMMUTATING VOLTAGE = -.0176 VOLTS

OUTPUT TORQUE= 48.20 FT-LBS

LOSSES

ARMATURE I2R	1388.2 WATTS
FIELD I2R	97.0 WATTS
FIELD POLE FACE	73.3 WATTS
CONDUCTOR EDDY LOSS	10.5 WATTS
CORE RING	42.5 WATTS
INTERPOLE I2R	836.6 WATTS
ARMATURE TEETH	180.3 WATTS
BRUSH FRICTION	143.6 WATTS
BRUSH CONTACT	616.0 WATTS
FRICTION AND WINDAGE	56.7 WATTS

8.	37.1	4109.	26317.	3453.	280.	.667	88.4	.616	106.00	0.	2

COMMUTATING VOLTAGE = -.0188 VOLTS

OUTPUT TORQUE= 45.14 FT-LBS

LOSSES

ARMATURE I2R	1388.2 WATTS
FIELD I2R	82.9 WATTS
FIELD POLE FACE	69.8 WATTS
CONDUCTOR EDDY LOSS	11.9 WATTS
CORE RING	41.1 WATTS
INTERPOLE I2R	836.6 WATTS
ARMATURE TEETH	192.3 WATTS
BRUSH FRICTION	153.2 WATTS
BRUSH CONTACT	616.0 WATTS
FRICTION AND WINDAGE	68.8 WATTS

9.	39.2	4345.	26287.	3471.	280.	.628	88.3	.573	106.00	0.	2

COMMUTATING VOLTAGE = -.0198 VOLTS

OUTPUT TORQUE= 42.64 FT-LBS

LOSSES

ARMATURE I2R	1388.2 WATTS
FIELD I2R	72.6 WATTS
FIELD POLE FACE	67.0 WATTS
CONDUCTOR EDDY LOSS	13.3 WATTS
CORE RING	40.0 WATTS
INTERPOLE I2R	836.6 WATTS
ARMATURE TEETH	203.4 WATTS
BRUSH FRICTION	162.0 WATTS
BRUSH CONTACT	616.0 WATTS
FRICTION AND WINDAGE	81.3 WATTS

10.	41.2	4564.	26258.	3491.	280.	.596	88.3	.539	106.00	0.	2

COMMUTATING VOLTAGE = -.0208 VOLTS

OUTPUT TORQUE= 40.55 FT-LBS

LOSSES

ARMATURE I2R	1388.2 WATTS
FIELD I2R	64.7 WATTS
FIELD POLE FACE	64.6 WATTS
CONDUCTOR EDDY LOSS	14.7 WATTS
CORE RING	39.0 WATTS
INTERPOLE I2R	836.6 WATTS
ARMATURE TEETH	213.6 WATTS
BRUSH FRICTION	170.2 WATTS
BRUSH CONTACT	616.0 WATTS
FRICTION AND WINDAGE	94.3 WATTS

11.	43.0	4768.	26228.	3513.	280.	.569	88.2	.510	106.00	0.	2

COMMUTATING VOLTAGE = -.0218 VOLTS

OUTPUT TORQUE= 38.78 FT-LBS

LOSSES

ARMATURE I2R	1388.2 WATTS
FIELD I2R	58.5 WATTS
FIELD POLE FACE	62.5 WATTS
CONDUCTOR EDDY LOSS	16.1 WATTS
CORE RING	38.2 WATTS
INTERPOLE I2R	836.6 WATTS
ARMATURE TEETH	223.2 WATTS
BRUSH FRICTION	177.8 WATTS
BRUSH CONTACT	616.0 WATTS
FRICTION AND WINDAGE	107.5 WATTS

12.	44.7	4960.	26200.	3536.	280.	.546	88.1	.487	106.00	0.	2

COMMUTATING VOLTAGE = -.0227 VOLTS

OUTPUT TORQUE= 37.24 FT-LBS

LOSSES

ARMATURE I2R	1388.2 WATTS
FIELD I2R	53.5 WATTS
FIELD POLE FACE	60.7 WATTS
CONDUCTOR EDDY LOSS	17.4 WATTS
CORE RING	37.4 WATTS
INTERPOLE I2R	836.6 WATTS
ARMATURE TEETH	232.1 WATTS
BRUSH FRICTION	184.9 WATTS
BRUSH CONTACT	616.0 WATTS
FRICTION AND WINDAGE	121.0 WATTS

13.	46.4	5140.	26172.	3560.	280.	.526	88.0	.466	106.00	0.	2

COMMUTATING VOLTAGE = -.0235 VOLTS

OUTPUT TORQUE= 35.90 FT-LBS

LOSSES

ARMATURE I2R	1388.2 WATTS
FIELD I2R	49.4 WATTS
FIELD POLE FACE	59.1 WATTS
CONDUCTOR EDDY LOSS	18.7 WATTS
CORE RING	36.8 WATTS
INTERPOLE I2R	836.6 WATTS
ARMATURE TEETH	240.6 WATTS
BRUSH FRICTION	191.6 WATTS
BRUSH CONTACT	616.0 WATTS
FRICTION AND WINDAGE	134.7 WATTS

14.	47.9	5311.	26144.	3584.	280.	.508	87.9	.449	106.00	0.	2

COMMUTATING VOLTAGE = -.0243 VOLTS

OUTPUT TORQUE= 34.71 FT-LBS

LOSSES

ARMATURE I2R	1388.2 WATTS
FIELD I2R	45.9 WATTS
FIELD POLE FACE	57.7 WATTS
CONDUCTOR EDDY LOSS	19.9 WATTS
CORE RING	36.2 WATTS
INTERPOLE I2R	836.6 WATTS
ARMATURE TEETH	248.6 WATTS
BRUSH FRICTION	198.0 WATTS
BRUSH CONTACT	616.0 WATTS
FRICTION AND WINDAGE	148.5 WATTS

15.	49.4	5472.	26117.	3608.	280.	.492	87.9	.434	106.00	0.	2

COMMUTATING VOLTAGE = -.0250 VOLTS

OUTPUT TORQUE= 33.65 FT-LBS

LOSSES

ARMATURE I2R	1388.2 WATTS
FIELD I2R	43.0 WATTS
FIELD POLE FACE	56.4 WATTS
CONDUCTOR EDDY LOSS	21.1 WATTS
CORE RING	35.6 WATTS
INTERPOLE I2R	836.6 WATTS
ARMATURE TEETH	256.1 WATTS
BRUSH FRICTION	204.0 WATTS
BRUSH CONTACT	616.0 WATTS
FRICTION AND WINDAGE	162.5 WATTS

16.	50.7	5625.	26090.	3632.	280.	.478	87.8	.420	106.00	0.	2

COMMUTATING VOLTAGE = -.0257 VOLTS

OUTPUT TORQUE= 32.70 FT-LBS

LOSSES

ARMATURE I2R	1388.2 WATTS
FIELD I2R	40.5 WATTS
FIELD POLE FACE	55.2 WATTS
CONDUCTOR EDDY LOSS	22.3 WATTS
CORE RING	35.1 WATTS
INTERPOLE I2R	836.6 WATTS
ARMATURE TEETH	263.3 WATTS
BRUSH FRICTION	209.7 WATTS
BRUSH CONTACT	616.0 WATTS
FRICTION AND WINDAGE	176.5 WATTS

17.	52.1	5771.	26064.	3656.	280.	.466	87.7	.408	106.00	0.	2

COMMUTATING VOLTAGE = -.0264 VOLTS

OUTPUT TORQUE= 31.84 FT-LBS

LOSSES

ARMATURE I2R	1388.2 WATTS
FIELD I2R	38.3 WATTS
FIELD POLE FACE	54.2 WATTS
CONDUCTOR EDDY LOSS	23.5 WATTS
CORE RING	34.7 WATTS
INTERPOLE I2R	836.6 WATTS
ARMATURE TEETH	270.1 WATTS
BRUSH FRICTION	215.2 WATTS
BRUSH CONTACT	616.0 WATTS
FRICTION AND WINDAGE	190.6 WATTS

18.	53.3	5910.	26038.	3679.	280.	.454	87.6	.398	106.00	0.	2

COMMUTATING VOLTAGE = -.0270 VOLTS

OUTPUT TORQUE= 31.07 FT-LBS

LOSSES

ARMATURE I2R	1388.2 WATTS
FIELD I2R	36.4 WATTS
FIELD POLE FACE	53.2 WATTS
CONDUCTOR EDDY LOSS	24.7 WATTS
CORE RING	34.3 WATTS
INTERPOLE I2R	836.6 WATTS
ARMATURE TEETH	276.6 WATTS
BRUSH FRICTION	220.4 WATTS
BRUSH CONTACT	616.0 WATTS
FRICTION AND WINDAGE	204.7 WATTS

19.	54.5	6043.	26013.	3703.	280.	.444	87.5	.388	106.00	0.	2

COMMUTATING VOLTAGE = -.0276 VOLTS

OUTPUT TORQUE= 30.36 FT-LBS

LOSSES

ARMATURE I2R	1388.2 WATTS
FIELD I2R	34.7 WATTS
FIELD POLE FACE	52.4 WATTS
CONDUCTOR EDDY LOSS	25.8 WATTS
CORE RING	33.9 WATTS
INTERPOLE I2R	836.6 WATTS
ARMATURE TEETH	282.8 WATTS
BRUSH FRICTION	225.3 WATTS
BRUSH CONTACT	616.0 WATTS
FRICTION AND WINDAGE	218.8 WATTS

20.	55.6	6170.	25988.	3726.	280.	.434	87.5	.379	106.00	0.	2

COMMUTATING VOLTAGE = -.0282 VOLTS

OUTPUT TORQUE= 29.71 FT-LBS

LOSSES

ARMATURE I2R	1388.2 WATTS
FIELD I2R	33.2 WATTS
FIELD POLE FACE	51.6 WATTS
CONDUCTOR EDDY LOSS	26.9 WATTS
CORE RING	33.5 WATTS
INTERPOLE I2R	836.6 WATTS
ARMATURE TEETH	288.8 WATTS
BRUSH FRICTION	230.0 WATTS
BRUSH CONTACT	616.0 WATTS
FRICTION AND WINDAGE	232.9 WATTS

21.	56.7	6291.	25963.	3749.	280.	.426	87.4	.371	106.00	0.	2

COMMUTATING VOLTAGE = -.0287 VOLTS

OUTPUT TORQUE= 29.11 FT-LBS

DESIGN POINT.....

CLUTCH OUTPUT SPEED RPM	ROAD POWER HP	TERM. VOLTS	BACK EMF	ARM. CURRENT AMPS	FIELD P.U.	MOTOR LOSS WATTS	MOTOR EFF. PERCENT	SECONDS OPERATING	FIELD CURRENT P.U.	CLUTCH LOSS WATTS	GEAR
3000.00	15.81	113.7	108.0	125.6	.9959	1339.698	90.726	1.0	.8174	0.	2.

COMMUTATING VOLTAGE = -.0062 VOLTS

LOSSES

ARMATURE I2R	279.5 WATTS
FIELD I2R	158.0 WATTS
FIELD POLE FACE	116.0 WATTS
CONDUCTOR EDDY LOSS	1.3 WATTS
CORE RING	61.0 WATTS
INTERPOLE I2R	168.5 WATTS
ARMATURE TEETH	140.4 WATTS
BRUSH FRICTION	111.9 WATTS
BRUSH CONTACT	276.4 WATTS
FRICTION AND WINDAGE	26.8 WATTS

CLUTCH OUTPUT SPEED RPM	ROAD POWER HP	TERM. VOLTS	BACK EMF	ARM. CURRENT AMPS	FIELD P.U.	MOTOR LOSS WATTS	MOTOR EFF. PERCENT	SECONDS OPERATING	FIELD CURRENT P.U.	CLUTCH LOSS WATTS	GEAR
			10% UPHILL GRADEBILITY								
3873.89	32.00	106.6	96.8	267.5	.6918	3223.715	88.736	300.0	.6266	0.	2.

COMMUTATING VOLTAGE = -.0169 VOLTS

LOSSES

ARMATURE I2R	1267.5 WATTS
FIELD I2R	92.8 WATTS
FIELD POLE FACE	74.7 WATTS
CONDUCTOR EDDY LOSS	9.7 WATTS
CORE RING	43.2 WATTS
INTERPOLE I2R	763.9 WATTS
ARMATURE TEETH	181.3 WATTS
BRUSH FRICTION	144.4 WATTS
BRUSH CONTACT	588.6 WATTS
FRICTION AND WINDAGE	57.6 WATTS

CLUTCH OUTPUT SPEED RPM	ROAD POWER HP	TERM. VOLTS	BACK EMF	ARM. CURRENT AMPS	FIELD P.U.	MOTOR LOSS WATTS	MOTOR EFF. PERCENT	SECONDS OPERATING	FIELD CURRENT P.U.	CLUTCH LOSS WATTS	GEAR
			DOWNHILL REGENERATION								
3323.08	-33.00	127.8	134.5	156.5	.5600	2107.460	90.161	120.0	.4018	0.	1.

COMMUTATING VOLTAGE = -.0170 VOLTS

LOSSES

ARMATURE I2R	433.9 WATTS
FIELD I2R	38.2 WATTS
FIELD POLE FACE	106.1 WATTS
CONDUCTOR EDDY LOSS	9.7 WATTS
CORE RING	63.6 WATTS
INTERPOLE I2R	261.5 WATTS
ARMATURE TEETH	311.1 WATTS
BRUSH FRICTION	247.8 WATTS
BRUSH CONTACT	344.4 WATTS
FRICTION AND WINDAGE	291.1 WATTS

55 MPH CRUISE

CLUTCH OUTPUT SPEED RPM	ROAD POWER HP	TERM. VOLTS	BACK EMF	ARM. CURRENT AMPS	FIELD P.U.	MOTOR LOSS WATTS	MOTOR EFF. PERCENT	SECONDS OPERATING	FIELD CURRENT P.U.	CLUTCH LOSS WATTS	GEAR
6093.07	10.30	115.9	111.4	81.0	.5062	1250.598	86.731	4000.0	.3431	0.	2.

COMMUTATING VOLTAGE = -.0081 VOLTS

LOSSES

ARMATURE I2R	116.3 WATTS
FIELD I2R	27.8 WATTS
FIELD POLE FACE	73.6 WATTS
CONDUCTOR EDDY LOSS	2.2 WATTS
CORE RING	45.6 WATTS
INTERPOLE I2R	70.1 WATTS
ARMATURE TEETH	285.2 WATTS
BRUSH FRICTION	227.2 WATTS
BRUSH CONTACT	178.3 WATTS
FRICTION AND WINDAGE	224.3 WATTS

4% UPHILL GRADEBILITY

CLUTCH OUTPUT SPEED RPM	ROAD POWER HP	TERM. VOLTS	BACK EMF	ARM. CURRENT AMPS	FIELD P.U.	MOTOR LOSS WATTS	MOTOR EFF. PERCENT	SECONDS OPERATING	FIELD CURRENT P.U.	CLUTCH LOSS WATTS	GEAR
4435.40	18.00	113.0	106.9	139.2	.6670	1508.537	90.448	4000.0	.4837	0.	2.

COMMUTATING VOLTAGE = -.0101 VOLTS

LOSSES

ARMATURE I2R	343.2 WATTS
FIELD I2R	55.3 WATTS
FIELD POLE FACE	84.7 WATTS
CONDUCTOR EDDY LOSS	3.4 WATTS
CORE RING	49.2 WATTS
INTERPOLE I2R	206.9 WATTS
ARMATURE TEETH	207.6 WATTS
BRUSH FRICTION	165.4 WATTS
BRUSH CONTACT	306.3 WATTS
FRICTION AND WINDAGE	86.5 WATTS

CLUTCH OUTPUT SPEED RPM	ROAD POWER HP	TERM. VOLTS	BACK EMF	ARM. CURRENT AMPS	FIELD P.U.	MOTOR LOSS WATTS	MOTOR EFF. PERCENT	SECONDS OPERATING	FIELD CURRENT P.U.	CLUTCH LOSS WATTS	GEAR
			5% UPHILL GRADEBILITY								
5544.46	28.40	108.3	99.4	234.2	.4964	2857.471	88.748	60.0	.3944	0.	2.

COMMUTATING VOLTAGE = -.0212 VOLTS

LOSSES

ARMATURE I2R	971.0 WATTS
FIELD I2R	36.8 WATTS
FIELD POLE FACE	60.8 WATTS
CONDUCTOR EDDY LOSS	15.2 WATTS
CORE RING	38.1 WATTS
INTERPOLE I2R	585.2 WATTS
ARMATURE TEETH	259.5 WATTS
BRUSH FRICTION	206.7 WATTS
BRUSH CONTACT	515.2 WATTS
FRICTION AND WINDAGE	169.0 WATTS

CLUTCH OUTPUT SPEED RPM	ROAD POWER HP	TERM. VOLTS	BACK EMF	ARM. CURRENT AMPS	FIELD P.U.	MOTOR LOSS WATTS	MOTOR EFF. PERCENT	SECONDS OPERATING	FIELD CURRENT P.U.	CLUTCH LOSS WATTS	GEAR
			DRIVING CYCLE								
138.84	1.25	116.1	111.6	78.7	1.3790	1725.934	82.887	1.0	2.0000	7323.	1.

COMMUTATING VOLTAGE = -.0029 VOLTS

LOSSES

ARMATURE I2R	109.8 WATTS
FIELD I2R	945.7 WATTS
FIELD POLE FACE	155.7 WATTS
CONDUCTOR EDDY LOSS	.3 WATTS
CORE RING	75.5 WATTS
INTERPOLE I2R	66.2 WATTS
ARMATURE TEETH	104.9 WATTS
BRUSH FRICTION	83.5 WATTS
BRUSH CONTACT	173.2 WATTS
FRICTION AND WINDAGE	11.2 WATTS

CLUTCH OUTPUT SPEED RPM	ROAD POWER HP	TERM. VOLTS	BACK EMF	ARM. CURRENT AMPS	FIELD P.U.	MOTOR LOSS WATTS	MOTOR EFF. PERCENT	SECONDS OPERATING	FIELD CURRENT P.U.	CLUTCH LOSS WATTS	GEAR
416.52	3.76	116.1	111.6	78.9	1.3790	1727.193	82.912	1.0	2.0000	5264.	1.

COMMUTATING VOLTAGE = -.0029 VOLTS

694.20	6.26	116.1	111.6	78.9	1.3790	1726.689	82.902	1.0	2.0000	3183.	1.
COMMUTATING VOLTAGE =			-.0029 VOLTS								
971.89	8.76	116.1	111.6	78.8	1.3790	1726.474	82.898	1.0	2.0000	1107.	1.
COMMUTATING VOLTAGE =			-.0029 VOLTS								
1248.81	11.25	115.6	110.9	88.0	1.2289	1189.577	88.686	1.0	1.1958	0.	1.
COMMUTATING VOLTAGE =			-.0036 VOLTS								
1525.73	13.74	114.6	109.3	108.5	.9914	1187.588	90.557	1.0	.7953	0.	1.
COMMUTATING VOLTAGE =			-.0054 VOLTS								
1801.14	16.29	113.5	107.6	130.2	.8267	1367.377	90.804	1.0	.6266	0.	1.
COMMUTATING VOLTAGE =			-.0077 VOLTS								
2075.79	18.30	112.6	106.2	148.1	.7079	1574.899	90.594	1.0	.5244	0.	1.
COMMUTATING VOLTAGE =			-.0100 VOLTS								
2343.60	19.13	112.2	105.6	156.2	.6233	1711.012	90.260	1.0	.4543	0.	1.
COMMUTATING VOLTAGE =			-.0119 VOLTS								
2598.66	19.11	112.2	105.5	156.7	.5641	1777.152	89.912	1.0	.4052	0.	1.
COMMUTATING VOLTAGE =			-.0132 VOLTS								
2806.41	19.09	112.1	105.5	157.3	.5201	1846.293	89.551	1.0	.3701	0.	1.
COMMUTATING VOLTAGE =			-.0144 VOLTS								
3003.67	19.07	112.1	105.4	157.8	.4857	1917.016	89.184	1.0	.3433	0.	1.
COMMUTATING VOLTAGE =			-.0155 VOLTS								
3184.99	19.06	112.1	105.4	158.5	.4578	1989.757	88.814	1.0	.3220	0.	1.
COMMUTATING VOLTAGE =			-.0165 VOLTS								
3353.42	19.04	112.0	105.3	159.1	.4347	2062.250	88.443	1.0	.3046	0.	1.
COMMUTATING VOLTAGE =			-.0174 VOLTS								
3509.72	19.02	112.7	106.3	146.6	.8383	1527.701	90.809	1.0	.6508	0.	2.
COMMUTATING VOLTAGE =			-.0084 VOLTS								
3656.90	19.01	112.7	106.3	146.7	.8045	1532.004	90.781	1.0	.6159	0.	2.
COMMUTATING VOLTAGE =			-.0088 VOLTS								
3794.98	18.98	112.7	106.3	146.6	.7753	1536.552	90.743	1.0	.5868	0.	2.
COMMUTATING VOLTAGE =			-.0091 VOLTS								
3926.24	18.97	112.7	106.3	146.7	.7494	1544.247	90.697	1.0	.5619	0.	2.
COMMUTATING VOLTAGE =			-.0094 VOLTS								
4050.66	18.95	112.7	106.3	146.6	.7264	1552.035	90.645	1.0	.5404	0.	2.
COMMUTATING VOLTAGE =			-.0097 VOLTS								
4169.02	18.93	112.7	106.3	146.6	.7057	1560.503	90.590	1.0	.5216	0.	2.
COMMUTATING VOLTAGE =			-.0100 VOLTS								
4282.07	18.92	112.7	106.3	146.7	.6871	1570.336	90.532	1.0	.5049	0.	2.
COMMUTATING VOLTAGE =			-.0102 VOLTS								
4389.80	18.90	112.7	106.3	146.6	.6702	1579.617	90.472	1.0	.4901	0.	2.
COMMUTATING VOLTAGE =			-.0105 VOLTS								
4492.98	18.88	112.7	106.3	146.6	.6549	1589.137	90.411	1.0	.4767	0.	2.
COMMUTATING VOLTAGE =			-.0107 VOLTS								
4591.61	18.86	112.7	106.3	146.6	.6408	1598.775	90.349	1.0	.4647	0.	2.
COMMUTATING VOLTAGE =			-.0110 VOLTS								
4686.45	18.85	112.7	106.3	146.6	.6278	1609.387	90.287	1.0	.4537	0.	2.
COMMUTATING VOLTAGE =			-.0112 VOLTS								
4777.49	18.83	112.7	106.3	146.6	.6159	1619.158	90.224	1.0	.4436	0.	2.
COMMUTATING VOLTAGE =			-.0114 VOLTS								
4863.98	18.82	112.7	106.3	146.6	.6049	1629.651	90.162	1.0	.4345	0.	2.
COMMUTATING VOLTAGE =			-.0116 VOLTS								

LOSSES

ARMATURE I2R	380.7 WATTS
FIELD I2R	44.6 WATTS
FIELD POLE FACE	78.1 WATTS
CONDUCTOR EDDY LOSS	4.6 WATTS
CORE RING	46.5 WATTS
INTERPOLE I2R	229.4 WATTS
ARMATURE TEETH	227.7 WATTS
BRUSH FRICTION	181.4 WATTS
BRUSH CONTACT	322.6 WATTS
FRICTION AND WINDAGE	114.1 WATTS

4948.20	16.81	112.7	106.3	146.7		.5946	1640.239	90.100	1.0	.4261	0.	2.
COMMUTATING VOLTAGE =			-.0118 VOLTS									
4989.93	6.62	117.4	113.7	52.2		.6307	922.167	85.068	50.0	.4339	0.	2.
COMMUTATING VOLTAGE =			-.0043 VOLTS									
4157.64	-15.90	124.0	128.5	80.4		.8554	1085.059	88.681	10.0	.6298	0.	2.
COMMUTATING VOLTAGE =			-.0055 VOLTS									
3198.65	-26.52	126.3	132.1	126.8		.5717	1744.426	89.798	1.0	.4009	0.	1.
COMMUTATING VOLTAGE =			-.0132 VOLTS									
2926.28	-26.55	126.4	132.2	127.5		.6252	1662.338	90.177	1.0	.4440	0.	1.
COMMUTATING VOLTAGE =			-.0122 VOLTS									
2615.22	-26.58	126.4	132.2	128.1		.6998	1585.957	90.464	1.0	.5071	0.	1.
COMMUTATING VOLTAGE =			-.0109 VOLTS									
2245.73	-26.56	126.4	132.3	128.3		.8150	1520.875	90.520	1.0	.6137	0.	1.
COMMUTATING VOLTAGE =			-.0094 VOLTS									
1839.83	-23.88	125.8	131.2	115.3		.9871	1378.775	89.629	1.0	.7960	0.	1.
COMMUTATING VOLTAGE =			-.0069 VOLTS									
1432.41	-18.59	124.3	129.0	86.9		1.2464	1305.757	84.147	1.0	1.2431	0.	1.
COMMUTATING VOLTAGE =			-.0041 VOLTS									
1023.48	-13.29	.0	.0	.0	*	.0000	.000	.000	1.0	.0000	0.	1.
COMMUTATING VOLTAGE =			.0000 VOLTS									
613.78	-7.98	.0	.0	.0	*	.0000	.000	.000	1.0	.0000	0.	1.
COMMUTATING VOLTAGE =			.0000 VOLTS									
204.85	-2.66	.0	.0	.0	*	.0000	.000	.000	1.0	.0000	0.	1.
COMMUTATING VOLTAGE =			.0000 VOLTS									
.00	.00	.0	.0	.0	*	.0000	.000	.000	25.0	.0000	0.	0.
COMMUTATING VOLTAGE =			.0000 VOLTS									

---------- MOTOR ----------

INPUT ENERGY 952992.8 WATT SEC. ENERGY LOSS 111775.6 WATT SEC.

[redacted] 16877.7 WATT SEC.

* SPECIFIED VALUE

****
***
****

APPENDIX C

MULTI-SPEED TRANSMISSION STUDY

C.1 - Introduction

A vehicle propulsion system was proposed that uitlized a D.C. motor operated with simple field control, in which the motor could be operated only with full battery voltage applied to the armature. This propulsion system requires some means to achieve vehicle speeds (and accelerations) below those corresponding to motor base speed. A simple electrically or hydraulically controlled slip clutch element was proposed, which could be operated in a feedback control mode to achieve any desired motor armature current (torque) by controlling the clutch engagement. To evaluate the energy efficiency of this propulsion system over a typical D-cycle, a series of computer simulation runs were performed using a variety of transmissions including a direct reduction drive, a 2-speed and a 3-speed transmission. These were compared to the cycle efficiency of the reference (armature chopper, direct reduction drive) system.

C.2 - Assumptions

For these simulations the following assumptions were made:

- Battery Voltage = $V_o - I_B R_B$
  $= 120 - 0.05\ I_B$
- Armature Chopper Efficiency = 95% below base speed
  100% above base speed

- Drive Train Efficiency

  Direct Reduction: G.R. = 7.5, η = 95%

  2-speed: G.R. = 15, η = 90%
  G.R. = 7.5, η = 94%

  3-speed: G.R. = 30, η = 90%
  G.R. = 15, η = 92%
  G.R. = 7.5, η = 94%

C.3 - Results

The results of the computer simulation are given in Table C1. The predicted range of the vehicle is obviously optimistic, presumably because the battery model is quite optimistic. However, the comparative results are presumed valid.

The results show that the substitution of a slip clutch for armature control using a direct reduction drive will result in a 22% increase in losses, primarily in the clutch (starting) and brakes (stopping), and a corresponding 18% reduction in vehicle range. With such a drive, vehicle cruise speeds below approximately 20 mph would be achieved with clutch slippage. Beside the obvious loss in vehicle range, the heat dissipated in the clutch during low speed stop and go driving would be an obvious limitation.

When a 2-speed transmission is used, the slip clutch locks up at approximately 10 mph, operates with field control up to approximately 30 mph, then shifts into second gear, again under field control. The computed energy losses using this drive train are only 5% greater than the reference (chopper) drive, and the range 5% less. Moreover, the 0-30 mph acceleration capability of the vehicle is improved from 8 seconds to 5 seconds at a peak armature current of 280 amps. Heat generated in the clutch under abnormal (low speed) driving conditions may still be a problem.

TABLE C1

D-CYCLE ENERGY LOSS ANALYSIS

(LOSSES PER CYCLE, KILOJOULES)

SOURCE	DIRECT DRIVE WITH CHOPPER	DIRECT DRIVE WITH CLUTCH	2-SPEED TRANS. WITH CLUTCH	3-SPEED TRANS. WITH CLUTCH
MOTOR	122	110	112	111
CHOPPER	8	-	-	-
CLUTCH **	-	59	17	4
TRANS.	43	43	52	59
BATT.	40	48	42	40
BRAKES	0	73	18	5
NET ROAD	342	342	342	342
TOTAL	555 (100%)	675 (122%)	583 (105%)	561 (101%)
RANGE* (MI)	128	105	122	127

* BASED ON USEABLE BATTERY CAPACITY OF 20 KWH @ 120V. (72,000 KJ)

** IGNORES ROTATIONAL INERTIA OF DRIVE TRAIN

When a 3-speed transmission is used, the clutch locks up at approximately 5 mph, which is comparable to a conventional I.C.E. vehicle with manual transmission. The associated losses in the clutch and brakes are negligible and the vehicle range is comparable to the chopper-controlled direct drive. The 0-30 mph acceleration time is reduced to 4 seconds at an armature current of 280 amps.

The conclusion of this study was that a 3-speed shifting transmission mated to a field-controlled D.C. motor is a practical, inexpensive, efficient, and reliable alternative to a chopper-controlled D.C. motor with direct reduction drive that also offer improved acceleration capability.

C.4 - Motor Inertia Limitations

The foregoing analysis ignores the inertia of the rotary elements in the vehicle drive system in computing vehicle and transmission performance. However, when using a shifting multi-speed transmission, without proper control excessive motor inertia can have an adverse impact upon the transmission shift clutches, and in the extreme can have an adverse effect upon vehicle acceleration. To investigate possible problems in this regard the inertia and rotary kinetic energy of the motor were calculated and compared in Table C2. As pointed out in the main body of this report, the axial field D.C. motors developed under this contract have appreciably more inertia than a conventional drum armature machine as typified by the motor in the ETV-1. The table indicates that the rotational kinetic energy of the two axial field motors at any speed in direct drive (G.R. = 7.5) are approximately 9-12% of the linear kinetic energy of the total vehicle. Thus ignoring this energy in the computer simulations creates a small but significant error. Moreover, since the kinetic energy varies as the square of speed, using an additional 2:1 gear reduction increases this percentage ratio by a factor of four when the transmission is in low gear. And with a 3-speed transmission having an overall reduction ratio of, say 4:1 in low gear, the ratio of motor kinetic energy to vehicle linear kinetic

TABLE C2

ROTARY INERTIA COMPARISON

	ETV-1	FUNCT. MODEL	ENGR. MODEL
MOMENT OF INERTIA OF ROTOR (I IN LB-FT^2)	2.2	8.5	5.7
KINETIC ENERGY OF ROTOR (FT. LB @ RPM)	9360 (@ 5000)	39,200 (@ 4800)	50,300 (@ 7200)
VEHICLE K.E. @ 65 MPH (FT. LB)	423,400	423,400	423,400
ROTOR/VEHICLE K.E. (DIRECT DRIVE)	2.2%	9%	12%
(2:1 G.R.)	8.8%	37%	47%
ACCL TIME (SEC)*	-	-	0.35 SEC
DECEL TIME (SEC)**	-	-	1.40 SEC

* ZERO TO 3000 RPM WITH IMAX = 500A

** 6000 TO 3000 RPM WITH IMAX = 500A

energy varies from 35% for the ETV-1 drum armature machine to 148% for the engineering model of the axial field motor. The effect upon vehicle performance is equivalent to a comparable increase in vehicle mass. Aside from the obvious detrimental effect on the vehicle acceleration and deceleration, the accommodation of such rotational energies by the transmission shift mechanism presents a significant design problem. To avoid excess energy dissipation in the clutches, motor and clutch speed sensors would probably be required so that excess motor rotational energy could be regenerated back into the battery during an upshift. A similar scheme may be required for downshifting.

ELECTRIC VEHICLE TEST CYCLE D

per SAE J-227a

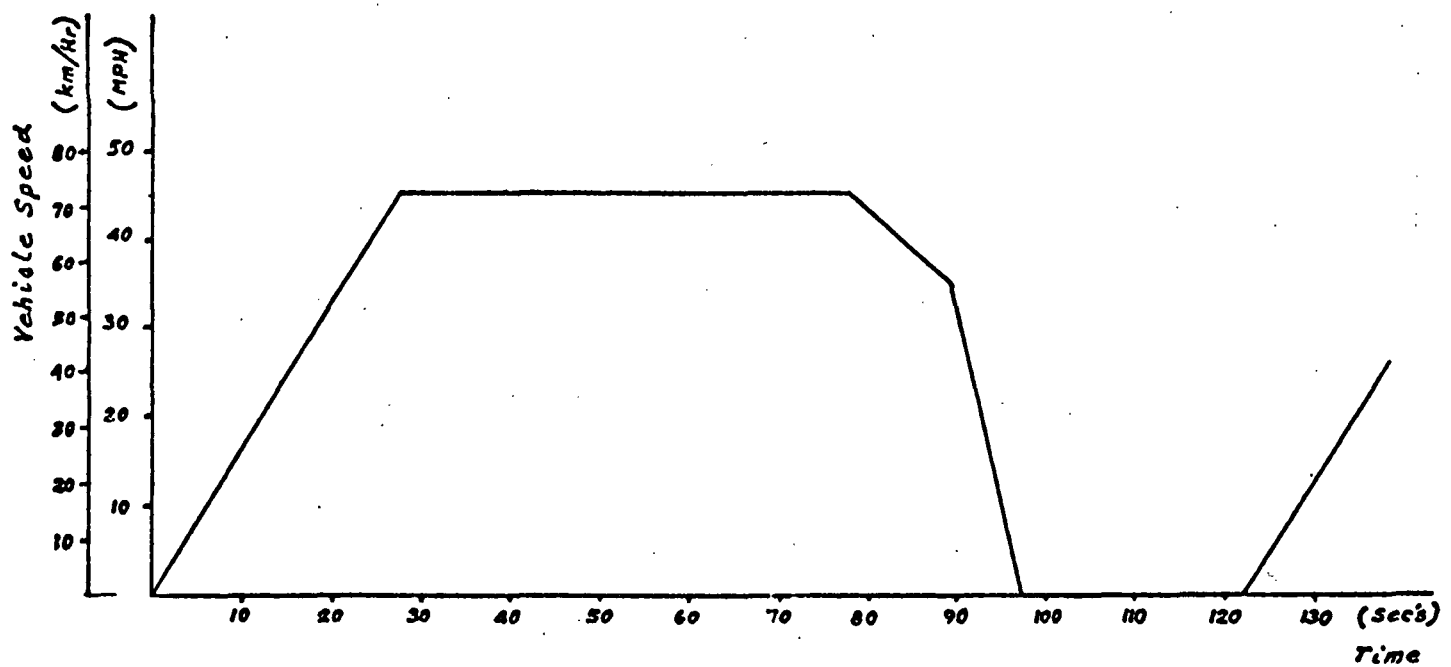

Characterized by	Testing Cycle	Vehicle Cruise Speed		Accel. Time Sec.	Cruise Time Sec.	Coast Time Sec.	Braking Time Sec.	Idle Time Sec.
		km/Hr	MPH					
Suburban Commuter Car	D	72 ± 1.5	45 ± 1	28 ± 2	50 ± 2	10 ± 1	9 ± 1	25 ± 2

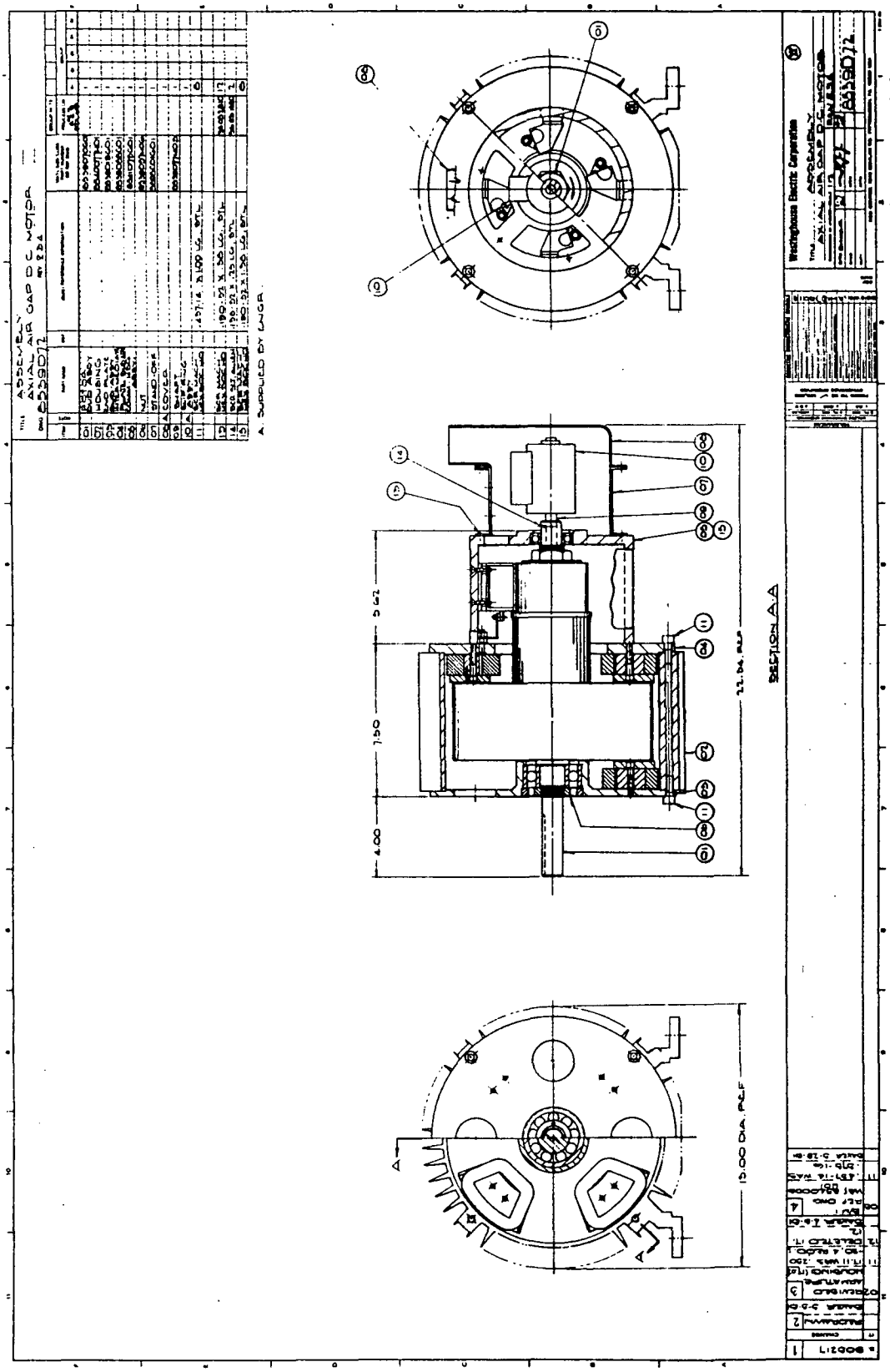
ASSEMBLY
AXIAL AIR GAP D.C. MOTOR
6239D72
SECTION A-A
5.62
7.50
4.00
13.94 REF
15.00 DIA. REF
Westinghouse Electric Corporation
ASSEMBLY
AXIAL AIR GAP D.C. MOTOR
6239D72

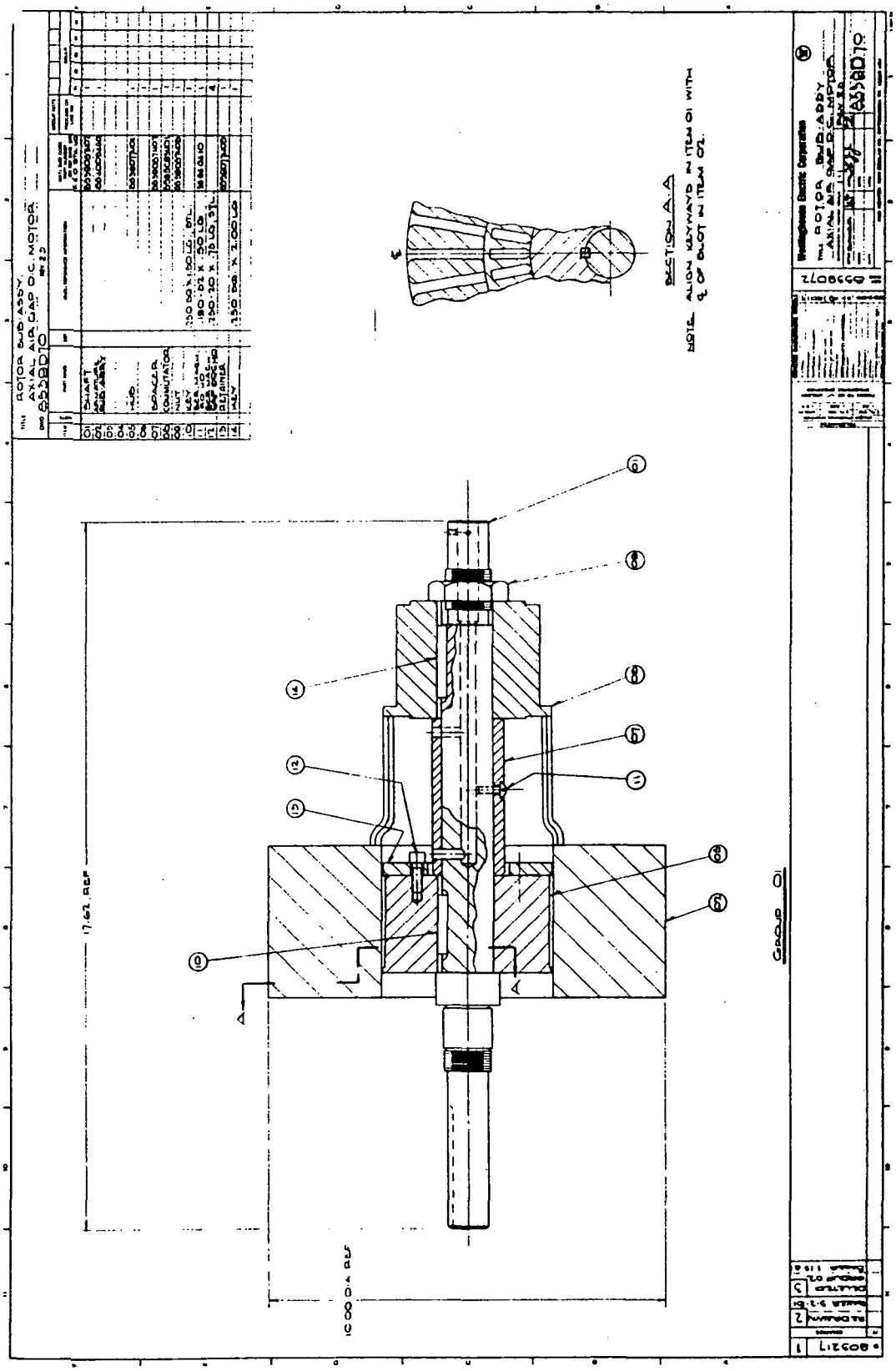

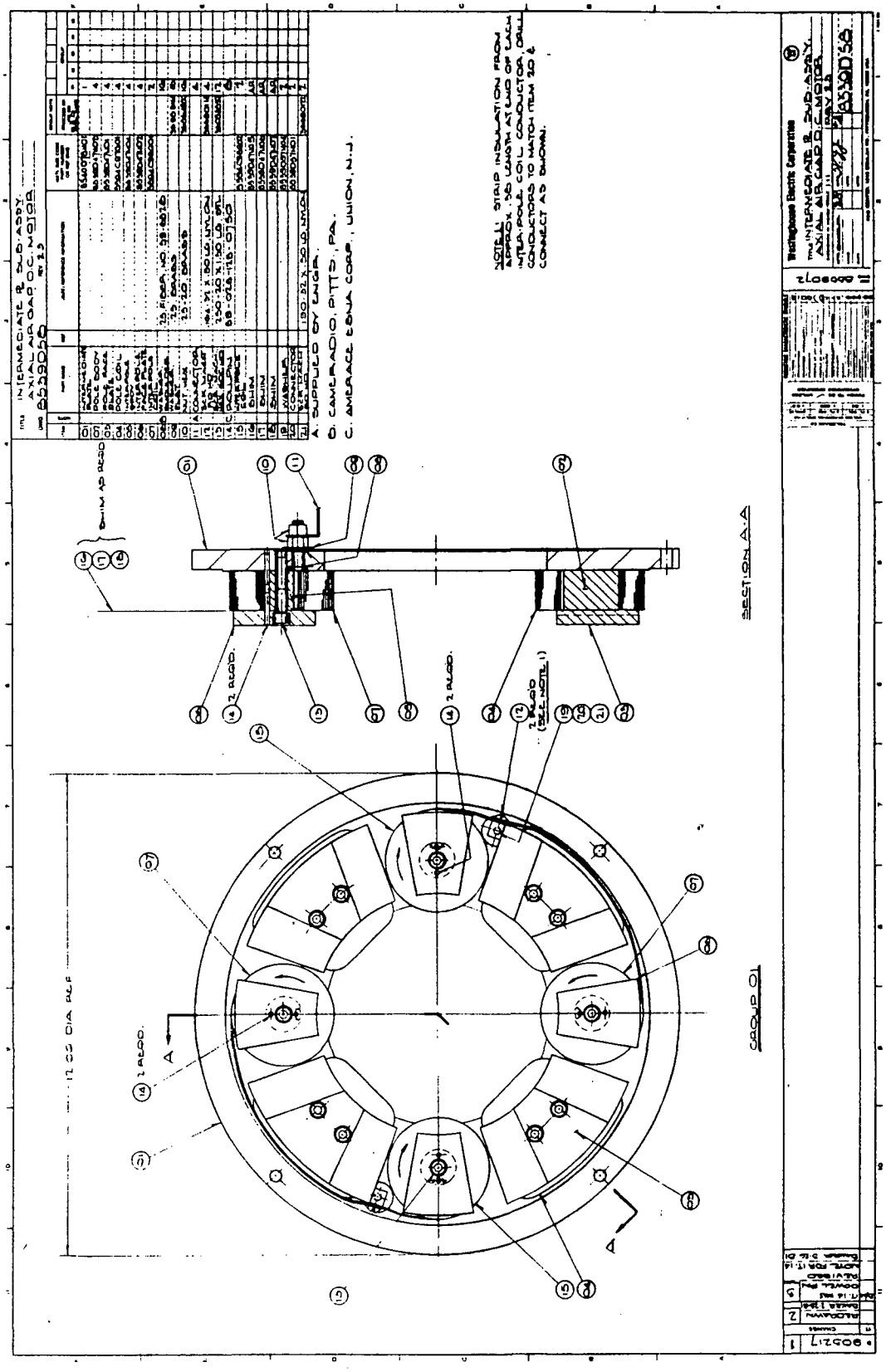

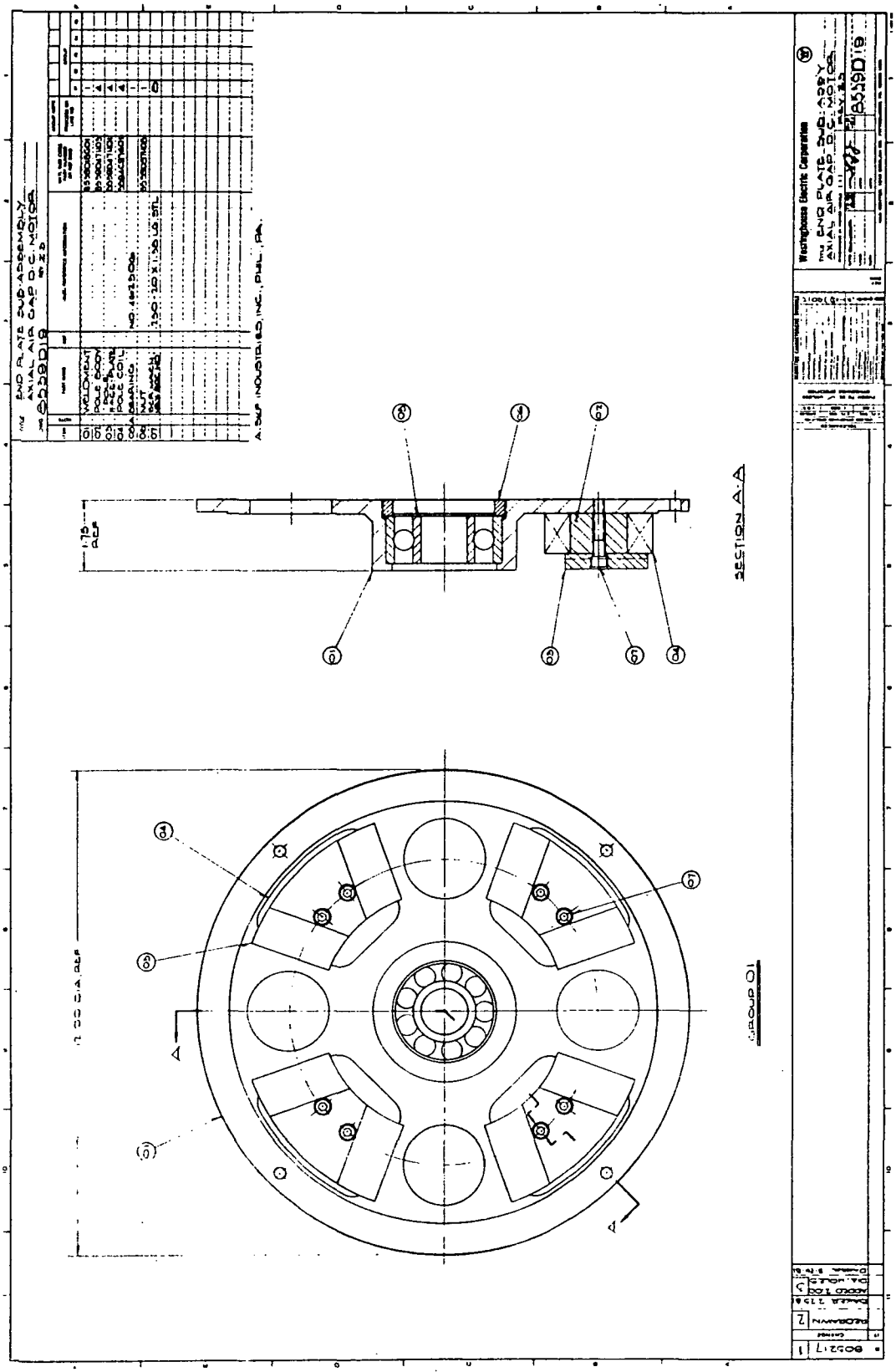

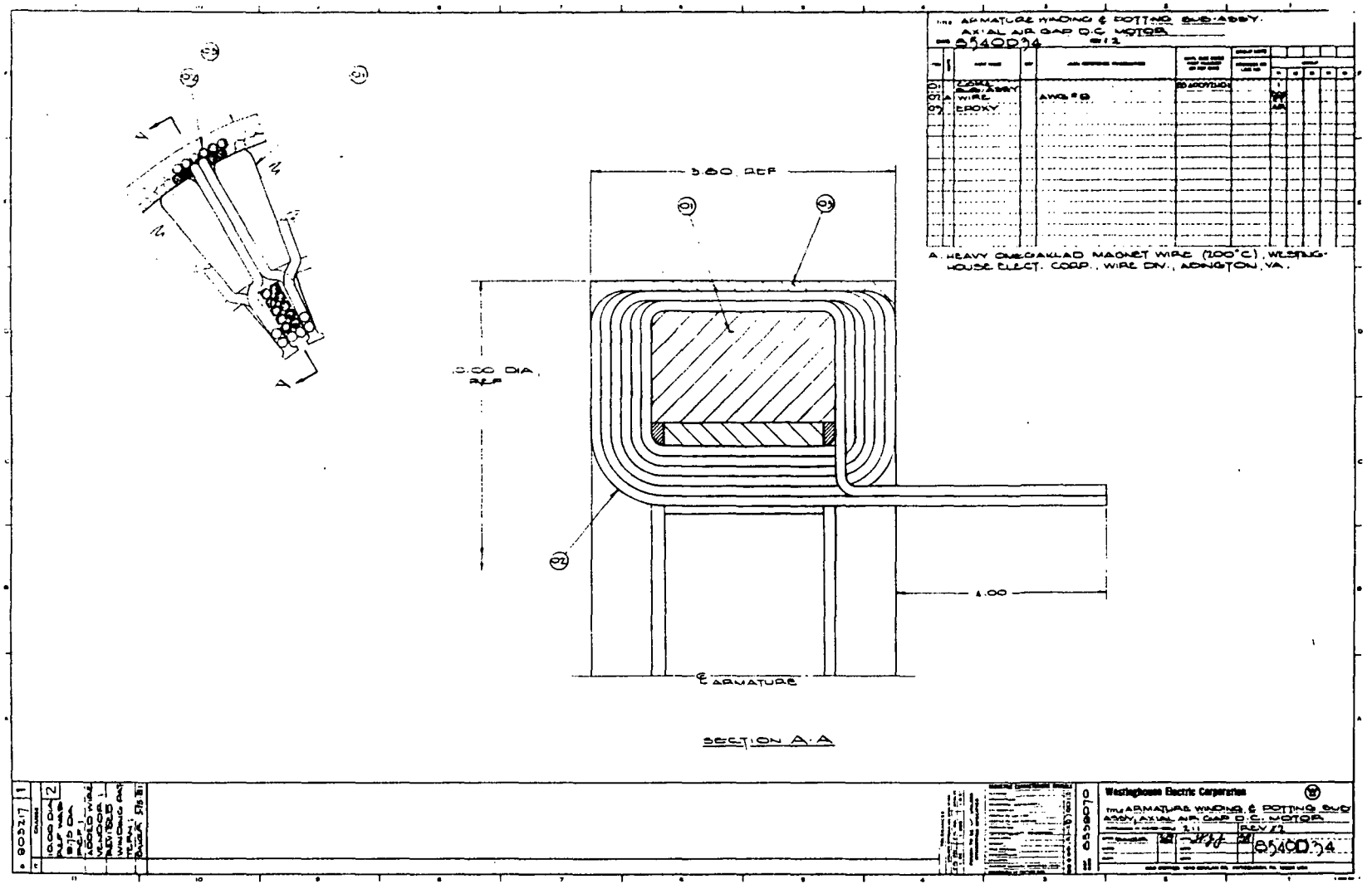
ARMATURE WINDING & POTTING SUB-ASSY.
AXIAL AIR GAP D.C. MOTOR
SIZE 2
NOTES:
A. HEAVY OMEGAKLAD MAGNET WIRE (200°C), WESTINGHOUSE ELECT. CORP., WIRE DIV., ARLINGTON, VA.
5.80 REF
3.60 DIA REF
4.00
ARMATURE
SECTION A-A
Westinghouse Electric Corporation
ARMATURE WINDING & POTTING SUB ASSY, AXIAL AIR GAP D.C. MOTOR
SIZE 2
REV 12
85400J24

1. Report No.	2. Government Accession No.	3. Recipient's Catalog No.
NASA CR 167985		

4. Title and Subtitle	5. Report Date
ADVANCED AXIAL FIELD D.C. MOTOR DEVELOPMENT FOR ELECTRIC PASSENGER VEHICLE	December 1982
	6. Performing Organization Code
7. Author(s)	8. Performing Organization Report No.
William J. Jones	83-8J22-EVMOT-R1
	10. Work Unit No.
9. Performing Organization Name and Address	
Westinghouse Research & Development Center Westinghouse Electric Corporation Pittsburgh, PA 15235	11. Contract or Grant No. DEN 3-75
	13. Type of Report and Period Covered Contractor Report
12. Sponsoring Agency Name and Address	
National Aeronautics and Space Administration Washington, D.C. 20546	14. Sponsoring Agency Code DOE/NASA 0076-82/1

15. Supplementary Notes

Project Manager, B.R. Hatvani, NASA Lewis Research Center, Cleveland, Ohio
Final Report, Report Prepared Under Interagency Agreement DE-A101-77CS51044

16. Abstract

A wound-field axial-flux D.C. motor was developed for an electric vehicle drive system. The motor is essentially an axial-flux version of the classical Gramme-ring winding motor, but the active conductors are recessed into slots cut into the two opposite faces of the laminated tape-wound core ring. Three motors were built and tested in the program. The second (functional) model was a six-pole machine which weighed 88.5 kg. It developed 16.9 kw (22.0 hp) at a base speed of 2400 rpm, with a peak power rating of 25.3 kw (33.0 hp), and a max speed of 4800 rpm. Full load efficiency was 92% and predicted SAE D-cycle efficiency was 88%. The last (engineering) model was a 4-pole machine with compoles, allowing a weight reduction to 45 kg (100 lbs.) while addressing some manufacturability problems. The engineering model was rated at 13.2 kw (17.6 hp) at 3000 rpm, with a peak power of 19.8 kw (26.4 hp) and a max speed of 7200 rpm. Initial test results on this motor showed poor commutation and efficiency; the program was terminated without resolution of these problems.

17. Key Words (Suggested by Author(s))	18. Distribution Statement
D.C. motor electric vehicle axial flux motor disc motor	Unclassified - unlimited STAR Category 33 DOE Category UC-96

19. Security Classif. (of this report)	20. Security Classif. (of this page)	21. No. of Pages	22. Price*
	Unclassified	105	

*For sale by the National Technical Information Service, Springfield, Virginia 22151